Florian Steindl, BSc

Simulation and comparison of power losses in an E-Drive transmission

MASTER THESIS
to obtain the academic degree Diplom-Ingenieur

Master programme Production Science and Management

Graz University of Technology

Faculty of Mechanical Engineering and Economic Sciences

Institute of Automotive Engineering

Member of Frank Stronach Institute

Supervisor: Univ.-Prof. Dipl.-Ing. Dr.techn. Peter Fischer

Supervisor (external): DI Daniel Zirhan

Graz, 26.06.2018

Restricted access until 26.06.2023

Acknowledgement

My special thanks go to Mr. Univ.-Prof. Dipl.-Ing. Dr.techn. Peter Fischer, head of the department of Automotive Engineering at the TU Graz, for the supervision and the technical support of my master thesis.

My thanks also go to my external supervisors DI Daniel Zirhan and Dr. Bernhard Steiner, who supported me from the beginning until the end of the thesis with their know how. I want thank them for all the time invested to support me in the best way possible.

Furthermore, I want to thank all employees of the department Driveline systems with the team leader DI Reinhard Buchberger at the Engineering Center Steyr for their collegial input and assistance during my time at ECS.

I also want to express my gratitude to my parents Herbert and Christine who not only supported me financially, but also helped me in difficult times with the right motivating words. Last but not least, thanks to my girlfriend Lisa who has helped me in stressful times to manage the tricky exams and challenges of my studies.

Statutory Declaration

Ich erkläre an Eides statt, dass ich die vorliegende Arbeit selbstständig verfasst, andere als die angegebenen Quellen/Hilfsmittel nicht benutzt, und die den benutzten Quellen wörtlich und inhaltlich entnommenen Stellen als solche kenntlich gemacht habe.

Graz, am …….

(Unterschrift)

I declare that I have authored this thesis independently, that I have not used other than the declared sources/resources, and that I have explicitly marked all materials which have been quoted either literally or by content from the employed sources.

…….. ……

(Date) (Signature)

Abstract

The present diploma thesis deals with the computation of the transmission losses of a high-speed, electric vehicle transmission with two selected simulation software tools and the comparison of the calculated results with test results.

At the beginning of the thesis, the calculation of the different loss components such as gear losses, bearing losses and sealing ring losses are described. The associated calculation methods were determined by means of a literature research. For the simulation with the software KISSsoft/KISSsys and with the software LMS Amesim state of the art formulas are employed. In KISSsoft/KISSsys, a currently existing simulation model is adapted and applied for the calculation of the power loss. The calculation of the same loss- and efficiency map is performed with LMS Amesim and therefore a new simulation model is created. With this simulation model the efficiency map is evaluated automatically and the individual loss sources are identified. The transmission simulation model should be used as a template in future transmission development projects. Additionally the generated simulation results are compared with the test bench results of the selected transmission. These comparisons show the deviation of calculation results compared to the measured loss values. The deviation of the KISSsoft/KISSsys and the LMS Amesim simulation from the measurement results is in a range of 30 to 40 percent, depending on the respective transmission temperature. To reduce these deviations, calibration factors are introduced. This results in a deviation of the simulation from the measurement in a range of 10 percent. With the calibration factors an adjusted torque loss-and efficiency map for further simulations is created. The determined calibration factors can now be employed in future projects for similar transmissions until test bench results for comparisons are available.

In LMS Amesim, a temperature-dependent transmission model is created, which takes the change in power loss due to temperature changes into account. Input data of the simulation model such as the heat transfer coefficient of the different materials is determined by comparing the simulation with the test bench results. With this approach the simulation model is matched with the test bench measurements and thus verified. By applying the determined heat transfer coefficients a mean deviation of the measured from the simulated temperature curve in a range of -1 °C to 0 °C is achieved. The adjusted temperature-dependent transmission model is implemented in an existing 1D vehicle model adapted for the entire vehicle simulation. By using this vehicle simulation model, different driving cycles are simulated, such as the standardized WLTP driving cycle. Further simulations are executed with data generated from test drive measurements with battery electric vehicles. The gear, bearing and sealing ring losses have been evaluated with the help of the simulation model, to present the shares of the respective individual power losses for each driving cycle respectively test track. At the WLTP the bearing losses generate the greatest share of the total mean losses with 48% and the gear losses generate the second largest share with 30%. The remaining share consists of the sealing ring losses with 17% and the paddling losses with 5% of the total mean losses. At the measuring runs the distribution of the individual power losses is dependent on the velocity and slope trend.

For future gearbox developments at ECS it makes sense to perform the calculation of the transmission losses at first with KISSsoft/KISSsys. The reason for this recommendation is that KISSsoft/KISSsys is used for the dimensioning of all gearbox components, hence the simulation model is always held up to date. The torque loss maps which are implemented in the LMS Amesim vehicle simulation model should be derived from KISSsoft/KISSsys when the gearbox design has reached an advanced status. If the gearbox design changes the LMS Amesim model must be updated parallel to the KISSsoft/KISSsys model.

Kurzfassung

Die vorliegende Diplomarbeit befasst sich mit der Berechnung der Getriebeverluste eines hochdrehenden, elektrischen Fahrzeuggetriebes mit zwei unterschiedlichen Simulationsprogrammen und dem Vergleich der berechneten Ergebnisse mit Versuchsergebnissen.

Am Beginn der Arbeit wird die Berechnung der unterschiedlichen Verlusttherme wie Zahnradverluste, Lagerverluste und Dichtringverluste beschrieben. Die dazugehörigen Berechnungsmethoden wurden mittels einer Literaturrecherche ermittelt. Für die Simulationen im Programm KISSsoft/KISSsys und im Programm LMS Amesim werden Formeln nach dem Stand der Technik für die Berechnung der verschiedenen Verlustleistungen angewandt. Bei der Betrachtung des Softwaretools KISSsoft/KISSsys wird ein bereits bestehendes Simulationsmodell adaptiert und für die Berechnung der Leistungsverluste verwendet. Die Berechnung desselben Wirkungsgradkennfeldes wird mit einem neu erstellten Getriebemodell mit dem Simulationsprogram LMS Amesim durchgeführt. Mit diesem Simulationsmodell wird das Wirkungsgradkennfeld automatisiert ausgewertet und die einzelnen Verlustquellen können identifiziert werden. Das modulare Getriebesimulationsmodell soll als Vorlage für weitere Simulationen neuer Getriebeentwicklungen dienen. Mit den generierten Simulationsergebnissen wird ein Vergleich mit den Prüfstands-Messergebnissen des ausgewählten Antriebs durchgeführt. Mittels dieses Vergleichs wird gezeigt, wie weit die Berechnungsergebnisse der beiden Simulationen von gemessenen Werten abweichen. Die Abweichung der KISSsoft/KISSsys und der LMS Amesim Simulation von den Versuchsergebnissen liegt in einem Bereich zwischen 30 und 40 Prozent, abhängig von der jeweiligen Getriebetemperatur. Um die Abweichungen der Simulationsergebnisse zu den Messergebnissen zu reduzieren, werden Kalibierfaktoren eingeführt, mit denen ein abgeglichenes Verlustmomentkennfeld erstellt wird. Diese Faktoren führen zu einer Abweichung die sich in einem Bereich von 10% befinden.

In LMS Amesim wird ein temperaturabhängiges Getriebemodell erstellt, welches die Änderung der Verlustleistung bei Veränderung der Getriebetemperatur berücksichtigt. Das thermische Verhalten des Simulationsmodells ist mit den im Versuch ermittelten Testergebnissen verglichen und abgeglichen worden, um Randbedingungen wie die Wärmeübergangskoeffizienten der unterschiedlichen Materialien zu bestimmen. Unter Verwendung der ermittelten Wärmeüberganskoeffizienten wird eine mittlere Abweichung des gemessenen vom simulierten Temperaturverlauf in einem Bereich von -1 °C bis 0 °C erreicht. Das abgeglichene, temperaturabhängige Getriebemodell wird in ein bestehendes und für die Gesamtfahrzeugsimulation adaptiertes 1D-Fahrzeugmodell implementiert. Mit dem Fahrzeug Simulationsmodell werden unterschiedliche Fahrzyklen simuliert, wie zum Beispiel der standardisierte WLTP Fahrzyklus. Weitere Simulationen werden mit Messdaten durchgeführt, die aus Testfahrten mit batterieelektrischen Fahrzeugen generiert wurden. Die unterschiedlichen Verlustquellen werden mit Hilfe des Simulationsmodells ausgewertet, um die Anteile der jeweiligen Einzelverlustleistungen für jeden Fahrzyklus bzw. jede Messstrecke darzustellen. Beim WLTP generieren die Lagerverluste mit 48% den größten Anteil und die Verzahnungsverluste mit 30% den zweitgrößten Anteil des gemittelten Gesamtverlustes. Der restliche Anteil setzt sich aus den Dichtringverlusten mit 17% und den Planschverlusten mit 5% zusammen. Die Aufteilung der Einzelverluste bei den Messfahrten ist abhängig vom Geschwindigkeits- und Steigungsprofil.

Für die Berechnung der Getriebeverluste sollte in Zukunft KISSsoft/KISSsys verwendet werden. Ein Grund für diese Empfehlung ist, da KISSsoft/KISSsys für die Auslegung aller Getriebekomponenten verwendet wird und somit das Model immer auf dem neusten Stand ist. Im fortgeschrittenen Entwicklungsstadium sollen die Verlustmomentkennfelder mit Hilfe von KISSsoft/KISSsys generiert werden und in das Fahrzeugsimulationsmodell implementiert werden. Wenn sich das Getriebedesign ändert muss parallel zum KISSsoft/KISSsys Modell auch das LMS Amesim Modell aktualisiert werden.

Contents

Abbreviations

AL	Axial load
B	Bearing
BEV	Battery electric vehicle
CL	Clutch
eRAD245o	electric Rear Axle Drive, 245kW peak power of electric machine, offset design of transmission
ECS	Engineering Center Steyr
ECU	Engine Control Unit
NEDC	New European Driving Cycle
PSM	Permanent Magnet Synchronous Motor
RL	Radial load
S	Radial shaft sealing ring
SUV	Sports utility vehicle
UNECE	United Nations Economic Commission for Europe
VCU	Vehicle Control Unit
WLTP	Worldwide Harmonized Light Duty Test Procedure

Symbols

Symbol	Naming	Unit
b	gear width	[mm]
b_0	effective gear width	[mm]
d_M	mean bearing diameter	[mm]
d_{sh}	shaft diameter	[mm]
d_w	pitch circle diameter	[mm]
e_h	oil thickness	[mm]
f_g	slipping coefficient	[-]
f_0 f_1	bearing factors	[-]
g	gravity	[m/s²]
g_f	length off approach	[mm]
h_c	height contact point above immersed gear	[mm]
h_e	immersed gear height	[mm]
h_t	tooth height	[mm]
h_{t0}	scale factor of gear tooth height	[mm]
k	heat transmission coefficient	[W/m²K]
l_h	hydraulic length	[mm]
m_n	real pitch module	[mm]
q	heat transfer rate	[W]
p_e	base pitch	[-]
u	gear ratio	[-]

v_r	vehicle longitudinal velocity	[m/s]
v_S	oil jet velocity	[m/s]
v_t	circumferential speed	[m/s]
v_{t0}	reference tangential speed	[m/s]
$viscopress$	oil piezo viscosity coefficient	[1/Pa]
z_1	pinion teeth number	[-]
z_2	connected gear teeth number	[-]

Capital letters:

C	factor-churning losses	[-]
C_{side}	paddling torque losses on gear side	[Nm]
C_{Sp}	splash oil factor	[-]
C_{teeth}	paddling torque losses on gear teeth	[Nm]
C_0	static load capacity	[N]
F_a	axial force	[N]
F_{bt}	tangential force at pitch circle	[N]
F_N	normal force	[N]
F_{nu}	normal force per length unit	[N]
F_r	radial force	[N]
F_t	tangential force	[N]
Fro	Froude number on gear side	[-]
Fro_A	Froude number on gear teeth	[-]
G	mass force	[N]
H_V	gear loss factor	[-]

L_A	length of action	[mm]
M_0	rotational speed dependent friction torque	[Nm]
M_1	load dependent friction torque	[Nm]
P_a	input power	[W]
P_g	sliding friction loss	[W]
P_{VB}	bearing loss due to load	[W]
P_{VB0}	bearing idling losses	[W]
P_{VD}	sealing losses	[W]
P_{pad}	paddling losses	[W]
P_{VX}	other losses	[W]
P_{VZ}	load dependent gear losses	[W]
P_{VZ0}	idling losses of gears	[W]
P_1	decisive load for frictional torque	[N]
$\dot{Q}$	heat flow	[W]
R_p	pitch radius	[mm]
R_{pw}	working pitch radius	[mm]
R_t	tip radius	[mm]
Re	Reynolds number on gear side	[-]
Re_A	Reynolds number on gear teeth	[-]
T	temperature	[°C]
T_H	hydraulic loss torque	[Nm]
T_p	primary shaft torque	[Nm]

T_s	secondary shaft torque	[Nm]
V_g	sliding velocity	[m/s]
V_r	rolling velocity	[m/s]
$V_{\Sigma m}$	mean summing velocity at contact	[m/s]
V_p	immersed volume of the gear	[m/s]
V_0	oil volume in the gearbox	[mm³]
$\dot{V}_{oil}$	oil injection rate	[m/s]
$\dot{V}_0$	reference oil injection rate	[m/s]
X_1	curve radius for pinion gear	[mm]
X_2	curve radius for connected gear	[mm]
X_{eq}	equivalent curve radius	[mm]
X_R	roughness factor	[-]
Z	pulling force	[N]

Greek letters:

α	heat exchange coefficient	[W/m²K]
α_N	normal pressure angle	[°]
α_T	transverse pressure angle	[°]
α_{Tw}	working transverse pressure angle	[°]
β_b	helix angle at base circle	[°]
ε	addendum contact ratio	[-]
ε_α	transverse contact ratio	[-]
η	efficiency degree	[-]
ϑ	temperature	[K]

λ	thermal conductivity	[W/mK]
μ	oil absolute viscosity	[Ns/m²]
μ_{mZ}	mean friction coefficient	[-]
μ_z	friction coefficient	[-]
ν	oil kinematic viscosity	[m²/s]
ρ	oil density	[kg/m³]
ρ_m	mean curvature radius in normal section	[mm]
σ	Stefan-Boltzmann constant	[W/m²K^4]
φ	rotational angle	[rad]
$\ddot{\varphi}$	angular acceleration	[rad/s²]
ω	rotational speed	[rad/s]

Indices:

1	pinion gear
2	connected gear
max	maximum value
min	minimum value
x, y, z	coordinates

1 Introduction

Today phrases like global warming and CO2 emissions are used in context developing the sustainable vehicle of the future. Cars powered by fossil fuel are ranked by their CO2 emissions and the fuel consumption per 100 km. The car manufacturers have reduced the emissions over the last years and this process will continue for the next years as well. Yet, there is a new development, which has been going on for the last few years in the field of e mobility.

In the year 2017 the electro mobility increased compared to the year before and the variety of electric vehicles available on the market rises as well. The share of electric vehicles on the market in Austria and in Europe is likely to drastically increase in the near future. Hence, it is possible that in the year 2026 the number of produced electric vehicles will reach 100 million units. Some countries even have discussed the possibility to completely prohibit the use of cars powered by combustion engines using fossil. There are different dates mentioned, such as 2030 or 2040 and these dates depend on the policy in each country. However, these dates are not only dependent on politics but also on the development of air quality in large cities. [1]

To reduce air pollution in cities, it will be inevitable in the future to impose bans on cars with internal combustion engines. With the use of battery electric vehicles (BEV), the sound and air emission in big cities will decrease compared to currently used fossil fuel powered cars. Parallel to the BEVs fuel cell vehicles are developed. Compared to a BEV the fuel cell uses the energy of hydrogen to produce electric energy which is then employed to run an electric machine. Japanese car manufacturers have already invested a lot of research in that field and have launched the first series of vehicles. Hydrogen cars have the advantage of higher mileage and faster charging or refilling compared to BEVs. Hence, in the future there might be a mix of battery electric vehicles for shorter distances due to the price advantage and for longer distances a hydrogen car will satisfy the customer needs, as it provides comparably the same comfort as driving a fossil fuel powered vehicle.

The development of vehicles powered by electric current, fossil fuel or by hydrogen is done in shorter periods compared to the development times a few years ago. In order to ensure short development cycles new innovative simulation tools are necessary which enables analysis and evaluation of virtual vehicles. With the simulation of the vehicle in advance the evaluation of different drivetrain concepts becomes much faster. This kind of data and knowledge generation is also called frontloading. With appropriate software tools it is possible to start simulation runs with the whole vehicle model before any prototype exist. With these results of the simulation runs different drivetrain concepts can be analysed in the vehicle application and evaluated afterwards. Therefore, development of new vehicles is getting more and more efficient because the number of prototypes needed to evaluate the drivetrain is reduced which in turn results in a time and cost benefit as well. [2]

At the Engineering Center Steyr (ECS) different types of computation and simulation software are in use to develop new drivetrain components like a gearbox or an axle drive. One important indicator during the development is the efficiency because it is directly related to the energy consumption and especially concerning electric vehicles it is related to the range. Hence, the efficiency computation of a gearbox plays an important role in the drive train development. The efficiency simulation is done with the KISSsoft/KISSsys simulation tool that provides a good overview of the efficiency for different load points. With the software LMS Amesim it is also possible to set up a simulation model that computes the efficiency and losses of a gearbox. This software tool enables the simulation of a whole vehicle as well and it is possible to analyse different driving cycles. That leads to the task of this master thesis which includes the setup of a gearbox simulation model in LMS Amesim and the implementation of the gearbox model into a vehicle model to simulate various driving cycles.

1.1 Task

The first task of that thesis is the generation of a 1D simulation model of the electric drive gearbox, called eRAD245o at ECS, with the software tool LMS Amesim. In Figure 1-1 a cutaway model of the whole drive unit including the electric motor and the gearbox is displayed. Using the LMS Amesim simulation model it is possible to compute the different types of losses and the efficiency of that gearbox. In order to evaluate the results of the simulation, the results are compared with measurement results of test bench runs. At ECS several efficiency test bench runs were done to determine the losses at the different load points. After the setup of the simulation model and the definition of the most important parameters, the results of the LMS Amesim simulation are compared with the measured results. The same procedure is performed with the KISSsys model. A gearbox model was generated by an employee at ECS and this model is checked and completed to run an efficiency simulation. With that KISSsoft/KISSsys model the different types of losses are computed. The aim of the first part is the comparison of the LMS Amesim simulation results with the measurement results and with the KISSsoft/KISSsys calculation results. Afterwards the differences between the results is visible.

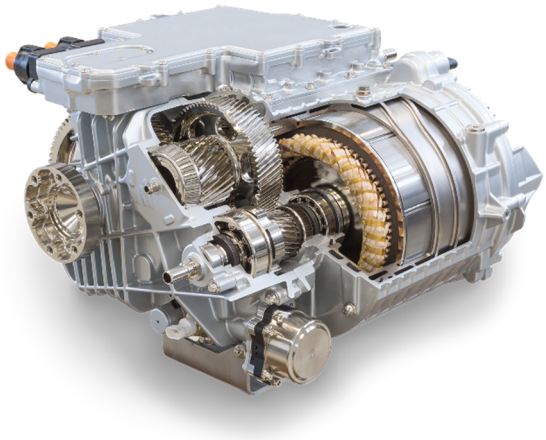

Figure 1-1: Cutaway model of the eRAD245o gearbox

The second part of the thesis includes the implementation of temperature dependencies into the LMS Amesim gearbox simulation model. In a gearbox the losses produce heat and this heat leads to an increase in temperature of the whole gearbox. Moreover, the increase of temperature leads to a change of the losses which is considered in the LMS Amesim simulation model. In order to determine the right input data which is employed for the simulation model the results of the simulation are compared with test run results. Using the calibration factors, the losses of the gearboxes can be calculated with reduced deviation over a temperature spectrum. The temperature dependent gearbox model is implemented into a 1D vehicle simulation model. With the vehicle simulation model standardized driving cycles like the WLTP or NEDC are simulated. The evaluation of gearbox losses and the evaluation of the shares of individual loss sources for the driving cycles is the last part of the second task.

The third and final task is the generation of a LMS Amesim simulation model template for the computation of the different gearbox power losses. The modelling template should help in the future to create a new simulation model for other transmissions.

1.2 E-Drive system

An Electric drive system is employed in electric vehicles and will play an important role in the near future. Today the electric vehicles market share is not that large, but due to stricter climate regulations from the legislation in the future the e-mobility will increase. The gearbox of an electric vehicle is an important part because it transmits the power of the electric motor to the wheels. Therefore, the efficiency of such a transmission should be as high as possible in order to use the energy of the batteries in an efficient way and thus increase the range of the vehicle. Figure 1-2 shows an electric vehicle schema with the most important electric and mechanical components of such a vehicle. The main parts of an electric vehicle are enumerated from one to nine and described in the following section.

1. **Electric machine**
   There are different types of electric machines available on the market. Electric machines can be used as a motor and as a generator. In the drive mode an electric power is required to produce torque at the output shaft. By usage in generator mode the mechanical power from the wheels is transferred into electric power which is employed to charge the batteries. [3]

2. **Transmission with differential**
   To transmit the power of the electric machine to the tires a transmission and a differential is needed. Referring to the speed range of the vehicle a one or two manual transmission is employed. One advantage of a two-speed gearbox is the higher efficiency of the vehicle due to the fact that the vehicle control unit operates the electric motor in the best load point of the efficiency map at any driving situation.

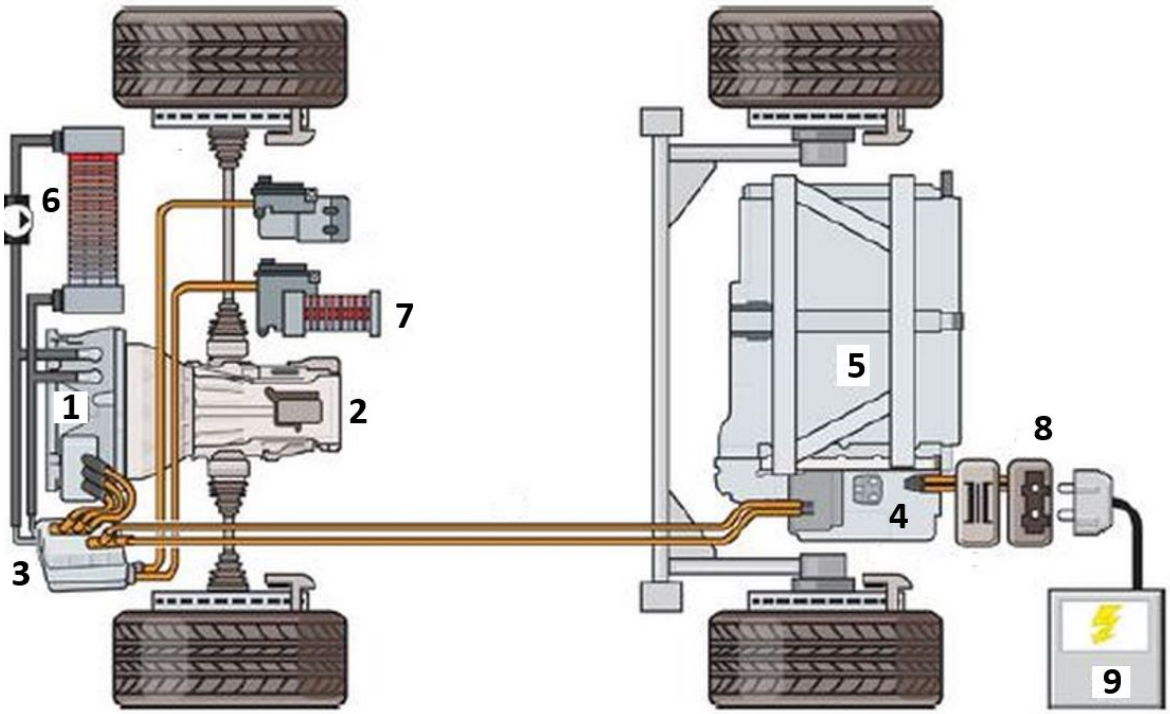

Figure 1-2: E-Vehicle schematic diagram [4]

3. **Power electronics including the inverter**
   One task of the power electronics is to adjust the electric energy of the energy storage, which is usually a battery, according to the requirements of the electric machine. The voltage from the energy storage is available as direct voltage. For the power supply of the electric machine a three-phase alternating voltage with variable amplitude, frequency and phase position is

needed in order to adjust the target torque and the target rotational speed. To get the alternating voltage, which is used for the machine in the driving mode, an inverter is needed. If the electric machine works as a generator, the inverter transforms the alternating current into direct current which is then employed for charging the battery. [3]

4. **Electronic box with control unit for battery regulation**
   The electric vehicle is charged by an external charging unit and hence a control unit for the charging of the battery is required. This control unit often includes a battery management system which is responsible for the charging status of the battery. [3]

5. **High voltage battery**
   Nowadays usually lithium ion batteries are applied in electric vehicles. This type of battery is used due to the high specific charging and discharging power and based on the high-power density. Other advantages of this battery are the charging efficiency of nearly 100% and the lifetime referring to the charging cycles. One weakness of the lithium ion battery is the sensibility against low discharging and overcharging. [3]

6. **Cooling system**
   The cooling system is needed to cool the electric machine and the inverter. There are several different types of cooling systems possible. One type is a cooling jacket around the electric machine and a cooling of the rotor shaft to cool the machine from inside and outside. At high load points the electric machine and the inverter produce a lot of heat which must be absorbed by the cooling system.

7. **High voltage heating system**
   Usually the electric machine and the power electronics are water cooled whereby the generated heat energy is employed for the heating of the passenger compartment. The heating system is employed to regulate the passenger compartment temperature. Furthermore, if an increase in temperature is required the electric powered heating system generates the needed heat energy.

8. **Battery charger with charging contact for external charging**
   For the charging of the battery a connection point is necessary to connect the vehicle with a power supply unit. Today usually a wire connection of the vehicle with the power unit is used. There are some future developments looking into ways to charge the vehicle without connecting it manually with a charging unit. One investigated possibility is the charging of the battery by induction, which however has the disadvantage of an additional power loss during the charging operation.

9. **External charging unit**
   It is possible to charge the electric vehicle at charging stations, which are more and more available. Concerning the charging speed, there are different types of charging units available, like fast charging stations which charge the battery up to 80% in 30 minutes.

2 Basics of gearbox losses

For the efficiency calculation of a gearbox it is necessary to know the losses and how these losses can be calculated. The losses in a gearbox generally consist of the losses the different machine elements of the gearbox produce. Therefore, the overall losses of a gearbox are subdivided into gear losses, bearing losses, sealing losses and other losses. [5] In the following formula (2.1) the different loss parts are displayed.

$$P = P_{VZ} + P_{VZ0} + P_{VB} + P_{VB0} + P_{VD} + P_{VX} \tag{2.1}$$

P_{VZ} … Load dependent gear losses

P_{VZ0} … Idling losses of gears

P_{VB} … Bearing loss due to bearing load

P_{VB0} … Bearing idling losses

P_{VD} … Sealing losses

P_{VX} … Other losses

It is possible to classify the terms in load-dependent and non-load dependent losses respectively speed dependent losses. Load-dependent losses are caused by loads in the contact area of bearings or gears. The non-load dependent losses occur also without any load applied like for example the paddling losses. Other losses include power losses of other power units like oil pumps which are employed in the gearbox. In the following subchapters the different types of losses and the associated calculation methods are described in detail. [5]

2.1 Gear losses

As mentioned before the losses are split up into load and non-load dependent losses. Concerning gear losses, the load dependent are losses due to the normal force acting in the tooth contact. The non-load-dependent losses are basically caused by the rotational speed of the gears during immersion in the oil and due to the crushing losses between the teeth. In the following two subchapters exclusively the power loss computation of spur gears is explained.

2.1.1 Load dependent gear losses

In a spur gear, the gears roll against each other and during this process, a combination of sliding and rolling takes place. Thus, sliding and rolling losses occur in the spur gear. This generated friction losses are described by Coulombs law with the normal force F_N, the friction coefficient μ_z and the sliding velocity V_g. In equation (2.2) the general formulation of the power loss is displayed. [5]

$$P_{VZ} = F_N \cdot \mu_z \cdot V_g \tag{2.2}$$

In order to get the power loss over the whole action length, the formula of the power loss is integrated over the length of action and divided by the spur base pitch. With equation (2.3) the average power loss over the length of action is calculated. [5]

$$P_{VZ} = \frac{1}{p_e} \int_A^E F_N(x) \cdot \mu_z(x) \cdot V_g(x)\, dx \tag{2.3}$$

According to Niemann [5] the friction coefficient is constant over the whole length of action and therefore is called μ_{mZ}. Directly at the pitch point the friction coefficient is equal to zero, but for the calculation of the power loss the mean friction coefficient is valid. Consequently, the whole integral is written as in equation (2.4) displayed. The input power P_a is multiplied with the mean friction coefficient μ_{mZ} and the gear loss factor H_V which leads to the load dependent power loss of the gear pair.

$$P_{VZ} = P_a \cdot \mu_{mZ} \cdot H_V \tag{2.4}$$

The calculation of the gear loss factor H_V is possible in several ways according to different approaches and testing procedures. Niemann uses the approach by Ohlendorf [6] which is defined in the following formula:

$$H_V = \frac{\pi \cdot (u+1)}{z_1 \cdot u \cdot \cos\beta_b} \cdot \frac{1}{\varepsilon_\alpha^{\,2}} \cdot \left(\varepsilon_1^{\,2} + \varepsilon_2^{\,2}\right) \tag{2.5}$$

Equation (2.5) consists of gear specific geometry related elements like the addendum contact ratio ε_1, ε_2, the transverse contact ratio ε_α, the gear ratio u of gear 2 to gear 1, and the helix angle β_b at the base diameter.

According to Niemann the calculation of the mean friction coefficient μ_{mZ} is dependent on several factors. Beside the load also the sliding and rolling velocity, the oil viscosity and the chemical structure of the lubricating oil have an impact onto this coefficient. For a first calculation it is possible to use equation (2.6). [5]

$$\mu_{mZ} = 0.045 \cdot \left(\frac{K_A \cdot \frac{F_{bt}}{b}}{V_{\Sigma m} \cdot \rho_m} \right)^{0.2} \cdot \eta_M^{-0.05} \cdot X_R \le 0.2 \tag{2.6}$$

The KISSsoft/KISSsys computation software uses the equations according to Niemann for the calculation of the load dependent losses, which are described in the section above. In KISSsoft/KISSsys there are currently no other methods available for calculating the load dependent losses.

In contrast to the KISSsoft/KISSsys software the software LMS Amesim uses a different computation method to calculate the load dependent losses. These losses are separated into slipping and rolling losses. For the calculation of the slipping losses the normal force F_N, the slipping coefficient f_g and the slipping velocity V_g are employed. With these terms the power loss due to teeth slipping is calculated as follows in formula (2.7). The normal force F_N is calculated with equation (2.8) including the tangential force F_t, the normal pressure angle α_N and the helix angle β. For the computation of the slipping coefficient f_g the equation (2.9) is in use, which is a correlation suggested by Benedict et Kelley [7]. With equation (2.10) the computation of the slipping velocity V_g is described. The equations (2.7), (2.8) and (2.10) from [8] are mentioned in the LMS Amesim help as well.

$$P_g = \frac{1}{L_a}\int_0^{L_a} F_N \cdot V_g \cdot f_g \; dl \tag{2.7}$$

$$F_N = \frac{F_t}{\cos\alpha_N \cdot \cos\beta} \tag{2.8}$$

$$f_g = 0.0127 \cdot \log_{10}\left(\frac{0.02912 \cdot F_{nu}}{\rho \cdot \mu \cdot V_g \cdot V_r^2}\right) \tag{2.9}$$

$$V_g(l) = \omega_2 \cdot \left|l - g_f\right| \cdot \left(1 + \frac{z_1}{z_2}\right) \tag{2.10}$$

For the determination of the rolling losses the rolling force F_r, rolling velocity V_r, oil thickness e_h, the equivalent Young's modulus E_{Eq} and the equivalent curve radius X_{Eq} are calculated with the following formulas [9]:

$$P_r = \frac{1}{L_a}\int_0^{L_a} F_r \cdot V_r \; dl \tag{2.11}$$

$$F_r = \frac{9.1^7 \cdot e_h \cdot b_0}{\cos\beta} \tag{2.12}$$

$$V_r = 2 \cdot \omega_1 \cdot R_{p1} \cdot \sin\left(\alpha_{Tw}\right) + \omega_1 \left|l - g_f\right| \cdot \left(1 - \frac{z_1}{z_2}\right) \tag{2.13}$$

$$e_h = X_{eq} \cdot 2.65 \cdot \left(\frac{\mu \cdot V_r}{2 \cdot E_{eq} \cdot X_{eq}}\right)^{0.7} \cdot \left(viscopress \cdot E_{eq}\right)^{0.54} \cdot \left(\frac{F_{nu}}{E_{eq} \cdot X_{eq}}\right)^{-0.13} \tag{2.14}$$

$$E_{eq} = \frac{2}{\frac{1-\nu_1^2}{E_1} + \frac{1-\nu_2^2}{E_2}} \tag{2.15}$$

$$X_{eq} = \frac{X_1 \cdot X_2}{X_1 + X_2} \tag{2.16}$$

These formulas are mentioned in the LMS Amesim help [9] and relate to the literature [8]. Equation (2.11) shows that the power loss due to rolling friction is calculated over the total contact length. The lower limit of the integral is zero and the upper limit is the length of action L_a. Based on this assumption, the power loss for the whole rolling motion of one tooth contact is calculated. For the calculation of the rolling force F_r equation (2.12) is employed and shows that the force is dependent on the oil thickness, the tooth width and the helix angle. The formula (2.13) is used for the computation of the rolling velocity V_r which is an important factor of the rolling friction power loss. For the calculation of V_r several gear specific parameters are used.

2.1.2 Non-load dependent gear losses

KISSsoft/KISSsys computes the non-load dependent losses according to ISO/TR 14179 [10]. The equations for the loss calculation differ between splash lubrication and injection lubrication. In the following equations the torque loss calculation for the splash lubrication are displayed and thereafter the equations for injection lubrication are explained. The torque loss formula (2.17) consists of the factors C_1, C_2, C_{Sp} and the rotational speed. With the factors C_1 and C_2 it is possible to consider the impact of the immersion depth and the width of the tooth which is shown in equation (2.19). The factor C_{Sp}, see equation (2.18), takes the effect of the splash oil supply depending on the immersion depth into account. In equation (2.20) the hydraulic characteristic length of the gearbox housing along the flow direction of the oil is described with the side face and the inner circumference of the gearbox housing. [10]

$$T_H = C_{Sp} \cdot C_1 \cdot e^{C_2\left(\frac{v_t}{v_{t0}}\right)} \tag{2.17}$$

$$C_{Sp} = \left(\frac{4 \cdot h_{e,\max}}{3 \cdot h_c}\right)^{1.5} \cdot \frac{2 \cdot h_c}{l_h} \tag{2.18}$$

$$C_1 = 0.063 \cdot \left(\frac{h_{e1} + h_{e2}}{h_{e0}}\right) + 0.0128 \cdot \left(\frac{b}{b_0}\right)^3$$
$$C_2 = \frac{h_{e1} + h_{e2}}{80 \cdot h_{e0}} + 0.2 \tag{2.19}$$

$$l_h = \frac{4 \cdot A_G}{U_M} \tag{2.20}$$

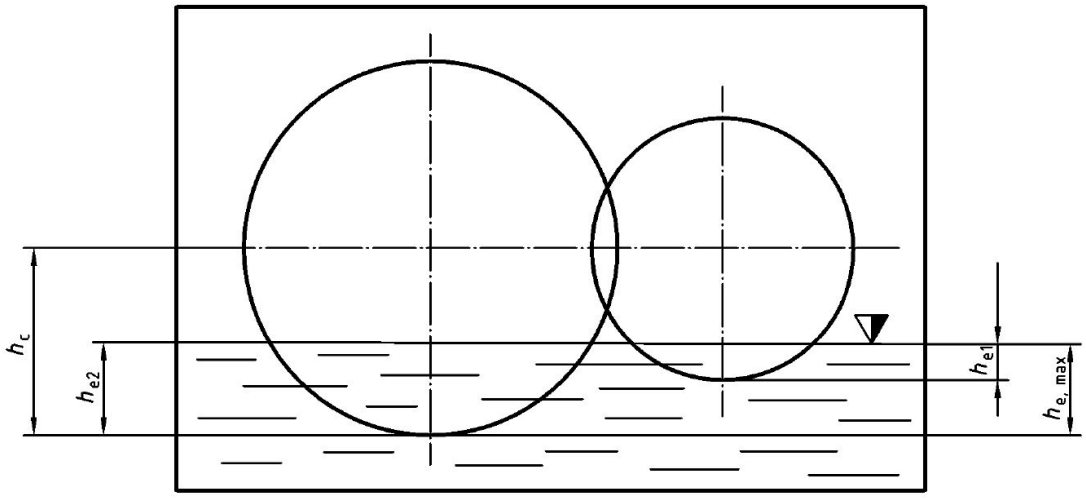

Figure 2-1: Immersion depth of gears [10]

Figure 2-1 shows gears with different immersion depths, where the immersion depth of the sprocket is defined as h_{e1}, the immersion depth of the gear as h_{e2}. The other dimensions are the distance of the pitch point to the lowest point of the immersing gear h_c and the maximum immersion depth $h_{e,\max}$. This different immersion depths are employed for the calculation of the factors which are required for the splash lubrication torque loss described in the section above.

The dependence of the power loss on the depth of immersion is reflected in the fact that the power loss increases with increasing oil level and vice versa. Another factor which has an impact on the torque loss is the oil viscosity. The results of experiments made by [11] showed that the influence of the oil viscosity in comparison with low immersion depths can be neglected. At the eRAD245o transmission, the immersion depth is not negligible and the oil viscosity is considered in the loss calculation. Thus, the power loss increases with the rise of the immersion depth and the rise of the peripheral speed.

The second type for the lubrication of a gearbox is the injection lubrication. In comparison to the splash lubrication there is no oil sump but injection nozzles which inject the lubricant at defined positions. For the calculation of the injection lubrication torque losses the type of calculation is distinguished between injection into the point of engagement and into the point of disengagement. Equation (2.21) shows the torque loss when the injection takes place at the point of engagement. To calculate the losses for the injection at the point of disengagement equation (2.22) is employed. In [10] these two formulas are mentioned and the reference oil injection volume is set with $\dot{V} = 2\ l/\min$. [10]

$$T_H = 1.67 \cdot 10^{-6} \rho \cdot \dot{V}_{oil} \cdot d_W \left(v_t - v_S \right) + 32 \cdot 10^{-9} \cdot \rho \cdot \nu^{0.065} \cdot d_W^{1.5} \cdot m_n^{0.18} \cdot v_t^{1.5 \cdot \left(\frac{\dot{V}_{oil}}{\dot{V}_0} \right)^{0.1}} + 0.1 \tag{2.21}$$

$$T_H = 8.33 \cdot 10^{-6} \rho \cdot \dot{V}_{oil} \cdot d_W \left(v_t - v_S \right) \tag{2.22}$$

The injection oil amount and the peripheral speed which are main components of the calculation formulas have the biggest influence on the hydraulic losses. Other factors that increase the torque loss due to injection lubrication are the module, tooth width, oil viscosity and tooth height. Gear specific parameters like the tooth clearance, backlash and the gear ratio have no impact on the torque loss. [11]

In comparison to the ISO/TR 141479-2 the LMS Amesim calculation model divides the gear paddling losses into gear teeth paddling and gear side paddling. The main influencing factors for the power loss are the oil properties, oil volume, immersed gear height, gear dimensions and the gear rotational speed. Equation (2.23) shows the whole power loss due to churning. [9]

$$P_{pad} = \left(C_{side} + C_{teeth} \right) \cdot \left| \omega \right| \tag{2.23}$$

For the calculation of the torque loss due to gear teeth paddling from [12] the equations (2.25) and (2.26) are employed. The equations differ between, laminar and turbulent flow condition. To decide between laminar and turbulent flow the Reynolds and Froude number are specified as follows:

$$Re_A = \left| \omega \right| \cdot \frac{Rp_1 \cdot ht}{\nu} \qquad Fro_A = \omega^2 \cdot \frac{Rp_1^2}{g \cdot ht} \tag{2.24}$$

For laminar flow: $Re_A^{0.32} \cdot Fro_A^{-0.23} < 12$

$$C_{teeth} = 616.6 \cdot Re_A^{-0.65} \cdot Fro_A^{-0.46} \cdot \left(\frac{ht}{ht_0} \right)^{-1.66} \cdot \left(\frac{b}{ht_0} \right)^{-0.46} \cdot \rho \cdot \omega^2 \cdot Rp_1^3 \cdot b \cdot ht \tag{2.25}$$

For turbulent flow: $Re_A^{0.32} \cdot Fro_A^{-0.23} \geq 12$

$$C_{teeth} = 5623 \cdot Re_A^{-0.88} \cdot Fro_A^{-0.78} \cdot \left(\frac{ht}{ht_0} \right)^{-1.6} \cdot \left(\frac{b}{ht_0} \right)^{-0.36} \cdot \rho \cdot \omega^2 \cdot Rp_1^3 \cdot b \cdot ht \tag{2.26}$$

These formulas are in force when the following validity ranges are fulfilled:

$$0.45 < \frac{b}{ht_0} < 1.8 \quad 1 < \frac{ht}{ht_0} < 1.6 \quad 7 < Re_A < 2110 \quad 22 < Fro_A < 3112 \tag{2.27}$$

The torque loss due to paddling on the gear side is calculated according to [13] and described in the following part. In the LMS Amesim model it is assumed that only one gear is immersed into the oil volume. For the calculation of the torque loss with laminar flow conditions two different equations exist. The validity ranges for deciding between the equations are stated below. Equation (2.29) and (2.30) show the difference in scope and the difference in the equations per se. The calculation of the Reynolds number and Froude number for this loss case is described as follows:

$$Re = |\omega| \cdot \frac{Rt_1}{\nu} \qquad Fro = \omega^2 \cdot \frac{Rt_1^2}{g} \tag{2.28}$$

For the laminar flow condition, the torque loss on the gear side is computed in the following way:

$$C_{side} = 4.57 \cdot Re^{-0.6} \cdot Fro^{-0.25} \cdot \left(\frac{V_p}{V_0}\right)^{-0.5} \cdot \left(\frac{b}{Rt_1}\right)^{-0.4} \cdot \left(\frac{h_e}{Rt_1}\right)^{1.5} \cdot \rho \cdot \omega^2 \cdot Rt_1^4 \cdot b \tag{2.29}$$

$$Re < 2250 \quad \text{and} \quad Re^{-0.6} \cdot Fro^{-0.25} \geq 8.7 \cdot 10^{-3}$$

$$C_{side} = 2.63 \cdot Re^{-0.6} \cdot Fro^{-0.25} \cdot \left(\frac{V_p}{V_0}\right)^{-0.73} \cdot \left(\frac{b}{Rt_1}\right)^{-0.4} \cdot \left(\frac{h_e}{Rt_1}\right)^{1.5} \cdot \rho \cdot \omega^2 \cdot Rt_1^4 \cdot b \tag{2.30}$$

$$Re < 2250 \quad \text{and} \quad Re^{-0.6} \cdot Fro^{-0.25} < 8.7 \cdot 10^{-3}$$

For the turbulent flow condition, it is calculated as follows: $Re \geq 2250$

$$C_{side} = 0.97 \cdot Re^{-0.31} \cdot Fro^{-\left(0.464 + 0.037 \cdot \frac{Rt_1}{h}\right)} \cdot \left(\frac{V_p}{V_0}\right)^{-0.576} \cdot \left(\frac{b}{Rt_1}\right)^{-0.124} \cdot \left(\frac{h_e}{Rt_1}\right)^{0.74} \cdot \rho \cdot \omega^2 \cdot Rt_1^4 \cdot b \tag{2.31}$$

In order to guarantee a correct calculation following ranges must be valid:

$$0.006 < \frac{b}{ht_0} < 1 \quad 0.025 < \frac{ht}{ht_0} < 1 \quad 10 < Re < 36000$$
$$1.6 < Fro < 1400 \quad 0.01 < \frac{V_p}{V_0} < 0.25 \tag{2.32}$$

2.2 Bearing losses

The friction losses of roller bearings are caused by the rolling friction, slipping friction of the rolling elements and the cage, the fluid friction and the friction of a bearing seal. The applied load on the bearing and the load direction, the rotational speed and the oil characteristic data have an impact on the friction losses. Regarding the idling losses the rotational speed, the oil properties and the oil volume play a major role. When using a lubricating oil, a part of the heat energy is dissipated by the oil. The remaining part of the heat energy is transmitted to the shaft and the housing. [14]

The bearing loss calculation according to Schaeffler [14] separates the overall friction torque into a load dependent and rotational speed dependent term and is explained in the section below.

Overall friction torque M_R:

$$M_R = M_0 + M_1 \tag{2.33}$$

Rotational speed dependent friction torque M_0:

$$\begin{aligned} M_0 &= f_0 \cdot (\nu \cdot n)^{\frac{2}{3}} \cdot d_M^3 \cdot 10^{-7} \quad \text{for } \nu \cdot n \geq 2000 \\ M_0 &= f_0 \cdot 160 \cdot d_M^3 \cdot 10^{-7} \quad \text{for } \nu \cdot n < 2000 \end{aligned} \tag{2.34}$$

Load dependent friction torque M_1 for cylindrical- and needle roller bearings:

$$M_1 = f_1 \cdot F \cdot d_M \tag{2.35}$$

Load dependent friction torque M_1 for radial ball bearings, tapered roller bearings and spherical roller bearing:

$$M_1 = f_1 \cdot P_1 \cdot d_M \tag{2.36}$$

The roller bearing coefficients f_0 and f_1 are selected from the tables of the bearing catalogue for the respective bearing type. These coefficients are dependent on the lubricating system and partly on the bearing load. In Figure 2-2 the calculation of P_1 for the different bearing types is displayed.

Bearing type	Single bearing P_1	Bearing pair P_1
Deep groove ball bearings	$3{,}3 \cdot F_a - 0{,}1 \cdot F_r$	–
Angular contact ball bearings, single row	$F_a - 0{,}1 \cdot F_r$	$1{,}4 \cdot F_a - 0{,}1 \cdot F_r$
Angular contact ball bearings, double row	$1{,}4 \cdot F_a - 0{,}1 \cdot F_r$	–
Four point contact bearings	$1{,}5 \cdot F_a + 3{,}6 \cdot F_r$	–
Tapered roller bearings	$2 \cdot Y \cdot F_a$ or F_r, use the larger value	$1{,}21 \cdot Y \cdot F_a$ or F_r, use the larger value
Spherical roller bearings	$1{,}6 \cdot F_a/e$ if $F_a/F_r > e$ $F_r\{1 + 0{,}6 \cdot [F_a/(e \cdot F_r)]^3\}$ if $F_a/F_r \leqq e$.	

If $P_1 \leqq F_r$, then $P_1 = F_r$.

Figure 2-2: P1 Calculation [14]

Using the KISSsoft/KISSsys software, it is possible to choose between the calculation method according to SKF and according to Schaeffler. In LMS Amesim the general formulation computation according to Schaeffler is one possibility which can be employed for the loss calculation. Other computation methods in LMS Amesim are the calculation according to NTN and TIMKEN, which are two other bearing manufacturers. So different calculation methods exist to calculate the bearing losses and with each method the results vary in a certain range.

2.3 Sealing ring losses

Compared to gear losses the sealing ring losses have a smaller influence on the total power loss, but can't be neglected in case of high rotational speeds. Sealing ring losses occur due to contact friction between the sealing lip and the shaft. If contactless seals are in use the losses are neglected relating to the standard ISO/TR 14179-2 [9]. Influencing factors for the calculation of the sealing ring loss are the rotational shaft speed and the diameter of the shaft. With these parameters the power loss of the

sealing can be calculated with the equation (2.37) according to the standard ISO/TR 14179-2 [10]. The calculation method is employed in KISSsoft/KISSsys and is also chosen for the LMS Amesim simulation.

$$P_{VD} = 7.69 \cdot 10^{6} \cdot d_{sh}^{2} \cdot n \tag{2.37}$$

2.4 Thermal losses

The power loss which is generated in a gearbox at certain components is converted into heat. For example, at a spur gear pair, which is one of the loss generating components, the power loss is created in the contact zone. This power loss leads to a temperature increase of the gear and the oil, which is employed for the lubrication of the gearbox. The thermal conduction, the convection and the thermal radiation are the three different types of heat transfer which exist. These types of heat transfer are explained in the following subchapters.

2.4.1 Conduction

Basically, conduction occurs in solids, liquids and gases and is a heat transfer inside a part. The energy transfer is from the higher temperature side to the lower temperature side. All elements which have a temperature coefficient can also conduct heat. The conduction is subdivided into stationary and transient heat conduction. If there is a constant heat flow and the temperature is constant at every position this is called stationary conduction. Transient conduction is the right term, if due to a constant heat flow the temperature of a body increases or decreases and the local temperature is changing dependent on the time. Equation (2.38) shows the calculation of the heat transfer rate q_x in x-direction including the thermal conductivity λ, the surface area A and the temperature gradient $d\vartheta / dx$ in x-direction. The formula (2.38) is a general one which was first stated by Fourier in 1822 and can be used for further calculations. [15] [16]

$$\frac{q_x}{A} = -\lambda \, \frac{d\vartheta}{dx} \tag{2.38}$$

2.4.2 Convection

The term convection is defined as exchange of energy between a surface and a fluid which is in contact with this surface. One type of convection is called free convection where the circulation of the fluid element is caused by the density differences due to temperature changes in a defined layer. The second type of convection is the forced convection which means that the flow of a fluid past the solid boundary layer is done with an external source like a pump or a fan. To describe the convection process by a general formulation, equation (2.39) is in use. The equation consists of the area A which is orthogonal to the flow direction, the convective heat exchange coefficient α, the temperature difference between the fluid ΔT and the convective heat flow rate q. With these terms the convective heat exchange is described. In most applications the convective heat exchange coefficient α needs to be estimated or determined by measurements. [15]

There are general factors which were gained out of empirical studies and these factors can be used for the first calculations. Concerning the area and the temperature difference, these two variables are measurable. [15]

$$\frac{q}{A} = \alpha \cdot \Delta T \tag{2.39}$$

Mechanism	α [W/m²K]
Air free convection	5-50
Air forced convection	25-250
Water forced convection	250-15000
Boiling water	2500-25000
Condensing water vapour	5000-100000

Table 2-1: Convective heat transfer coefficient approximate values [15]

In Table 2-1 approximate values for the convective heat exchange coefficient are shown. These values are averaged ones and can be used for the calculation of the convective heat flow rate. The values have a wide range and can vary depending on the certain application.

2.4.3 Radiation

The heat transfer through radiation differs from the conductive and convective heat transfer because no backing medium is needed to transfer energy from a body to the surrounding. Concerning conductive and convective heat exchange a medium is necessary to transfer energy from a body to the other or from a body to a fluid. By means of heat exchange through radiation no medium is required and therefore the process of heat exchange is possible in a vacuum as well. With equation (2.40) the calculation of the radiation of a body is described and the radiation energy is calculated with the emitting surface area A, the Stefan-Boltzmann constant σ and the absolute Temperature T. The Stefan-Boltzmann constant is equal to $5.676 \cdot 10^{-8}$ [W / m^{2}K^4] and was named after Stefan who generated this value out of experimental observations and Boltzmann because he derived the equation (2.40) theoretically. [15]

$$\frac{q}{A} = \sigma \cdot T^4 \tag{2.40}$$

2.5 Heating of a gearbox

The heat which is generated in a gearbox due to friction losses is dissipated via conduction, convection and radiation. For the cooling of the gearbox conventional air cooling or a separate oil cooling circuit is employed. During the operation of a gearbox the temperature rises to a certain level at which the temperature stays nearly constant and this level is called the constant mean gearbox temperature. This mean gearbox temperature is interesting for the design of gearboxes. If the mean transmission temperature is in a range that negatively affects the aging of the gearbox oil, this also affects the lifetime of different components, such as roller bearings and radial shaft seals. The difficulty of the development of a gearbox is to reach the thermal performance defined in theory also in practice. A transmission with gears, bearings and sealing rings is a complex model because a lot of influencing factors have an impact on the calculation results and thus in some cases only approximation methods are used. A gearbox used in a vehicle is air cooled in most cases and therefore a layer of dirt decreases the convective heat exchange of the transmission housing with the surrounding. There are other factors which can change the heat transfer in practice and it is difficult to consider them in the early development stage. [17]

The power loss generated in a gearbox is equal to the dissipated heat flow in a quasi-stationary state and is displayed in equation (2.41).

$$P_V = \dot{Q} \tag{2.41}$$

Equation (2.42) shows the different heat flow terms which are summed up and result in the dissipated heat flow. [17]

$$\dot{Q} = \dot{Q}_K + \dot{Q}_S + \dot{Q}_F + \dot{Q}_W + \dot{Q}_U \tag{2.42}$$

The different heat flow terms are described as follows [17]:

$\dot{Q}_K$ … Heat flow through convection
$\dot{Q}_S$ … Heat flow due to radiation
$\dot{Q}_F$ … Heat flow due to conduction through the mounting of the gearbox
$\dot{Q}_W$ … Heat flow due to conduction through the rotating parts
$\dot{Q}_U$ … Heat flow due to cooling system

One important part for the calculation of the gearbox temperature is the heat transfer to the surrounding air through convection and radiation. Equation (2.43) shows the heat transfer of the gearbox to the ambience. The heat transmission coefficient k for a plane plate is described with the equation (2.44) and consists of the heat transfer by convection on the inner and outer side of the plate and the heat conduction through the plate. For the convection from the oil to the gearbox housing the coefficient α_i is approximately between 150 and 300 W/(m²K). The outer convection coefficient α_a which is employed for the heat transfer from the housing to the ambience is approximately 20 W/(m²K) and can be neglected in case of natural air stream. At a forced air flow an external convection coefficient α_a of up to 50 W/(m²K) should be considered. [17]

$$\dot{Q}_G = \dot{Q}_K + \dot{Q}_S = k \cdot A \cdot \left(\vartheta_O - \vartheta_R\right) \tag{2.43}$$

$$k = \frac{1}{\frac{1}{\alpha_i} + \frac{s}{\lambda} + \frac{1}{\alpha_a}} \tag{2.44}$$

2.6 Gearbox efficiency

The total efficiency of a gearbox is calculated with the total losses of a gearbox and the propulsion power P_a. In equation (2.45) the computation of the transmission total efficiency is shown. It is possible to determine the efficiency for the single loss terms as well. With equation (2.46) the efficiency of the toothing is computed with the total gear losses and the propulsion power. [5]

$$\eta_G = 1 - \frac{P_V}{P_a} \tag{2.45}$$

$$\eta_Z = 1 - \frac{P_{VZ} + P_{VZ0}}{P_a} \tag{2.46}$$

3 Gearbox simulation

In this chapter the measurement on the test bench and the efficiency simulations of the eRAD245o gearbox with the selected software tools are described in detail. Furthermore, the results of both simulations are compared with each other and in each case the simulation is compared with the measurement results. During the calculation of the losses for different load points advantages and disadvantages of both programmes have appeared and these facts are mentioned in chapter 3.4.5.

3.1 Gearbox data

The eRAD245o drivetrain was developed at the ECS and some prototypes were produced to generate measurement results at test benches. This drivetrain consists of a three-shaft gearbox with two stages which is employed to transfer the mechanical power of the electric machine to the wheels with a gearbox ratio of 8.895. The maximum rotational speed of the electric machine is 16500 rpm and the maximum power is 245 kW. The rotor shaft of the electric machine is connected to the gearbox input shaft via an involute spline. Due to cooling purpose the rotor shaft and the input shaft are hollow. The torque at the output gear wheel is distributed via the differential gear unit to the output shaft and to the drive shaft and therefore to the wheels.

Figure 3-1 shows the cross section of the eRAD245o gearbox assembly drawing including the rotor shaft of the electric machine. In order to get a better overview of the gearbox some components like the gearbox cover and the system housing are hidden to focus on the main parts which are relevant for the simulation model.

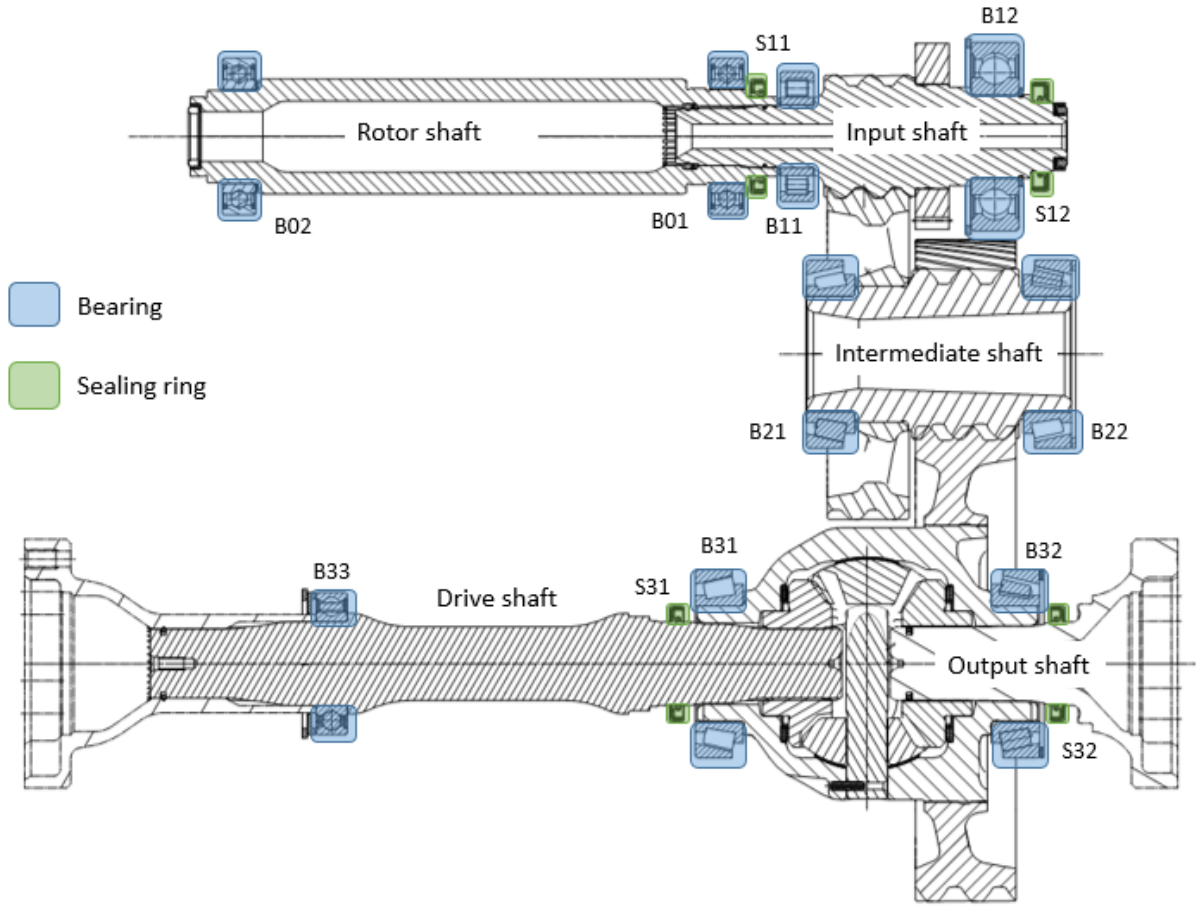

Figure 3-1: Cross-sectional drawing of the gearbox

In Figure 3-1 the positioning and naming of the different shafts, bearings and sealing rings is shown as well. The designation of the different components is used in further descriptions of the parts itself and in the LMS Amesim simulation model.

The gear parameters of the transmission, which are employed for the test and simulation runs, are shown in the following Table 3-1.The input shaft is a pinion shaft with the parameters of gear one. This first gear transmits the torque to the intermediate shaft gear which is gear two of the first spur gear stage. With the second spur gear stage the torque is transmitted to the differential gear unit and thereafter split up to the output shaft and the drive shaft. All parameters in the table below were predefined and are not changed for the simulation runs.

Parameter	Unit	Spur gear 1		Spur gear 2	
		Gear 1	Gear 2	Gear 1	Gear 2
Number of teeth	-	27	79	25	76
Normal module m_n	mm	1.86	1.86	2.72	2.72
Normal pressure angle α_n	°	18	18	18	18
Helix angle β	°	18	18	21.5	21.5
Hand of helix	-	right	left	left	right
Width of tooth face b	mm	42	39	51	48
Root diameter	mm	48.516	148.73	66.75	213.354
Working pitch diameter	mm	52.804	154.502	73.085	227.226
Tip diameter	mm	58.411	158.08	81.565	222.18
Center distance	mm	90		148	

Table 3-1: Gear parameters

In Table 3-2 and Table 3-3 the simulation relevant data of the different bearings used in the gearbox are displayed. The bearings of the rotor shaft and the drive shaft are grease lubricated bearings and hence sealed. Concerning the designation of the rotor shaft bearings the star * means that the sealing of the bearing is friction optimized. All other bearings used on the different shafts are oil lubricated with the oil used in the gearbox. The sealing ring S11 is used to seal the gearbox to the housing of the electric machine, because in the housing of the electric machine no oil is required.

Parameter	Unit	Rotor shaft		Input shaft	
		B01	B02	B11	B12
Bearing designation	-	Groove ball bearing 6009-2RS*	Groove ball bearing 6009-2RS*	Cylindrical roller bearing NU206	Groove ball bearing 6308
Inner diameter	mm	45	45	30	40
Outer diameter	mm	75	75	62	90
Width	mm	16	16	16	23
Static load rating C_0	kN	14.6	14.6	37.5	25
Dynamic load rating C_{dyn}	kN	22.1	22.1	46	45.5

Table 3-2: Rotor and input shaft bearing parameters

Parameter	Unit	Intermediate shaft Output shaft		Drive shaft
		B21, B22	B31, B32	B31
Bearing designation	-	Tapered roller bearing 32011	Tapered roller bearing 32011	Groove ball bearing 6008-2RS-C4
Inner diameter	mm	55	55	40
Outer diameter	mm	90	90	68
Width	mm	23	23	15
Static load rating C_0	kN	118	118	11.5
Dynamic load rating C_{dyn}	kN	96	96	17.8

Table 3-3: Intermediate, Output and Drive shaft bearing data

The gearbox is lubricated with a special oil and therefore at the shaft end of the input and output shaft radial sealing rings are needed to keep the oil in the gearbox housing. In Table 3-4 the different radial sealing ring types are displayed and the relevant parameters are mentioned in that table. On the input shaft are two different types of radial shaft sealing rings in use. The radial sealing rings used on the output shaft are both of the same type.

Parameter	Unit	Input shaft		Output shaft	
		S01	S02	S31	S32
Design type	-	BAUM3X7	BAUM2SLX7	BAUM3SLX7	BAUM3SLX7
Inner diameter	mm	38	34	40	40
Outer diameter	mm	55	52	55	55
Width	mm	7	8	7	7
Material	-	75 FKM 585	75 FKM 585	75 FPM 585	75 FPM 585

Table 3-4: Radial shaft sealing ring parameters

For the lubrication of the gearbox the lubricating oil BOT350M3 is used and the relevant properties of that oil are mentioned in Table 3-5. The fill capacity of the investigated transmission is 1200 ml with a deviation of ± 60 ml. The grease lubricated bearings make use of the RHENUS NORLITH STM3 grease. This grease has different specific properties compared to the lubricating oil and these properties are shown in the table below.

Parameter	Unit	Physical properties	
Designation	-	BOT350M3	RHENUS NORLITH STM3
Kinematic viscosity at 40 °C	mm²/s	32	80
Kinematic viscosity at 100 °C	mm²/s	6.3	10
Density at 15 °C	kg/m³	852	950
Dynamic viscosity at 40 °C	mPas	26.6	74.4
Specific heat capacity at 40 °C	kJ/kgK	1.991	1.991
Heat conduction at 15 °C	W/mK	0.1368	0.1227
Piezo viscosity coefficient at 40 °C	1/bar	$2.4 \cdot 10^{-3}$	$2.4 \cdot 10^{-3}$

Table 3-5: Oil and grease properties

3.2 Measurements on the test bench

The gearbox was tested on a test bench to evaluate the efficiency at different load points and two temperatures. The results of the test bench tests are compared with the simulation results. In the following subchapters the setup of the test bench and the results of the measurement runs are stated and described.

3.2.1 Test bench setup

The test bench setup consisted of two shafts and two electric machines, which are test bench electric machines. With these test bench electric machines, it is possible to perform load spectrum runs. The electric machine of the eRAD245o is not used for the test runs. One electric machine provides the input power and the other electric machine was used to regulate the output speed. The test bench setup is shown in Figure 3-2 and the blue box in the image displays the gearbox as it is shown in the cross-sectional drawing in Figure 3-1. At the output side of the gearbox is the differential gear unit which transmits the torque to the left and right drive shaft. Due to the setup with two shafts the differential was locked and the full torque was transmitted to one side where the electric machine was placed. Two torque measurement flanges were in use, one at the drive side and one at the output side. With

the measured torque at the two shafts it is possible to calculate the gearbox power loss during the test runs. For the test runs a load point spectrum was defined by the testing department which includes different variations of input torques and output shaft rotational speeds.

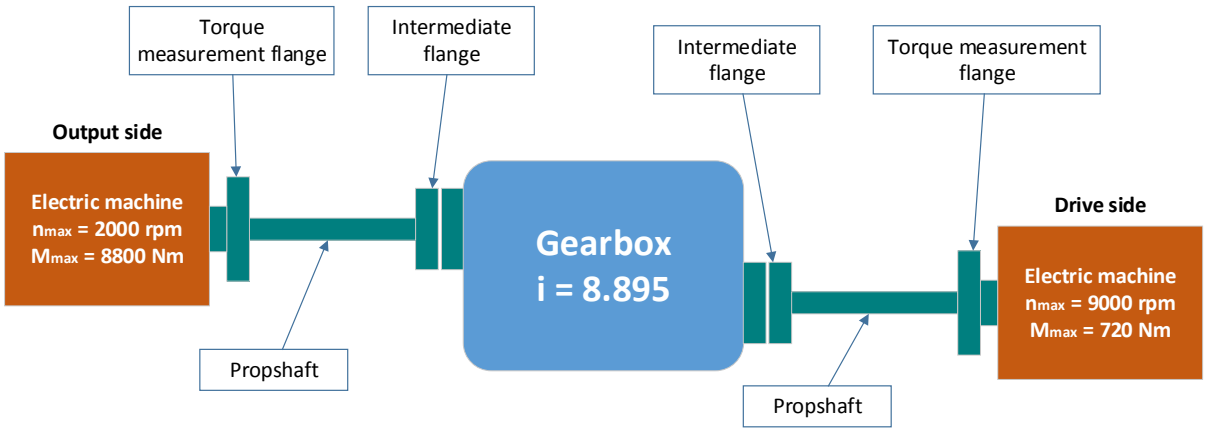

Figure 3-2: Test bench setup

3.2.2 Experimental results

With the test results, the power loss for each load point of the spectrum is calculated. The power loss is defined as the power difference between the drive side and the output side. The tables bellow show the results of these calculations for every load point. To get information about the temperature dependency of the power losses, the gearbox was tested at two different temperatures. The gearbox power losses at 40 °C is shown in Table 3-6 and the losses at 80 °C are displayed in Table 3-7.

		Output shaft speed [rpm]				
	P_{loss} [W]	**110**	**186**	**315**	**532**	**900**
Output shaft torque [Nm]	**50**	58	142	315	661	1652
	97	63	144	315	624	1421
	189	77	165	337	643	1421
	367	108	212	408	741	1527
	714	177	313	560	971	1840
	1388	333	547	906	1465	2535
	2700	678	1073	1679	2577	

Table 3-6: Total power losses at 40 °C oil temperature

		Output shaft speed [rpm]				
	P_{loss} [W]	**110**	**186**	**315**	**532**	**900**
Output shaft torque [Nm]	**50**	34	66	136	311	869
	97	44	79	157	345	914
	189	64	107	196	403	980
	367	110	174	286	523	1142
	714	210	310	468	762	1487
	1388	406	596	842	1293	2220
	2700	833	1188	1688	2504	

Table 3-7: Total power losses at 80 °C oil temperature

The power loss maps display the power loss at the certain load points. To display the efficiency of the gearbox for the whole spectrum an efficiency diagram is used. In Figure 3-3 the efficiency map of the gearbox at 40 °C oil temperature is displayed. The second tested oil temperature was 80 °C and the efficiency map for that temperature is shown in Figure 3-4. In the two figures the output shaft torque is on the y-axis and the output shaft speed is on the x-axis. The efficiency of the gearbox is displayed in a span from 90 to 99 percent. The gearbox efficiency is approximately 90% at low output shaft torque over the whole output shaft speed range.

The power loss of the gearbox rises with an increasing output shaft torque. Contrary to that the gearbox efficiency increases with increasing torque. The reason for that is the ratio of the power loss regarding the input power. With a decreasing share of the power loss in comparison with the input power the efficiency of the gearbox increases. The gearbox efficiency at 80 °C oil temperature, especially at low output torque is higher compared to the 40 °C gearbox temperature over the whole rotational speed range.

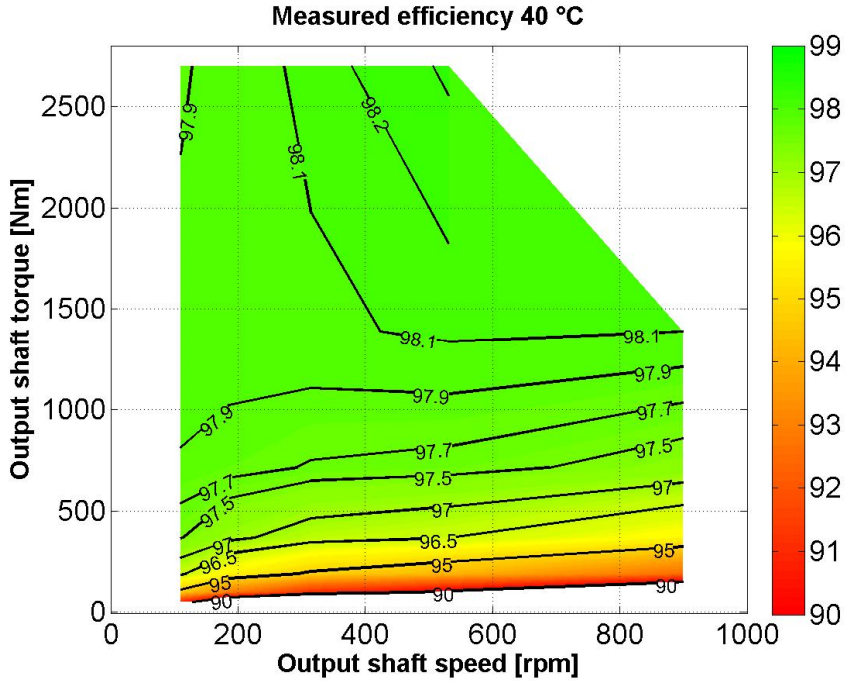

Figure 3-3: Efficiency map of measured gearbox at 40 °C

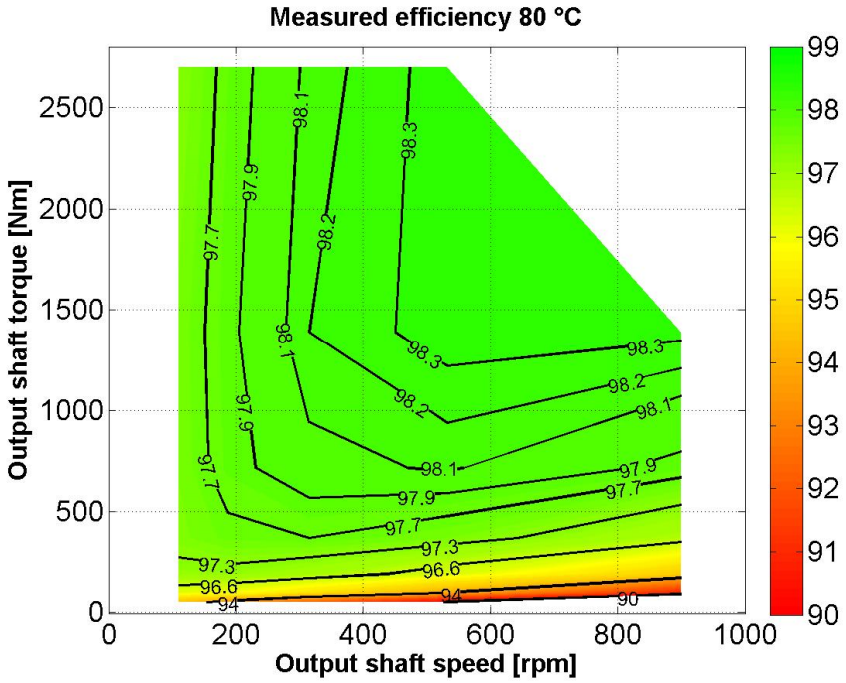

Figure 3-4: Efficiency map of measured gearbox at 80 °C

3.3 KISSsoft/KISSsys power loss calculation

In this chapter the loss calculation with the software KISSsoft/KISSsys is described. KISSsoft/KISSsys is a software applied for the configuration, calculation and optimization of machine elements. The software KISSsoft is the basic software including the individual modules, which enables the computation of e.g. gears, bearings, shaft-hub connections and press fits. Hence, this software can be used for the calculation of any mechanical components. The software KISSsys enables the automated computation of entire systems e.g. the setup of complete gearbox calculation models. It is possible to compute the losses of a gearbox that considers the housing stiffness to gain realistic results. In this thesis the KISSsys package is used for the gearbox loss computation and the software KISSsoft is used for the modulation of the different shafts, bearings and gears. [18]

3.3.1 Setup of the simulation model

The setup of the gearbox simulation model without the drive shaft bearing was done by a member of the analytical calculation powertrain team at the ECS and first simulations were carried out. In order to calculate the losses of the gearbox as it was tested on the test bench, it is necessary to add the drive shaft bearing B33 at the output side of the gearbox. There is no load acting on that bearing, but the rotational speed dependent losses of that bearing are considered.

In Figure 3-5 the configuration of the KISSsoft/KISSsys model is displayed in an isometric view. The sealing rings can't be displayed in the software. With a rotational constraint between the rotor shaft and the input shaft the power created by the electric machine is transmitted to the gearbox. The gear parameters and type of bearings are defined as mentioned in the chapter of the gearbox data.

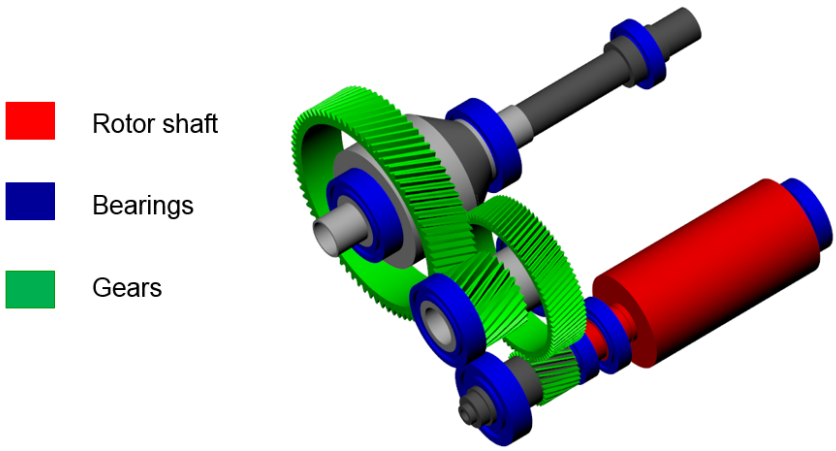

Figure 3-5: KISSsoft/KISSsys simulation model

In KISSsoft/KISSsys it is possible to choose different types of calculation methods and in terms of power loss this is dependent on the specific machine element. For the power loss calculation of the bearings the SKF and Schaeffler method can be chosen. Due to lessons learned in former ECS projects the Schaeffler calculation method is at ECS currently seen as more accurate than the SKF method and is therefore used for the simulation of the bearing losses. The gear power losses are separated into meshing losses which are calculated according to Niemann and into churning losses which are calculated referring to the ISO/TR 14179. It is not possible to change the computation method of the gear losses. For the calculation of the sealing ring losses it is possible to choose different methods. In order to receive comparable results, the computation method according to ISO/TR 14179-2 is used for the sealing ring power loss computation. In chapter 2 the power loss computation methods which are used in the KISSsoft/KISSsys simulation are explained in detail.

The gearbox has an oil bath lubrication with a predefined oil volume, which is considered in the simulation model with the height of the oil in the housing. If a shaft has two equal bearings the setting of the oil level must be done only ones. If different bearings are mounted at one shaft, such as the bearings at the input shaft of the eRAD245o gearbox, it is initially necessary to define the oil level for one bearing and then perform the efficiency simulation. Then this process must be repeated for the second bearing with the related oil level. After the simulation the power loss of the bearings with the appropriate oil level are summed up to get the complete bearing losses of the gearbox. This procedure is done to compute the total bearing losses with the KISSsoft/KISSsys software tool in a proper way.

The testing department defined the load spectrum and this spectrum is also used for the power loss calculation in KISSsoft/KISSsys. With the implemented spectrum, KISSsoft/KISSsys calculated the losses for every single load point. In the following chapter the results of the KISSsoft/KISSsys simulation are shown.

3.3.2 Results of simulation

The simulations are performed with a gearbox oil temperature of 40 °C and 80 °C. In Table 3-8 and Table 3-9 the total power loss of each load point is shown. To get the total power loss for every load point the part losses of the transmission are summed up in relation to the data points. The output shaft speed and output shaft torque are the data points at which the losses are related to.

		Output shaft speed [rpm]				
	P_{loss} [W]	**110**	**186**	**315**	**532**	**900**
Output shaft torque [Nm]	**50**	70	131	258	536	1213
	97	84	152	290	584	1287
	189	110	193	352	679	1433
	367	163	273	475	867	1721
	714	271	438	729	1258	2323
	1388	520	822	1320	2169	3729
	2700	1099	1711	2689	4274	

Table 3-8: KISSsoft/KISSsys power loss results at 40 °C

		Output shaft speed [rpm]				
	P_{loss} [W]	**110**	**186**	**315**	**532**	**900**
Output shaft torque [Nm]	**50**	47	82	149	285	584
	97	62	106	186	342	672
	189	93	153	258	453	843
	367	152	244	399	670	1179
	714	269	424	676	1096	1838
	1388	533	830	1301	2058	3322
	2700	1145	1768	2745	4277	

Table 3-9: KISSsoft/KISSsys power loss results at 80 °C

The two tables show the trend that the total power loss rises with an ascending output shaft torque and output shaft speed. A maximum torque loss is reached at the maximum output shaft torque and at an output shaft speed of 532 rpm.

Percentage of single losses

The total power loss of the simulation is split up into the single losses. To display the loss distribution in an appropriate way the mean value over the whole spectrum for every loss term is calculated. In Figure 3-6 the share of gear, bearing, sealing ring and paddling losses are plotted. The percentages of the different losses are mentioned as well. Over the whole load spectrum, the mean value of the gear losses has the highest share and the mean value of the bearing losses has the second largest share. Although the paddling losses are part of the gear losses and hence belong to the non-load dependent gear losses, they are mentioned separately and have a small share in the pie chart. The mean total power loss is calculated over the entire load spectrum for the two different oil temperatures and is displayed in Figure 3-6.

At lower gearbox temperatures the bearing and paddling losses have a higher share. One reason for the higher share is the kinematic viscosity of the oil which is larger at lower temperatures. The non-load dependent gear losses are dependent of the oil properties and therefore a higher share at lower temperatures is the consequence.

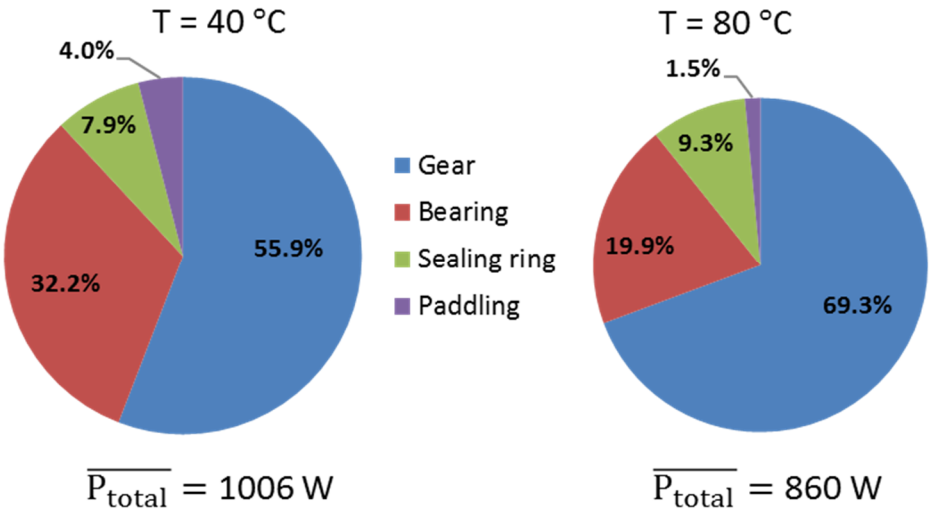

Figure 3-6: KISSsoft/KISSsys percentage of single losses at 40 °C and 80 °C oil temperature

3.3.3 Comparison of KISSsoft/KISSsys results with measurement

The KISSsoft/KISSsys simulation model results are compared with the results of the test bench measurements. In Table 3-10 and Table 3-11 the deviation of the KISSsoft/KISSsys results in comparison with the test bench results are displayed. For the calculation of the power loss deviation equation (3.1) is used and the deviation is shown as percentage with the test results as base in the tables below. If the deviation is negative the total power loss of the KISSsoft/KISSsys simulation is larger than the power loss measured at the test bench and with a positive deviation is vice versa. This positive and negative deviation condition is shown in equation (3.2).

$$\Delta P_{loss} = \left(1 - \frac{P_{loss,KISSsys}}{P_{loss,measurement}}\right) \cdot 100 \tag{3.1}$$

$$\begin{aligned} Positive\ (+) &: P_{loss,measuement} > P_{loss,KISSsys} \\ Negative(-) &: P_{loss,measuement} < P_{loss,KISSsys} \end{aligned} \tag{3.2}$$

		Output shaft speed [rpm]				
	ΔP_{loss}	**110**	**186**	**315**	**532**	**900**
Output shaft torque [Nm]	**50**	-20.8%	7.7%	18.1%	18.9%	26.5%
	97	-32.8%	-5.5%	8.0%	6.4%	9.4%
	189	-44.1%	-17.2%	-4.2%	-5.6%	-0.8%
	367	-51.4%	-29.0%	-16.4%	-17.0%	-12.7%
	714	-52.9%	-39.9%	-30.2%	-29.6%	-26.2%
	1388	-56.4%	-50.4%	-45.6%	-48.0%	-47.1%
	2700	-62.1%	-59.5%	-60.1%	-65.8%	

Table 3-10: Deviation of KISSsoft/KISSsys from measurement results at 40 °C

		Output shaft speed [rpm]				
	ΔP_{loss}	**110**	**186**	**315**	**532**	**900**
Output shaft torque [Nm]	**50**	-37.9%	-25.3%	-9.8%	8.6%	32.8%
	97	-41.7%	-34.9%	-18.4%	1.0%	26.5%
	189	-46.2%	-43.3%	-32.1%	-12.5%	14.0%
	367	-38.2%	-40.5%	-39.7%	-28.2%	-3.2%
	714	-28.1%	-36.5%	-44.4%	-43.9%	-23.6%
	1388	-31.4%	-39.3%	-54.5%	-59.2%	-49.7%
	2700	-37.6%	-48.9%	-62.6%	-70.8%	

Table 3-11: Deviation of KISSsoft/KISSsys from measurement results at 80 °C

The deviations of the KISSsoft/KISSsys from the measurement results display the tendency of an increasing deviation with ascending torque and rotational speed. If the red cell colour darkens, the KISSsoft/KISSsys results are larger than the measured ones. With increasing output shaft speed the calculated power loss is getting closer to the tested results. At high rotational speeds and low axle torques the KISSsoft/KISSsys power losses are smaller than the tested ones, as displayed in tables with the green cell colour. Regarding different oil temperatures the deviation is not the same. The deviation at high torque is almost in the same range. At the 40 °C simulation a mean deviation of all load points of 30.2% and at the 80 °C simulation of 34.3% is computed.

3.4 LMS Amesim power loss calculation

In this chapter the calculation of the power losses with the software LMS Amesim is explained in detail. To get a better overview the used software is characterized in the next sections.

For the computation of the power losses in the transmission, the simulation of the thermal and the overall vehicle model the software LMS Imagine.Lab Amesim version 15.1 is in use. The software is designated in this thesis as LMS Amesim or only Amesim. With this software it is possible to set up, simulate and analyse physical multi-domain systems.

LMS Amesim provides libraries for different application segments like drive systems, mechanical systems or fluid systems. Each library consists of different items which can be used for the selected simulation. The items are kind of a physical component, which has several input and output ports and enables the connection of the items with each other if it is physically possible. That means it allows the connection of items that exchange physical quantities in a proper way like a spring damper system. On the one hand the items are connected and on the other hand the items calculate the output values with time based analytical equations which are implemented in the models. If all for the simulation relevant components are connected, an entire simulation model is formed. [19]

All items of the different libraries are explained in the LMS Amesim help the so called LMS Amehelp. The formulas used by LMS Amesim for the calculation are described in the next chapter and are taken from the LMS Amehelp. [9]

3.4.1 Structure of the simulation model

With LMS Amesim it is possible to modulate a gearbox with the different shafts and the corresponding parts. In the drive library different types of gearbox models are available, like a 5-speed manual gearbox or an automatic gearbox. This kind of gearbox model is described in detail in chapter 4.4, where it is applied in the thermal simulation model. For the determination of the different loss parts a model with gears, bearings and sealing rings is defined. Such a simulation model represents the loss

relevant components of the entire gearbox and these components are used in the power loss computation.

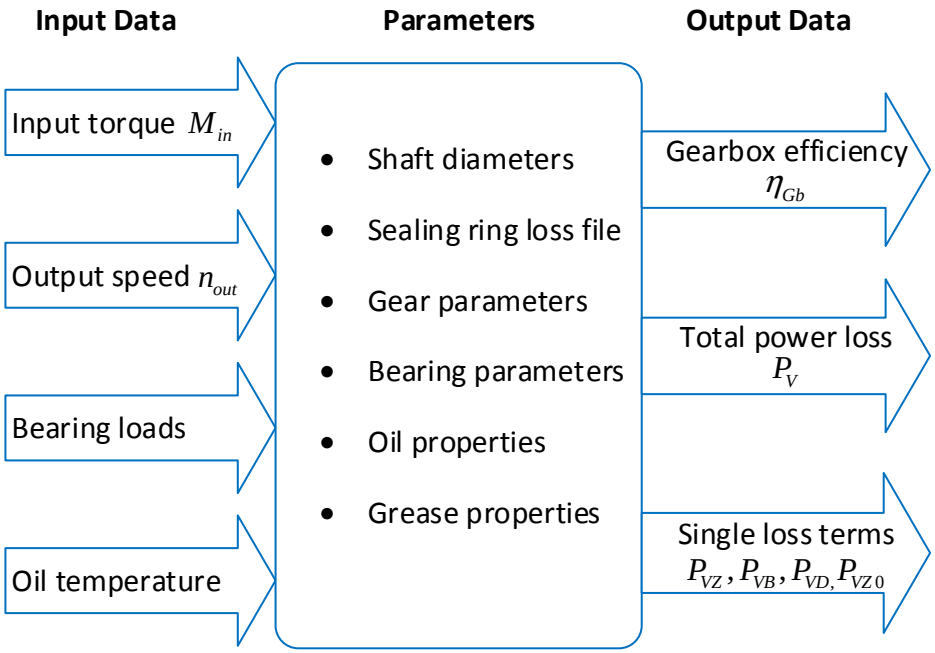

Figure 3-7: Input and Output data of the LMS Amesim simulation

The important parameters, input and output data of the load spectrum simulation are shown in Figure 3-7. It describes summarized, which boundary conditions are required for the simulation. The input torque and output speed are two quantities that are defined to start a simulation. Furthermore, the bearing loads, oil temperature and all other required parameters are implemented in the simulation model. As a result, the simulation provides the total loss and the shares of the individual losses. From these results, the gearbox efficiency for each load point is calculated.

The LMS Amesim simulation model consists of the following main components:

- Gears
- Bearings with load ports
- Sealing rings
- Fluid properties
- Clutches
- Sensors and Converters
- Signal elements

In Figure 3-9 the simulation model with the relevant items is displayed. It shows how the elements relate to each other and which signal elements are set at the input and output ports. The bearings have the same denotation as in Figure 3-1 and are positioned in the same way.

Description of the simulation model

An electric machine has the characteristic to operate in motor and generator mode. This means that in motor mode the torque is applied on the input shaft and the rotational speed is defined on the output shaft. For the determination of the contact force of the gears in the motor mode the first gear on the input shaft is the driving gear and the second gear of the first stage is the driven gear. The same

is valid for the second spur gear stage. When the electric machine is in generator mode the torque direction is inversed and therefore the drive gears become driven gears and vice versa. During the generator mode the torque is applied on the output shaft and the rotational speed is defined on the input shaft. To consider the motor and generator mode in the simulation model, two clutches on the input side and two clutches on the output side are applied. If the gearbox is in motor mode the clutch CL2 on the input side is closed and clutch CL3 on the output shaft is closed as well. The same is done with the two other clutches during the generator mode. A logical query is used to detect the two different modes and operate the clutches in the correct way.

One part of the present thesis is the automation of the simulation run in LMS Amesim. To make this possible the software tool Microsoft Excel is employed as an interaction program. In the LMS Amehelp the simulation scripting of visual basic and the required syntax for the data exchange from LMS Amesim to Excel are described in detail. With the use of Excel the load spectrum simulation is done automatically. By use of the visual basic script file the simulation relevant data is transferred to the LMS Amesim model and after one simulation run is completed, the results of the simulation are published in the Excel file. Hence, the simulation model and the evaluation file are set up in a way that the computation of the power loss map is possible.

Gear model

In Figure 3-8 the icon of the gear model is displayed and this model is used for every gear wheel of the transmission. The gear model is a three-port model that includes two rotary ports and one linear port. For each gear wheel it is necessary to implement the associated gear parameters which are mentioned in chapter 3.1. With these parameters the load and non-load dependent losses are calculated. To consider the paddling losses the immersed gear height is inserted in the gear parameters. In case of the eRAD245o gearbox only the gear wheel at the output shaft is immersed into the oil bath. All other gears are lubricated with the splashing oil in the gearbox due to the churning of the large output gear at the differential gear unit. The oil viscosity is temperature dependent and is one part of the gear loss computation equation, hence the gear losses are also temperature dependent. It is possible to calculate other gear related parameters with the gear model like the contact stiffness of the gear wheel, but these computations are not relevant for the determination of the power loss.

Figure 3-8: Gear wheel model

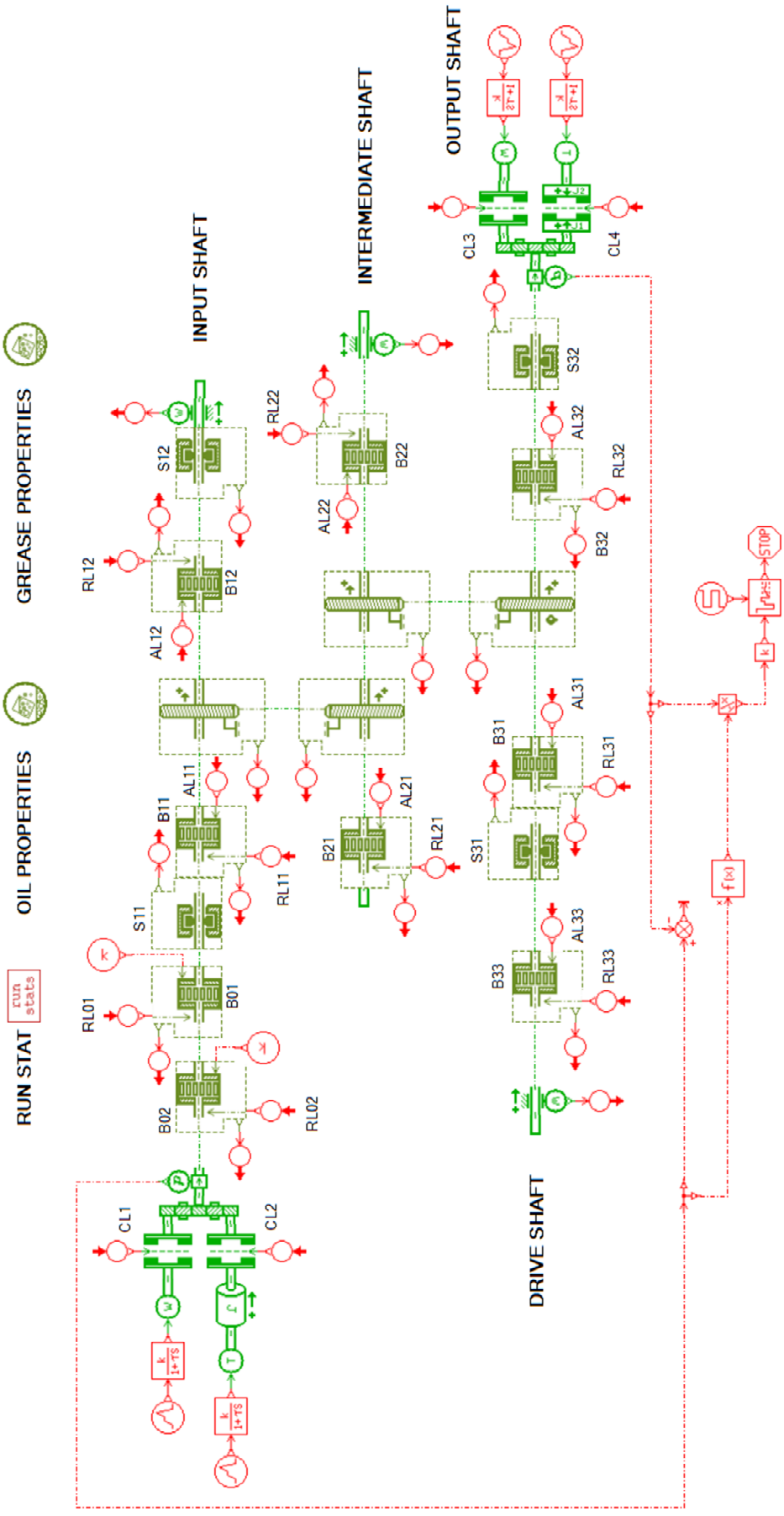

Figure 3-9: LMS Amesim simulation model

Bearing model with load ports

The model used to calculate the bearing losses is shown in Figure 3-10. To apply forces to the bearing, port one and two are used as input channels. At port one the radial load and at port two the axial bearing load is applied. The radial and axial bearing forces results out of the calculation of the gear forces and the geometrical situation on a shaft. It is possible to calculate the bearing forces in the LMS Amesim simulation as well, but for a better comparison of the power loss calculation results, the radial and axial bearing forces are used from the KISSsoft/KISSsys computation. In the KISSsoft model all geometry constraints and all bearing specific parameters e.g. the preload and the bearing stiffness are defined to calculate the bearing forces in a correct way. Concerning the bearing power loss computation the bearing force and the oil viscosity are the two temperature dependent components. The KISSsoft bearing force calculation considers the change of the preload dependent on the bearing temperature. The KISSsoft/KISSsys computed bearing forces are set in the global parameters of the simulation model. In LMS Amesim the forces are delivered to the respective bearings via transmitters and receivers. The transmitters and receivers are signal elements which are used to transfer signals from one submodel to another without any visible connection in the gearbox model. Normally the bearing and gear models relate to each other by connecting them, but for a better overview the models are not linked directly by a line. For a better process understanding, the steps required to read in the bearing forces are explained in terms of the first bearing on the intermediate shaft, the so-called bearing B21. In the global parameters the axial load AL21 and the radial load RL21 are defined and the forces are set referring to the actual load condition of the gearbox. Global parameters have the property that the variable names defined in the parameters are used as variables in the simulation model. The variable name is set in a defined signal element which is called constant and then the bearing load is transferred via a transmitter and a receiver to the bearing B21. That is the way the bearing force calculated in KISSsoft/KISSsys is set in the LMS Amesim bearing model.

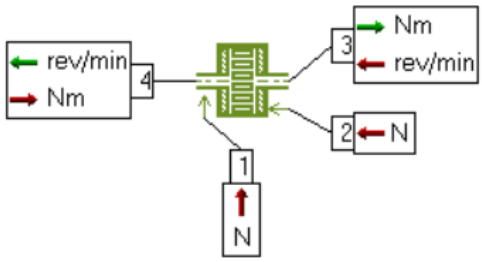

Figure 3-10: Bearing model with in-and output ports

In Figure 3-10 two other ports are shown which are used to transmit the torque and rotational speed of the shaft. Regarding the loss calculation method it is necessary to choose the standard formulation in the parameters of the model, because then the loss calculation in done in the way as it is described in chapter 2.2. Equation (3.3) and (3.4) represents the calculation of the equivalent dynamic load P_1. This calculated load is dependent on the ratio between the axial and radial bearing force.

$$P_1 = X_1 \cdot F_r + Y_1 \cdot F_a \quad \text{when} \quad \frac{F_a}{F_r} \leq e \tag{3.3}$$

$$P_1 = X_2 \cdot F_r + Y_2 \cdot F_a \quad \text{when} \quad \frac{F_a}{F_r} > e \tag{3.4}$$

The variables X_1, X_2 are radial load factors and Y_1, Y_2 are axial load factors. In Figure 2-2 on page 11 a table for the P_1 calculation is shown. To calculate the equivalent load according to the calculation method by Schaeffler, the values of the radial and axial load factors are chosen as it is displayed in the table. For the different bearing types, the value for X_1, X_2 and Y_1, Y_2 varies, which is considered in the

parameters of the bearing model. When calculating the equivalent bearing load for tapered roller bearings, it should be observed that the bearing specific factor Y is not mixed up with the load factors Y_1, Y_2. For all other bearing types, the values of the load factors are predefined.

Sealing ring model

In Figure 3-11 the sealing ring model with the input and output parameters is displayed. A radial shaft sealing ring is not a contactless sealing and therefore generates a torque loss due to the contact of the sealing ring with a rotating shaft. It is possible to choose the calculation with a constant torque loss or set a torque loss table as a function of the rotational speed and the shaft diameter. For the calculation of the sealing ring torque loss the torque loss table is used. The rotational speed of the shaft is the input at port two and the diameter of the shaft is defined in the parameters of the model. With these two parameters it is possible to calculate the loss of various sealing rings.

Figure 3-11: Sealing ring simulation model

For the setup of the table equation (2.37) is used and transferred to calculate the torque loss.

Fluid properties

The properties of the lubricating fluid are defined with the fluid property model and this icon is shown in Figure 3-12. In the parameters of the fluid model the characteristic data which are relevant for the simulation are set. The needed characteristic data is the density, the kinematic viscosity and the piezo viscosity coefficient, which are all functions of the temperature. Additionally, the bulk modulus and the oil volume are set as a constant value in the model parameters. It is possible to define the kinematic viscosity of an oil by three reference points or with a table which includes the kinematic viscosity over a temperature range. For the simulation of the torque losses a kinematic viscosity table of the oil and the grease is used.

Figure 3-12: Fluid property symbol

The piezo viscosity coefficient, which is also called compressibility of fluids, is one parameter that is set in the parameters of the oil model. It is defined that fluids are not compressible in contrast to gases but an index exists which describes the compressibility of a fluid. One impact on the compressibility have dissolved gases that increases the compressibility of liquids. For the simulation of the gearbox the default curve is used with a compressibility of $2.4 \cdot 10^{-3}$ [1/bar] at 20 °C. [20]

Clutch model

The clutch submodel is used to control if power should be transmitted or not and this is defined by using the signal port two. In Figure 3-13 the clutch model is shown with the belonging input and output ports. When the command signal at port two is one than the clutch is closed and power is transferred. Contrary to that if the input signal at port two is zero, then the clutch is opened and no power is transmitted. In case of the power loss computation of the gearbox the clutch is required to simulate a motor and generator mode. The clutch transmits torque until the maximum Coulomb friction torque

is reached. It is necessary to set the maximum Coulomb torque in the parameters of the clutch model. For the gearbox simulation the value is set higher than the largest torque to be transmitted, because no slip is allowed during the calculation to generate representative results.

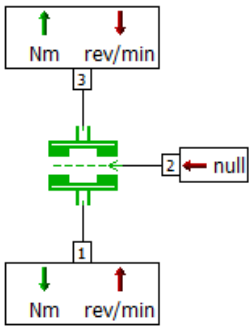

Figure 3-13: Clutch model with input and output signals

Signal elements

In Figure 3-9 some red elements are displayed, which are signal and control elements. The models of the signal and control library can be used e.g. for calculations, logical conditions, sources and tables. In the gearbox simulation model transmitters and receivers are used to transfer signals from one submodel to another. For a better overview some signals are not linked directly like the bearing load transmitters and receivers. These signal elements fulfil the same purpose of signal transformation. All other applied signal elements are functions and mathematical operations, used for post processing calculations.

Convergence condition

In the simulation run parameters the simulation time and the print interval are set. The simulation time is relevant if a simulation with a lot of different load points is done. In the case of the efficiency simulation it makes sense to define a stop condition when the simulation should end. This kind of stop condition is modelled with a convergence check. The convergence model detects the convergence of an input signal if it reaches a stable value. This model, which is shown in Figure 3-14, has two input ports, at input port three the checking signal and at input port two the reset signal is received. The mean value of the input signal is computed over a defined period set by a reset signal. Recording this mean value over a defined time period it enables the comparison with the values at the current time step. The model has one output port, where the number of converged periods are considered.

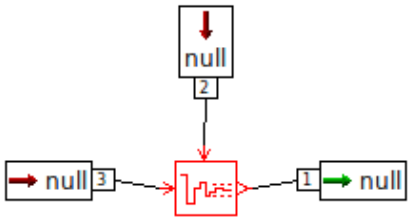

Figure 3-14: Discrete convergence check model

In combination with the stop model, which stops the simulation if the stopping condition is true, the simulation time is reduced to a minimum.

Sensors and Converters

In the mechanical library sensors are available which are used e.g. for the determination of the axle speed or axle power. The power sensors are used at the input and output shaft to compute the input and output power. Using that power signal, the power loss and the efficiency of the gearbox are calculated.

3.4.2 Results of simulation

The total power losses of the 40 °C and 80 °C oil temperature simulations are displayed in Table 3-12 and Table 3-13. In these tables the power loss is related to the output shaft torque and output shaft speed. The increase of the losses due to the rise of the output shaft torque has approximately a linear trend. For the increasing output shaft speed the total power loss also increases.

		Output shaft speed [rpm]				
	P_{loss} **[W]**	**110**	**186**	**315**	**532**	**900**
Output shaft torque [Nm]	**50**	71	130	248	487	997
	97	86	152	269	532	1057
	189	117	199	348	628	1191
	367	181	295	490	834	1480
	714	317	501	799	1288	2132
	1388	600	933	1452	2259	3552
	2700	1179	1823	2806	4288	

Table 3-12: LMS Amesim power loss map at 40 °C

		Output shaft speed [rpm]				
	P_{loss} **[W]**	**110**	**186**	**315**	**532**	**900**
Output shaft torque [Nm]	**50**	49	85	151	279	537
	97	67	111	191	337	620
	189	103	166	273	458	795
	367	177	279	443	709	1161
	714	327	509	791	1229	1926
	1388	631	979	1507	2306	3524
	2700	1250	1940	2981	4536	

Table 3-13: LMS Amesim power loss map at 80 °C

Percentage of individual losses

In Figure 3-15 the percentage of the individual losses at 40 °C and 80 °C gearbox oil temperature is displayed. The individual losses are the gear, bearing, sealing ring and paddling losses. To get the percentage over the whole load spectrum the mean value for every single loss term is divided by the total average power loss. The gear losses have the highest share referring to the two testing temperatures and referring to the whole test map. In the two pie charts it is visible that the share of the gear losses increases with the rise of the temperature. This leads to a decrease of the bearing loss share, but the paddling and sealing ring loss share stays nearly the same referring to the different temperatures. At 80 °C oil temperature the oil viscosity is lower and therefore the bearing losses decrease compared to 40 °C oil temperature. The computation of the bearing losses show that the oil viscosity is one component which is temperature dependent. With increasing temperature from 40 °C to 80 °C also the bearing prestress changes and therefore the bearing load.

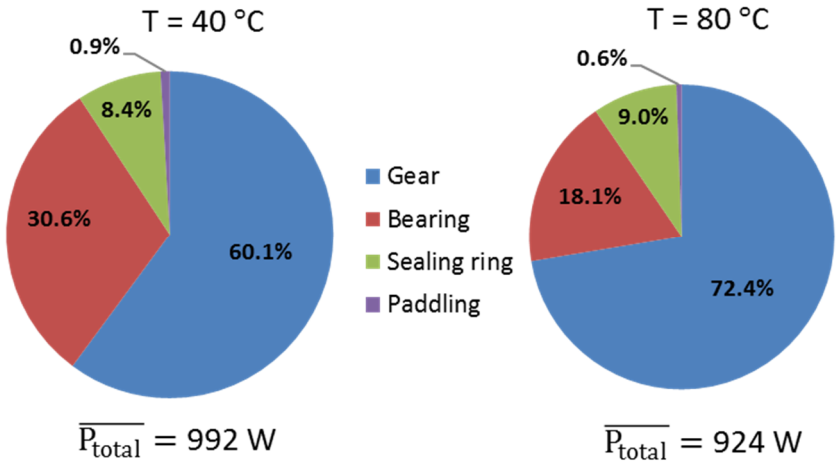

Figure 3-15: Percentage of single losses at 40 °C and 80 °C oil temperature

Single shaft bearing losses

With the results of the power loss calculation it is possible to detect the bearing losses for the single shafts and furthermore the bearing loss of each separate bearing. Therefore, the shaft and single bearing with the highest loss share are evaluated. Concerning the highest bearing loss per shaft the intermediate shaft causes the highest loss and the rotor shaft the second highest loss. Regarding the two different temperatures the power loss share of the intermediate shaft increases with the rise of the oil temperature. Contrary to that the share of the rotor shaft decreases over a temperature increase.

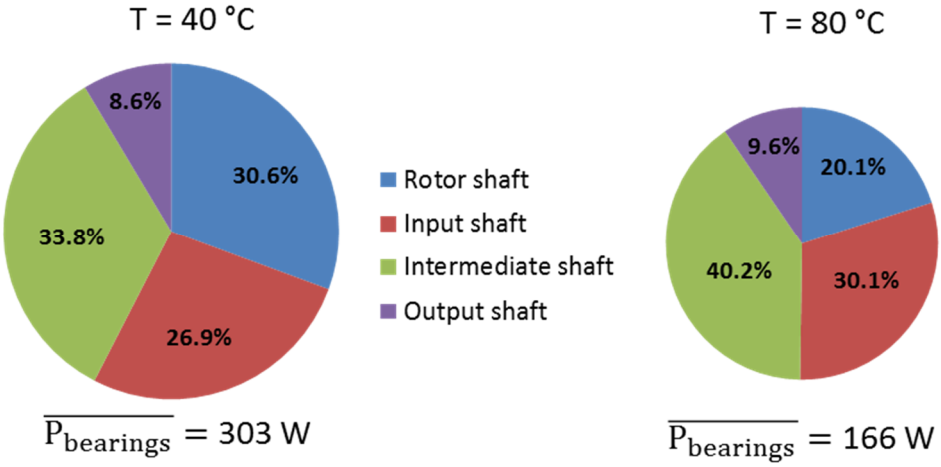

Figure 3-16: Percentage of single shaft losses at 40 °C and 80 °C oil temperature

Single bearing losses

The total bearing losses results out of the sum of the single bearing losses. In Figure 3-17 the share of the single bearing losses at 40 °C and 80 °C are displayed. These shares are the percentages of the average values for each bearing over the whole efficiency map computation. The designation of the bearings is the same as it is described in the cross-sectional drawing of the gearbox shown in Figure 3-1. At 40 °C oil temperature the ball bearing B12 at the input shaft has the highest share of the bearing power loss. The bearing B21 is the first tapered roller bearing at the intermediate shaft and produces the highest loss at 80 °C oil temperature. At that temperature the bearing B12 has the second highest loss share. The pie chart of the simulation at 80 °C shows that the loss of these two bearings, bearing B21 and B12, cause nearly half of the total bearing losses. Regarding the bearings at the output shaft,

bearing B31 and bearing B32, these two bearings only cause a small share of the total power loss. The smallest share of the bearing power losses has the drive shaft bearing B33, because at that bearing no forces act and hence only power loss due to hydraulic are considered. With the knowledge of the power loss share of each bearing, especially the bearings with a larger loss share, it is possible to take measures and try to reduce the total bearing power loss.

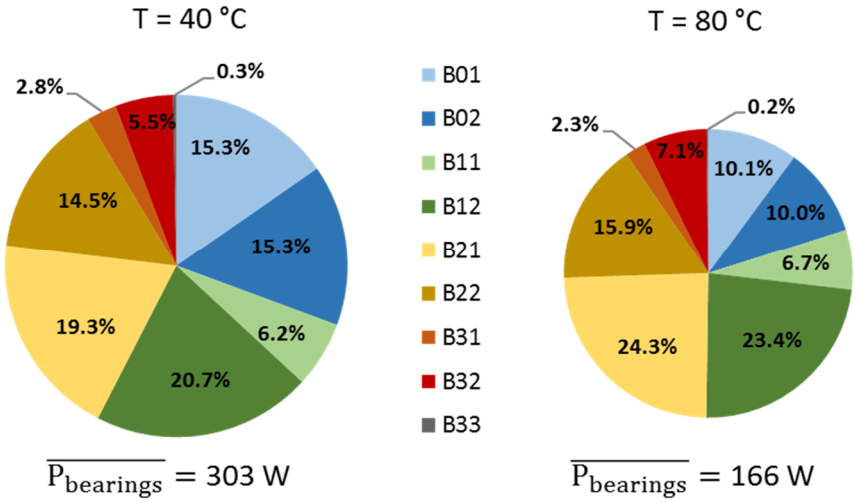

Figure 3-17: Single bearing losses at 40 °C and 80 °C oil temperature

The bearing losses are split up into load and rotational speed dependent losses. In chapter 2.2 the equations for the determination of the bearing losses are described. Concerning the rotor shaft bearings, the losses due to hydraulic are much larger as the losses due to load over the entire simulated load spectrum. The bearings of the intermediate shaft and the output shaft have the same trend referring to the loss distribution. At lower rotational speeds and higher input torques the losses due to hydraulic are lower than the load dependent losses. If the loads applied on the gearbox are low and the rotational shaft speeds are high, the losses due to hydraulic are larger than the losses due to the load. At high loads and high rotational shaft speeds the losses due to load are larger in relation to the losses due to hydraulic, but the share of the losses due to hydraulic is in a range of 20-40% of the total bearing loss. Relating to the input shaft bearings at high rotational speeds and high loads the losses due to hydraulic are larger in relation to the load dependent losses.

3.4.3 Comparison of LMS Amesim results with measurement

In this part the LMS Amesim simulation results are compared with the measurement results. The deviation of the LMS Amesim results from the testing results is given as a percentage. Under the usage of equation (3.5) the deviation is calculated and the power loss of the measurement is set as base. The deviation is positive if the power loss of the measurement is greater than the power loss of the LMS Amesim simulation. In case of a negative deviation the power loss of the simulation is greater than the power loss of the test run. These two conditions are described with equation (3.6). In Table 3-14 and Table 3-15 the deviation of the LMS Amesim simulation from the measurement results is displayed at the two different operation temperatures.

$$\Delta P_{loss} = \left(1 - \frac{P_{loss,Amesim}}{P_{loss,measurement}}\right) \cdot 100 \tag{3.5}$$

$$\begin{aligned} &Positive\ (+): P_{loss,measuement} > P_{loss,Amesim} \\ &Negative(-): P_{loss,measuement} < P_{loss,Amesim} \end{aligned} \tag{3.6}$$

		Output shaft speed [rpm]				
	ΔP_{loss}	110	186	315	532	900
Output shaft torque [Nm]	50	-22.1%	8.5%	21.3%	26.4%	39.7%
	97	-36.2%	-5.7%	14.4%	14.8%	25.6%
	189	-52.5%	-20.7%	-3.0%	2.4%	16.2%
	367	-68.1%	-39.2%	-20.2%	-12.6%	3.0%
	714	-79.0%	-59.8%	-42.6%	-32.6%	-15.9%
	1388	-80.3%	-70.7%	-60.2%	-54.2%	-40.2%
	2700	-73.8%	-70.0%	-67.1%	-66.4%	

Table 3-14: Deviation of LMS Amesim from measurement at 40 °C

		Output shaft speed [rpm]				
	ΔP_{loss}	110	186	315	532	900
Output shaft torque [Nm]	50	-43.9%	-29.1%	-11.5%	10.4%	38.3%
	97	-51.2%	-41.7%	-21.6%	2.3%	32.2%
	189	-61.6%	-55.4%	-39.7%	-13.8%	18.9%
	367	-60.1%	-60.2%	-54.9%	-35.7%	-1.6%
	714	-55.6%	-63.9%	-69.0%	-61.3%	-29.5%
	1388	-55.6%	-64.4%	-79.0%	-78.4%	-58.7%
	2700	-50.1%	-63.4%	-76.6%	-81.1%	

Table 3-15: Deviation of LMS Amesim from measurement at 80 °C

The comparison of the simulation to the measurement results show how much the simulation deviates from the test bench results. At the simulation with 40 °C gearbox temperature an overall mean deviation of 37.2% and at 80 °C simulation an overall mean deviation of 46.2% is computed. In some output shaft speed and torque ranges the deviation from the measurement reaches values up to -80%. This leads to the comprehension that the power losses calculated with the software tool are too high in a large range of the load spectrum. To find out which part loss leads to the high total power loss the single losses are analysed in detail. It showed that the gear losses rise too much in comparison with the increase of the shaft torque.

3.4.4 Comparison of KISSsoft/KISSsys results with LMS Amesim results

One task of this thesis is to show the differences of the two computation tools. In this section the total power losses of the KISSsoft/KISSsys simulation are compared to the LMS Amesim simulation. In chapter 3.3.3 the deviation of the KISSsoft/KISSsys computation from the measurement and in chapter 3.4.3 the deviation of the LMS Amesim simulation from the measurement is displayed via a deviation table. The deviation of the LMS Amesim simulation from the KISSsoft/KISSsys simulation is calculated according to equation (3.7). To point out the deviation of the LMS Amesim simulation from the KISSsoft/KISSsys computation the total power loss of the KISSsoft/KISSsys simulation is set as base in the deviation computation. The positive percentage deviation concludes out of the condition that the total power loss of the KISSsoft/KISSsys simulation is greater than the total power loss of the LMS Amesim simulation. If the percentage of the deviation is negative the total power loss of the KISSsoft/KISSsys computation is smaller than the total power loss of the LMS Amesim simulation.

$$\Delta P_{loss} = \left(1 - \frac{P_{loss,Amesim}}{P_{loss,KISSsys}}\right) \cdot 100 \tag{3.7}$$

$$Positive\ (+): P_{loss,KISSsys} > P_{loss,Amesim}$$
$$Negative(-): P_{loss,KISSsys} < P_{loss,Amesim} \quad (3.8)$$

		Output shaft speed [rpm]				
	ΔP_{loss}	110	186	315	532	900
Output shaft torque [Nm]	50	-1.1%	0.8%	3.9%	9.2%	17.9%
	97	-2.6%	-0.2%	7.0%	9.0%	17.9%
	189	-5.8%	-3.0%	1.2%	7.6%	16.9%
	367	-11.1%	-8.0%	-3.3%	3.8%	14.0%
	714	-17.1%	-14.2%	-9.5%	-2.3%	8.2%
	1388	-15.3%	-13.5%	-10.0%	-4.2%	4.8%
	2700	-7.2%	-6.6%	-4.4%	-0.3%	

Table 3-16: Deviation of LMS Amesim from KISSsoft/KISSsys at 40 °C

		Output shaft speed [rpm]				
	ΔP_{loss}	110	186	315	532	900
Output shaft torque [Nm]	50	-4.3%	-3.0%	-1.5%	2.0%	8.1%
	97	-6.7%	-5.0%	-2.7%	1.4%	7.7%
	189	-10.5%	-8.5%	-5.8%	-1.2%	5.7%
	367	-15.9%	-14.0%	-10.8%	-5.8%	1.5%
	714	-21.5%	-20.0%	-17.0%	-12.1%	-4.8%
	1388	-18.4%	-18.0%	-15.8%	-12.0%	-6.1%
	2700	-9.1%	-9.7%	-8.6%	-6.0%	

Table 3-17: Deviation of LMS Amesim from KISSsoft/KISSsys at 80 °C

In the Table 3-16 the deviation at 40 °C oil temperature is displayed and in Table 3-17 the deviation at 80 °C is shown. If the red cell colour darkens then the power loss computed with LMS Amesim is higher than the calculated power loss with KISSsoft/KISSsys. In the case that the power loss of the KISSsoft/KISSsys simulation is greater than the LMS Amesim power loss result then the green cell colour darkens. The almost white cells indicate a smaller deviation of the results of both calculation software tools. The results show the tendency that at high speeds and low torques, the calculated power loss of LMS Amesim is even lower than that of KISSsoft/KISSsys. In contrast, with increasing torque and lower speed, the calculated power loss of the LMS Amesim simulation is much higher than that of the KISSsoft/KISSsys calculation.

3.4.5 Differences between the two software tools

In this section the differences between the KISSsoft/KISSsys simulation and the LMS Amesim simulation are explained. During the setup of the simulation models, some advantages and disadvantages of the two calculation programs have emerged.

In the development phase of a new gearbox the software KISSsoft/KISSsys is used to define different components such as e.g. gears, bearings, shaft diameters. For the first concepts the single shafts with the gears and bearings are specified in KISSsoft and the whole gearbox is modeled in KISSsys. With this model the gearbox lifetime relevant parts are analyzed and the dimensions are defined. The existing model is used for the strength design of the gearbox components and hence the additional effort to run an efficiency simulation is not that high in comparison with the completely new setup of a LMS Amesim transmission model. In LMS Amesim the defined parameters are needed to establish a gearbox simulation model and therefore more time is needed to receive simulation results.

The calculation of the bearing losses in KISSsoft/KISSsys has one disadvantage, because the oil level for one shaft can be defined only ones in the current software release version 03/2017E. That means the oil level is set for one bearing in the middle of the rolling element, but if there is another bearing with a different size the oil level is incorrect and thus the calculated loss for that bearing would be wrong. To receive correct results the simulations must be done three times in the case of the eRAD245o gearbox to get the required results and sum up the correct calculated single bearing losses to determine the total bearing power loss. The repetition of the single simulation runs results in additional simulation time. In the LMS Amesim simulation the mean bearing diameter is used for the calculation of the torque loss due to hydraulic friction and no oil level must be defined.

One other disadvantage of the KISSsoft/KISSsys computation is that there is no possibility to set two different lubricants at one shaft. In case of the input shaft and the connected rotor shaft, the bearings of the input shaft are oil lubricated and the rotor shaft bearings are grease lubricated. These two different lubricants can't be considered in the loss calculation of KISSsoft/KISSsys. In LMS Amesim it is possible to define a second lubricant, which is allocated to the respective bearing. Therefore, in KISSsoft/KISSsys a small error is made in the calculation of the bearing losses if two lubricants are used in the gearbox design.

In case of the bearing loss computation in LMS Amesim it is possible to set the friction factor dependent on load and on speed in the parameters of the model. The factors are bearing type dependent and are defined in the bearing catalogue. KISSsoft/KISSsys doesn't have this input parameter window for bearing factors, but it enables the choice of oil bath lubrication or oil injection lubrication. By choosing one of the two lubrication types, the program itself uses the predefined loss factors depending on the bearing type for the power loss calculation of the various bearings. These predefined factors can't be changed for the calculation of the power loss.

The calculation of bearing forces is done in the shaft calculation of KISSsoft automatically, so this data exists after a simulation run. In KISSsoft the bearing stiffness and the temperature dependent preload are considered in the bearing force computation. Contrary to that in LMS Amesim the computation of the bearing forces must be determined by separate computations and the results aren't identical to the KISSsoft calculation. With the geometrical constraints and the gear contact forces it is possible to calculate the bearing forces in LMS Amesim but for a comparable result of the losses the bearing forces are imported from an Excel file. The KISSsoft/KISSsys computed bearing loads for each load point are exported in an Excel table and used for the LMS Amesim simulation as input boundary condition.

Concerning the simulation period, the KISSsoft/KISSsys calculation lasts much longer than the LMS Amesim calculation. In LMS Amesim the load spectrum with 33 load points takes approximately two minutes. Compared to the LMS Amesim computation the KISSsoft/KISSsys computation needs nearly 1 hour for a full load spectrum efficiency run, depending on the computer power.

3.5 Adjusting of simulation models with calibration factors

The simulations of the gearbox with the two different software tools show deviations of the results compared to the measurement results. In the context of this thesis calibration factors are determined by analyzing the computation results in detail to reduce the deviation. The calibration factors are only valid for the analyzed eRAD245o, but in the future these calibration factors can be used for the first computations in new projects where the gearbox has a similar design, because the deviations will probably vary in the same range. In chapter 3.3.3 and 3.4.3 the different simulation results are compared with the measurement. The evaluation of the simulations shows that at specific load points the deviation of the simulation is very high. By analysing the various power loss computation formulas, the cause for the deviations is determined. In the two following chapters the determination of the calibration factors for the two software tools is explained in detail.

3.5.1 KISSsoft/KISSsys adjusted simulation results

In the KISSsoft/KISSsys simulation different computation methods are employed to determine the power loss of the gearbox components. These power loss computation methods are described in chapter 2. The analysis of the calculation results shows that at higher output shaft torques the computation results are much higher compared with the measurement results. This leads to the conclusion that the computed load dependent losses are overestimated. The gear and bearing losses are separated in load and non-load dependent losses. For the adjusting of the computed results the load dependent share of the losses is one important part which is analysed in detail.

One other trend which is observed, is the decrease of the deviation with increasing shaft speed. In range of low level torques and higher output rotational speed the computed power loss is lower than the measured power loss. This leads to the assumption that the rotational speed dependent losses are underestimated at certain load points. Not only the rotational speed dependent losses have an impact on the computed power loss with increasing rotational shaft speed. The loss factors of the load dependent losses are influenced by the rolling and sliding velocity at the gear tooth and therefore load dependent gear losses also increase with increasing shaft speed.

In chapter 2.1.1 the computation method of the load dependent gear losses is described. The load dependent gear losses are computed according to Niemann and the formula for the calculation consists of the input power, the mean friction coefficient and the gear loss factor. One influencing factor is the gear loss factor which is computed by different gear specific parameters. The second influencing factor is the mean friction coefficient which is calculated with equation (2.6). To reduce the deviation of the KISSsoft/KISSsys simulation results from the measurement results, these two influencing factors should be revised by detailed analysis.

Losses which are dependent on the rotational speed and not on the loads acting on the gearbox are the sealing ring losses, one part of the bearing losses and the churning losses of a gear. All in all, there is a range of influencing factors which have an impact on the result of the power loss computation.

The improvement of the KISSsoft/KISSsys results is achieved by reducing the mean deviation value. This optimization process is accomplished with the help of the Excel solver. Excel uses the evolutionary algorithm to identify a global minimum in an interval range. Before an optimization run with the Excel solver is started, a permission range for the calibration factors is defined. With the defined constraints the factors are optimized to reach a minimum mean deviation over the entire load spectrum. This optimization run is performed for the two different operating temperatures. The results of this procedure indicate which kind of power loss is over- or underestimated referring to the load spectrum.

The aim is to find out calibration factors which are applied for both tested gearbox temperatures. With the help of the optimization results the factors are defined. Table 3-18 shows the calibration factors for the respective power loss component. The gear losses are multiplied with a factor of 0.6 and the paddling losses are multiplied with a factor of 2. Regarding the bearing and sealing ring losses, no improvement is detected by changing the calibration factors and therefore the calculated simulation results are used for the evaluation.

Gear factor	Bearing factor	Sealing ring factor	Paddling factor
0.6	1	1	2

Table 3-18: KISSsoft/KISSsys calibration factors and mean deviation

The mean overall deviation of the two different gearbox temperatures before and after the adjusting is shown in Table 3-19. By use of calibration factors a reduction of the overall mean deviation of approximately 20% is achieved for both gearbox temperatures.

Overall mean deviation before adjusting 40 °C	Overall mean deviation before adjusting 80 °C	Overall mean deviation after adjusting 40 °C	Overall mean deviation after adjusting 80 °C
30.2%	34.3%	8.5%	9.8%

Table 3-19: KISSsoft/KISSsys mean overall deviation before and after adjusting

The adjusted power losses are used to compute the optimized deviation map of the gearbox. Table 3-20 and Table 3-21 show the improvements of the deviation due to the calibration factors. At 40 °C gearbox temperature a maximum deviation of nearly 20% is reached but over the whole spectrum the overall mean deviation is reduced to 8.5%. The maximum deviation of 30% at 80 °C oil temperature is achieved at low torque and high rotational shaft speed. Over the entire load spectrum at 80 °C an overall mean deviation of 9.8% is computed. At 40 °C oil temperature the maximum negative deviation of -65% is reduced by the adjustment to -18%. In Table 3-21 the maximum negative deviation is -21% and this is much lower compared to the negative deviation before the adjustment of -71%.

		Output shaft speed [rpm]				
	ΔP_{loss}	**110**	**186**	**315**	**532**	**900**
Output shaft torque [Nm]	**50**	-11.5%	12.8%	19.9%	16.5%	17.8%
	97	-15.8%	5.1%	13.7%	6.8%	1.3%
	189	-16.7%	1.6%	8.2%	0.5%	-5.1%
	367	-13.4%	-0.1%	5.2%	-2.3%	-9.7%
	714	-7.8%	-1.5%	1.6%	-4.3%	-12.5%
	1388	-5.6%	-3.6%	-3.3%	-10.0%	-18.4%
	2700	-6.6%	-6.3%	-8.8%	-16.0%	

Table 3-20: Adjusted KISSsoft/KISSsys deviation table at 40 °C gearbox temperature

		Output shaft speed [rpm]				
	ΔP_{loss}	**110**	**186**	**315**	**532**	**900**
Output shaft torque [Nm]	**50**	-20.6%	-12.3%	-1.3%	11.6%	30.2%
	97	-15.6%	-13.3%	-2.7%	9.5%	27.3%
	189	-10.9%	-11.7%	-6.5%	4.3%	20.6%
	367	1.5%	-2.6%	-5.1%	-1.0%	12.5%
	714	12.4%	5.0%	-2.8%	-6.2%	3.2%
	1388	12.8%	6.4%	-5.5%	-11.4%	-9.0%
	2700	10.5%	2.2%	-8.0%	-15.3%	

Table 3-21: Adjusted KISSsoft/KISSsys deviation table at 80 °C gearbox temperature

To represent the share of the power losses for the two different gearbox temperatures, pie charts are used. The percentages are computed in the same way as in the other pie charts of the simulation results and hence are mean values of the entire load spectrum. In the left pie chart of Figure 3-18 the distribution of the single power losses at 40 °C oil temperature is shown. At 40 °C the proportion of bearing and gear losses is almost equal, which is no longer the case at 80 °C where the gear losses have the largest share.

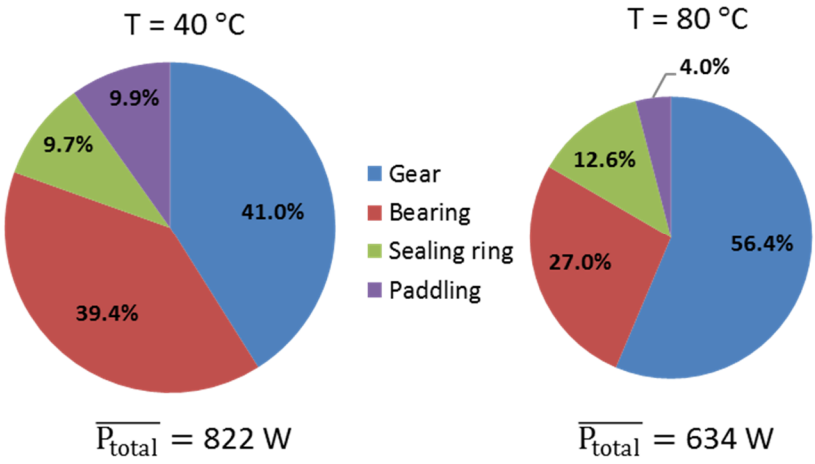

Figure 3-18: KISSsoft/KISSsys power loss distribution of adjusted loss map

3.5.2 LMS Amesim adjusted simulation results

In this subchapter the adjustment of the LMS Amesim computation results with the measurement results is described. The determination procedure of the calibration factors with the help of the Excel solver is the same, as mentioned in the chapter above. But there is a difference referring to the loss computation methods, because in the LMS Amesim simulation the gear and churning losses are calculated in a different way compared to the KISSsoft/KISSsys simulation. Therefore, the LMS Amesim calibration factors differ from the KISSsoft/KISSsys calibration factors.

In chapter 3.4.3 the comparison of the LMS Amesim simulation results with the measurement results is described. The two deviation tables at 40 °C and 80 °C gearbox temperature show that the deviation increases with increasing axle torque. In ranges of higher axle rotational speed, the simulation results are underestimated and thus lower than the measured results.

To understand the deviation of the power losses the computation method of the gear losses is analysed in detail. In chapter 2.1.1 the computation of the gear power loss is explained by means of equation (2.7). The gear power loss is split up in rolling and slipping friction losses. The share of the slipping losses is much larger in relation to the rolling losses. To compute the slipping friction losses of the gear wheel the normal force, the slipping velocity and the slipping coefficient are used. Therefore, the main influencing factor is the slipping coefficient which is computed by an equation based on empirical studies. If the deviation of simulation to the measurement should be reduced the equation of the gear slipping friction losses should be revised, especially the equation of the slipping coefficient. But for the generation of the torque loss tables, which are used for further simulations of the thermal and vehicle model, the computation of the gear loss results with a calibration factor is sufficient.

In chapter 2.1.2 the computation method of the non-load dependent gear losses is described. The computation method of the paddling losses is a different in relation to the KISSsoft/KISSsys computation. For the optimization of the mean deviation of the simulation results a calibration factor of 3 is defined for the paddling losses.

The results of the KISSsoft/KISSsys and the LMS Amesim adjusting procedure show that the gear losses must be reduced to minimize the deviation of the simulation to the measurement. In Table 3-22 the LMS Amesim calibration factors at the two different gearbox temperatures are shown. To reduce the deviation the gear losses are multiplied by 0.5, the paddling losses are multiplied by 3. The bearing and sealing ring losses are not multiplied by a factor, because the optimization shows no improvement of the mean deviation value.

Gear factor	Bearing factor	Sealing ring factor	Paddling factor
0.5	1	1	3

Table 3-22: LMS Amesim calibration factors and mean deviation

Overall mean deviation before adjusting 40 °C	Overall mean deviation before adjusting 80 °C	Overall mean deviation after adjusting 40 °C	Overall mean deviation after adjusting 80 °C
37.2%	46.2%	11.0%	12.9%

Table 3-23: LMS Amesim mean overall deviation before and after adjusting

In Table 3-23 the overall mean deviation before and after adjusting of the simulated power losses is displayed. By use of the calibration factors the overall mean deviation at the two gearbox temperatures is reduced to a minimum in a range of 12%.

The deviation of the LMS Amesim simulation results from the measured results without calibration factors is very high at certain load ranges. With the implementation of calibration factors a reduction of the average deviation is achieved. In Table 3-24 the deviation of the adjusted simulation results from the measured results of the entire load spectrum at 40 °C oil temperature is shown. At 40 °C gearbox temperature an overall mean deviation of 11.0% is reached with the factors, but in some low load and high rotational speed ranges the simulation results are underestimated. In that load ranges the calibration factors don't lead to an improvement of the computed results. With increasing output shaft torque at lower rotational shaft speeds the deviation value is decreasing. In Table 3-25 the deviation table with the adjusted simulation results at 80 °C oil temperature is displayed. A maximum deviation of 38% is reached at low output shaft torque and high output shaft speed. At 900 rpm the deviation is decreasing with increasing output shaft torque and reaches a low deviation. Over the entire load spectrum at 80 °C gearbox temperature a minimum deviation of 12.9% is reached.

The two deviation tables show that the deviations are not minimized in all ranges of the load spectrum, because it is not possible with general calculation factors which are not load and rotational speed dependent. For the vehicle simulation the adjusted loss maps are used for the determination of the individual power losses.

		Output shaft speed [rpm]				
	ΔP_{loss}	110	186	315	532	900
Output shaft torque [Nm]	50	-16.8%	11.2%	22.3%	26.1%	38.5%
	97	-19.6%	4.5%	20.4%	18.0%	26.4%
	189	-19.1%	1.9%	12.3%	12.6%	21.4%
	367	-15.7%	0.1%	9.1%	9.5%	16.7%
	714	-11.5%	-3.0%	3.8%	5.2%	11.1%
	1388	-5.7%	-2.6%	0.5%	-0.3%	3.3%
	2700	1.3%	1.7%	1.1%	-1.7%	

Table 3-24: Adjusted LMS Amesim deviation table at 40 °C gearbox temperature

		Output shaft speed [rpm]				
	ΔP_{loss}	110	186	315	532	900
Output shaft torque [Nm]	50	-26.5%	-16.8%	-4.0%	8.0%	38.8%
	97	-19.3%	-16.0%	-3.9%	3.5%	36.6%
	189	-13.4%	-13.3%	-6.6%	-5.4%	30.7%
	367	-1.6%	-4.9%	-5.7%	-15.3%	22.4%
	714	7.9%	0.7%	-5.6%	-25.1%	11.2%
	1388	11.6%	5.0%	-5.7%	-27.2%	-0.4%
	2700	16.3%	7.9%	-1.2%	-20.4%	

Table 3-25: Adjusted LMS Amesim deviation table at 80 °C gearbox temperature

Figure 3-19 shows the share of the different losses at 40 °C and 80 °C gearbox temperature. In the left pie chart, the percentages of the power losses at 40 °C are displayed. The gear losses are nearly equal to the bearing losses over the whole load spectrum. At 80 °C oil temperature the loss distribution is different, because of a higher share of the gear power loss. The bearing losses have the second highest share with a percentage of 26.6%. Regarding the sealing ring and paddling losses, the percentages are almost the same referring to the two oil temperatures.

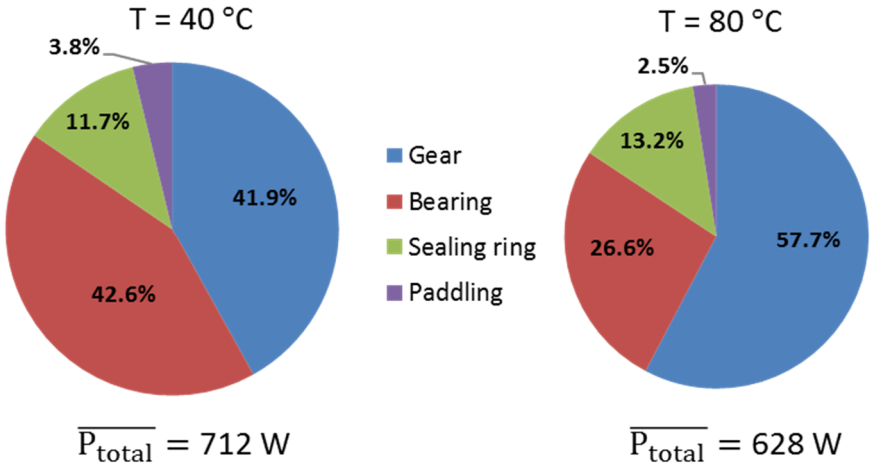

Figure 3-19: LMS Amesim power loss distribution of adjusted loss map

4 Thermal simulation of the gearbox

This chapter describes in detail the determination of the thermal model of the gearbox. In the early stage of a new gearbox development the oil temperature is an important parameter and difficult to identify without any empirical data. The temperature of the lubrication oil has influence onto the lifetime of the oil itself and if the oil temperature changes, the shares of the individual losses change as well. Therefore, the identification of a thermal model of the gearbox is relevant.

In chapter 4.1 the generation of the test bench results and the setup of the test bench are described. For a better understanding of a thermal transmission model in chapter 4.2 the heat transfer is explained in more detail. The thermal model is built with LMS Amesim and is described in chapter 4.3. To verify the thermal model, the results of different test runs are used to determine certain parameters. The temperature dependent transmission model is necessary for further simulations in a total vehicle model.

4.1 Measurement data

At ECS the eRAD245o gearbox was tested on the test bench to find out durability relevant data of the gears and bearings. The simulation runs were made with different damage related test cycles. To measure the gearbox temperature at different regions, temperature sensors were applied in the gearbox housing parts. The results of the test runs are used for the optimization of the thermal model of the gearbox. An important measurement result is the oil temperature of the transmission. Other quantities that have been measured are the input torque and input speed, as well as the output torque and output speed.

In Figure 4-1 a section of a whole test run cycle is shown. The plot displays the gradually changing input shaft torque in red and the output shaft speed in blue.

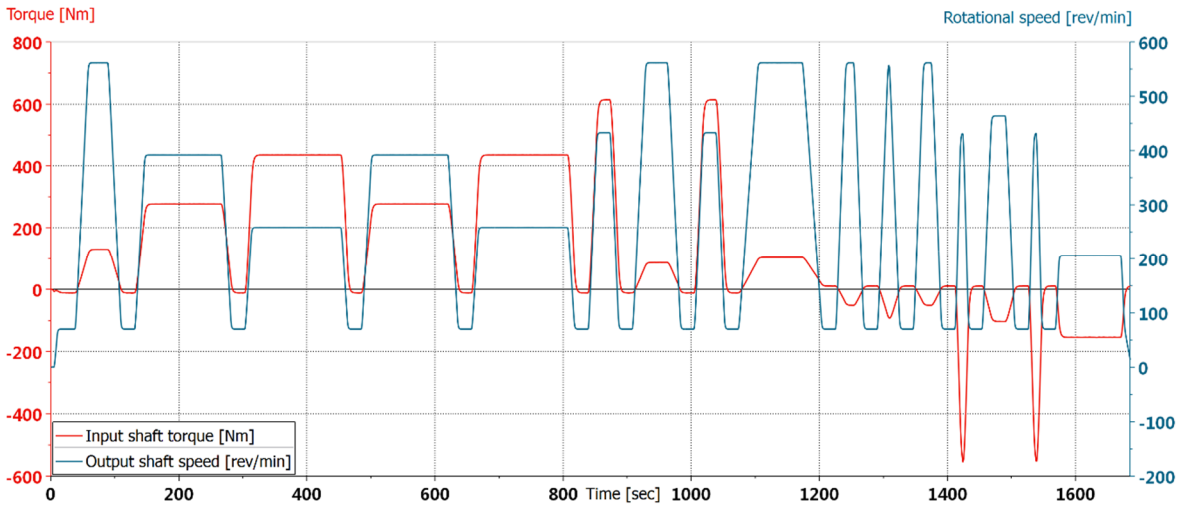

Figure 4-1: Input shaft torque and output shaft speed

4.1.1 Test bench setup

The measurements were carried out on the test bench in the powertrain testing and verification department of ECS. For the endurance runs the test bench setup was done with three electric machines. In Figure 4-2 the scheme of the endurance run test bench setup is displayed. At the test

bench the whole drive unit, consisting of the gearbox, the system housing and the rotor shaft of the electric machine, was installed. Instead of using the electric machine of the electric drive itself, an electric machine of the testing and verification department was used as power input for the test runs. At the output side two other electric machines were used for the test runs. The properties of the three electric machines are described in the image. With the use of three torque measurement flanges at the input and the two output shafts the determination of the axle torques was possible. For reasons of space a bevel gearbox was used to deflect the power by 90 degrees. Different propeller shafts were required for the connection of the electric machines with the drive unit. The used shafts are shown in the layout of the test bench.

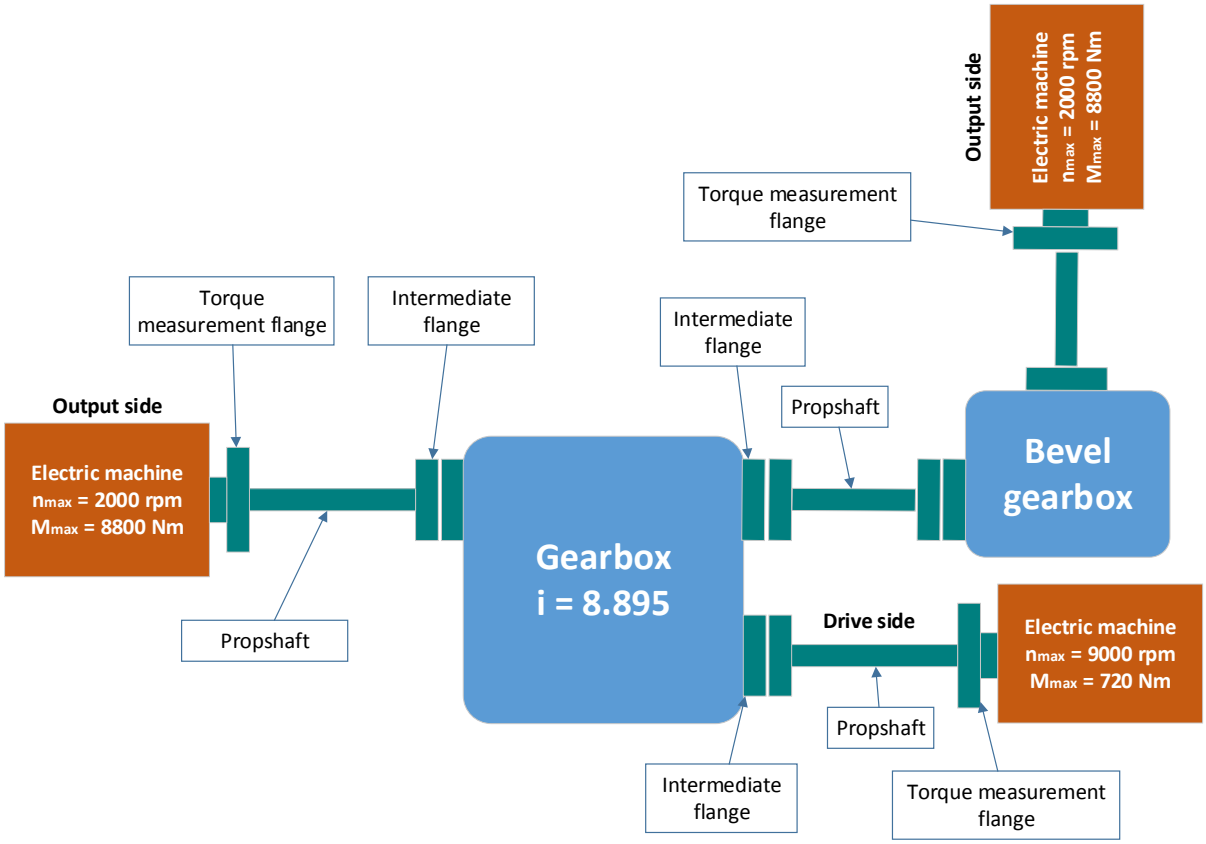

Figure 4-2: Gearbox endurance run test bench setup

4.1.2 Measurement results

The results of the measurement were analysed and the gearbox components were investigated in detail. For the establishing of the simulation model, data like the output shaft speed and the input torque is applied. The measurement points are gauged with a print interval of 0.05 seconds. In Figure 4-3 the test run results of test run M23 show the trend of the temperature at certain torques and speeds. The designation of the test run results was done by the testing and verification department and this naming is also used in the thesis that the interpretations remain comprehensible. Over the whole test run cycle, the lubricating oil reaches a maximum temperature of 76 °C from a starting temperature of 15 °C. The displayed cycle time is 3400 seconds and shows that the loads are repeated after nearly 1700 seconds. This is one test run cycle which was proceeded at the test bench. For the simulation and identification of the heat exchange coefficients a few more test cycles are used.

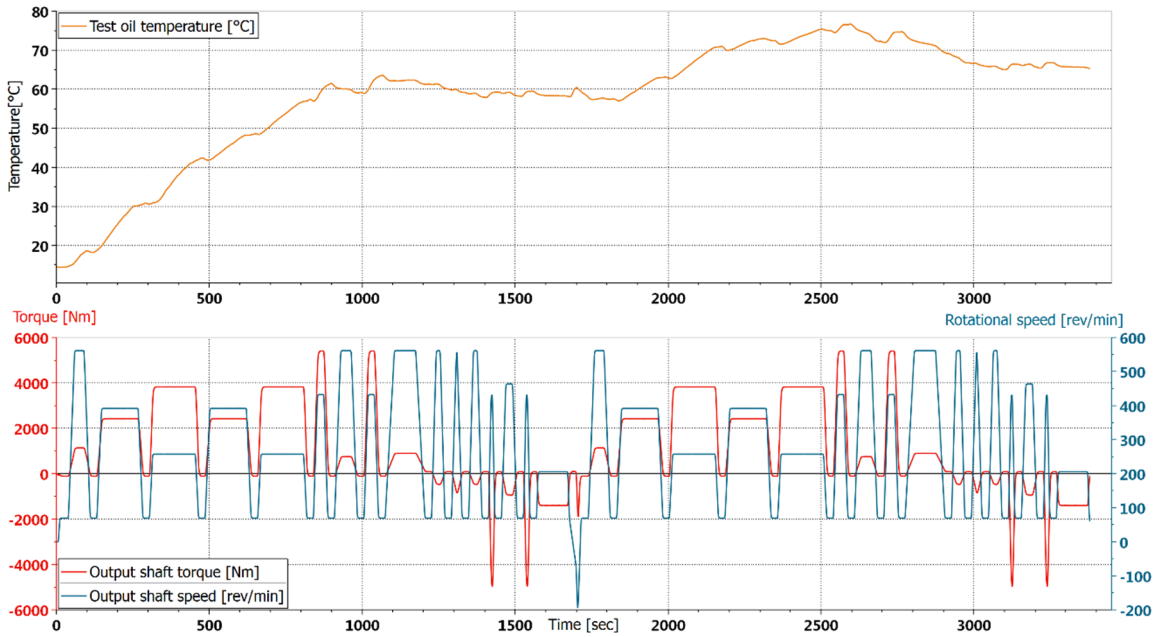

Figure 4-3: Temperature curve of test run cycle M23

4.2 Heat transfer in a gearbox

The gearbox is a complex model in terms of heat exchanges. A gearbox consists of several different elements and these elements are in contact at defined surfaces. Generally, the heat is generated at the parts where a loss exists. Considering a bearing the loss arises due to the rolling and hydraulic friction. This friction loss leads to an increase of the bearing temperature. The same applies to the other sources of loss.

To map a thermal model of a gearbox it is necessary to understand the direction and the type of heat transfer. In a transmission, the heat is transferred from the loss-generating components via the oil to the housing by heat conduction and convection. For a better understanding of the heat transfer path in Figure 4-4 the direction of the heat in the gearbox is displayed with arrows. The heat transfer path is shown only for the input shaft of the gearbox, because the same phenomenon also takes place at the other shafts of the gearbox.

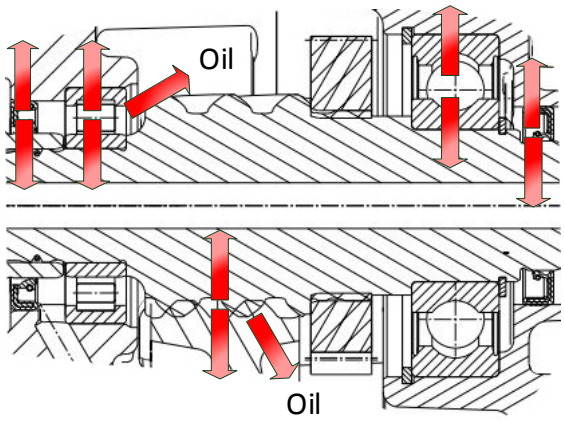

Figure 4-4: Heat transfer path of input shaft

One loss generator is the gear meshing, because at the contact zones of the teeth a rolling and sliding friction occurs and this friction leads to a temperature rise of the gear. The transfer of the heat to the shaft happens through conduction and the heat transfer of the gear to the oil happens through

convection. Paddling losses are part of the gear losses and occur due to the contact of the teeth with the oil. Looking at the bearings the loss is generated due to the friction loss between the bearing rings and roller parts of the bearing. The heat is transferred from the bearing through conduction to the housing and to the shaft. In the gearbox the bearings are oil lubricated and therefore heat is transmitted to the oil through convection. The losses of the sealing rings have the same heat transfer path as the bearings, because they are mounted in the aluminium housing parts. In the small contact zone of the sealing ring at the rotating shaft the loss occurs.

To model the heat flow path in a software tool, the components of the gearbox are summarized in point masses. In Figure 4-5 the simplified heat flow path and the specific heat capacity of the three different materials is displayed. At the beginning is the generated power loss of the gearbox. That loss originates around the steel parts and thus rises the temperature of these parts. The steel parts are wetted with oil and are partly in contact with the aluminium housing. To consider the convection from the steel parts to the oil a convective heat exchange coefficient, which is not known, must be defined. Another convective heat exchange happens between the oil volume and the aluminium housing. The housing is in contact with the oil volume and as a result the temperature of the aluminium parts rises as well. At the test bench the whole drive unit is surrounded by air that leads to a convective heat exchange with the air. To simplify the heat transfer simulation model the heat conduction of the steel components to the aluminium components is neglected. The heat conduction of the steel elements to the aluminium elements is very low and would hence only increase the complexity of the simulation model.

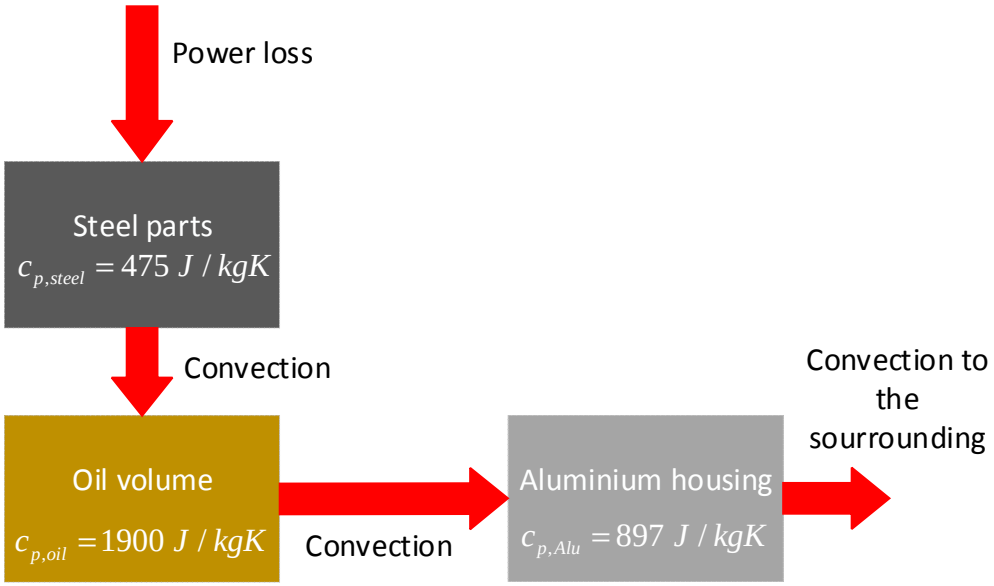

Figure 4-5: Simplified heat transfer model

4.3 Thermal simulation model

The simplified heat path model is used to build up the thermal simulation model in LMS Amesim. Figure 4-6 shows the layout of the thermal simulation model and the models which are used to set it up. The model consists of two thermal capacities, which represents the aluminium and steel point masses, and of a thermal hydraulic volume, which represents the gearbox oil. A convective heat exchange item is used to connect the point masses and oil volume with each other. At the input of the steel mass is the power loss of the gearbox. This power loss is generated in the gearbox and leads to an increase of the gearbox temperature.

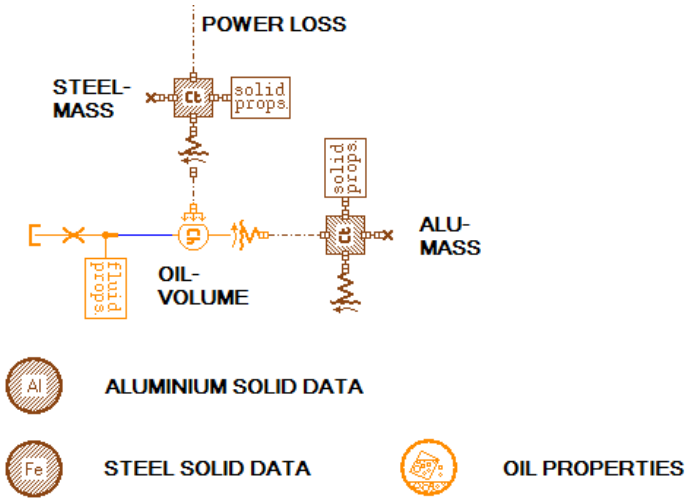

Figure 4-6: Thermal model of gearbox

For a better understanding the used items shown in Figure 4-6 are described in detail in the next section. All equations and figures of the following descriptions are taken from the LMS Amehelp [9].

Thermal capacity

This thermal capacity submodel is used to model the change in temperature of a solid mass. In Figure 4-7 the thermal mass model with four input ports is displayed. The four ports enable the input of four different heat flows and the output of the mass temperature. To calculate the temperature of the point mass, the incoming heat flux is considered. For a proper computation several input parameters are needed and set in the parameters of the submodel. One important value is the solid type index, which is linked to the defined solid material type. In the case of the gearbox the steel mass index is set with two and the aluminium index is set with one. The same value is defined in the parameters of the solid properties submodel. Another simulation relevant parameter is the mass of the thermal capacity. Therefore, it is necessary to define the mass of all aluminium parts and all steel parts of the gearbox. Using the 3D gearbox model, the masses of the gearbox parts are measured and summed up to a total mass. These two total masses are defined in Table 4-1. The temperature of the aluminium and steel mass is defined at the beginning of each simulation run. This value is dependent on the measurement run due to the starting temperature of the gearbox. The specific heat of the steel and aluminium mass changes over the temperature and this is also considered with the thermal capacity submodel.

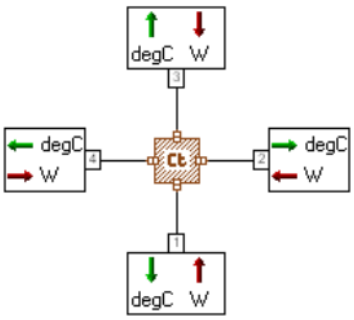

Figure 4-7: Thermal capacity model

To calculate the temperature of the thermal mass equation (4.1) is used. The temperatures at the output of the model are all equal at each port. With the specific heat of the material at temperature ϑ, the mass of the material and the heat flux h_i at the input ports, the actual temperature of the mass is calculated.

$$\frac{d\vartheta}{dt} = \frac{\sum_{i=1}^{4} dh_i}{m \cdot cp} \tag{4.1}$$

Thermal hydraulic volume

The thermal hydraulic volume represents the oil sump of the gearbox in the simulation model. At port three the oil volume is connected via the convective heat exchange with the steel mass. In the parameter mode of the model the oil volume and the index of the thermal hydraulic fluid are defined. For the thermal simulation only one lubrication fluid is in use and therefore the thermal hydraulic fluid index is one. With that index the oil volume is linked to the properties of the fluid. In Figure 4-8 the model symbol is displayed with the input and output quantities at the three ports. At port one and two more in- and output quantities are shown, but for the thermal simulation not all quantities are relevant. Due to the fact that the lubrication system in the gearbox is an oil sump lubrication and not an injection lubrication, the mass and volume flow of the oil is very low and hence neglected. Table 4-1 the oil volume which is used for the simulation is defined.

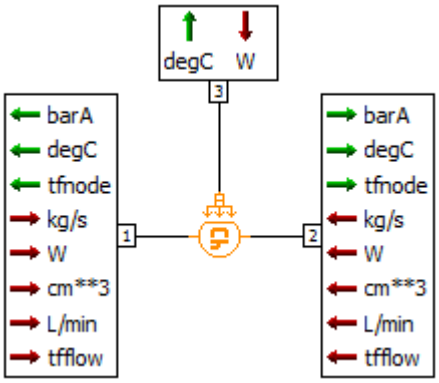

Figure 4-8: Thermal hydraulic volume model

In equation (4.2) the calculation of the oil temperature is described. The equation takes the incoming mass and heat fluxes into account, but in the case of oil sump lubrication the mass flux is negligible small. Other parameters which are relevant for the computation are the density ρ, the specific heat coefficient cp and the constant oil volume V.

$$\frac{d\vartheta}{dt} = \frac{\dot{Q} + \sum dmh_i - h\sum dm_i}{\rho \cdot cp \cdot V} + \frac{\alpha T}{\rho \cdot cp}\frac{dp}{dt} \tag{4.2}$$

Thermal hydraulic fluid properties

For the definition of the properties of a fluid in a simulation model the thermal hydraulic fluid property icon is used. In the parameters of the submodel the type of fluid is defined. A database with predefined liquids exists, but the lubrication oil BOT350M3 is not available. Therefore, the lubrication fluid is defined by use of the media property assistant. The procedure of the fluid property generation process is described in LMS Amehelp.

Figure 4-9: Fluid properties object

In the media property assistant all needed parameters are defined as a function of pressure and temperature. The necessary parameters are distinguished between the thermodynamic properties of the medium, which is the specific heat and the density, and the transport properties, which are the kinematic viscosity, the thermal conductivity and the dynamic viscosity. Another parameter which is also defined is the bulk modulus of the fluid.

Convection model

The convective heat exchange model is used to figure the convection between a solid material and a fluid. In Figure 4-10 the convective heat exchange model is displayed and used for the thermal model setup. It is possible to choose between different convective calculation methods. One possibility is the computation with either predefined or user defined Nusselt correlations. At the predefined correlations it is possible to choose between a flat plate or a cylinder, where the convective heat exchange is done. For the thermal simulation of the gearbox the case of a generic geometry with imposed heat exchange coefficient is used. Therefore, the convective heat exchange coefficient α is defined in advance to run a simulation. The difficulty is that the heat exchange coefficients are not known exactly for the convective heat exchange. In chapter 2.5 approximate values are mentioned, which can be used for the computation of the gearbox temperature. The second parameter which is important for the calculation of the heat exchange is the area of the respective gearbox component. In addition to that the heat exchange surface is measured by using the 3D gearbox model. The necessary surfaces are those of the steel parts, the aluminium parts and the lubricating oil. In Table 4-1 the heat exchange surfaces and coefficients of the relevant point masses are displayed.

Figure 4-10: Convective heat exchange model

In equation (4.3) the computation of the heat flux q of a convective heat exchange is shown. This formula is used in the simulation to calculate the amount of heat which is transferred by convection over a predefined surface A. Thus, the current temperatures of the oil and the solid contact member are used to calculate the temperature differential.

$$q = \alpha \cdot A \cdot \left(\vartheta_{Fluid} - \vartheta_{Wall} \right) \tag{4.3}$$

4.4 Test bench simulation model

To generate the results of the measurement with the simulation tool, the simulation model is set up in the same way as the experimental setup. The relevant input data which is necessary to run the simulation, is taken from the testing results. In this subchapter the gearbox model used for the thermal simulations is described, which has not the same layout as the simulation model described in chapter 3.4.

The simulation model setup

The simulation model displayed in Figure 4-11 is used for the thermal simulation of the gearbox and enables the comparison of the measurement results with the simulation results. As shown in the image at the input port of the gearbox the input torque signal is applied. At the gearbox output port the output shaft speed of the gearbox at the test run is used as input signal. To smoothen the test run results, which are used as an input signal, a first order lag is applied. The oil volume properties, the aluminium and steel solid data are defined in the simulation model. In Figure 4-11 the gearbox model

is connected via the thermal port with the thermal model. The temperature sensor is used to compare the simulated gearbox temperature with the oil temperature of the experimental run. All other red elements displayed in the image are signal elements which are used for post processing evaluations of the simulation results.

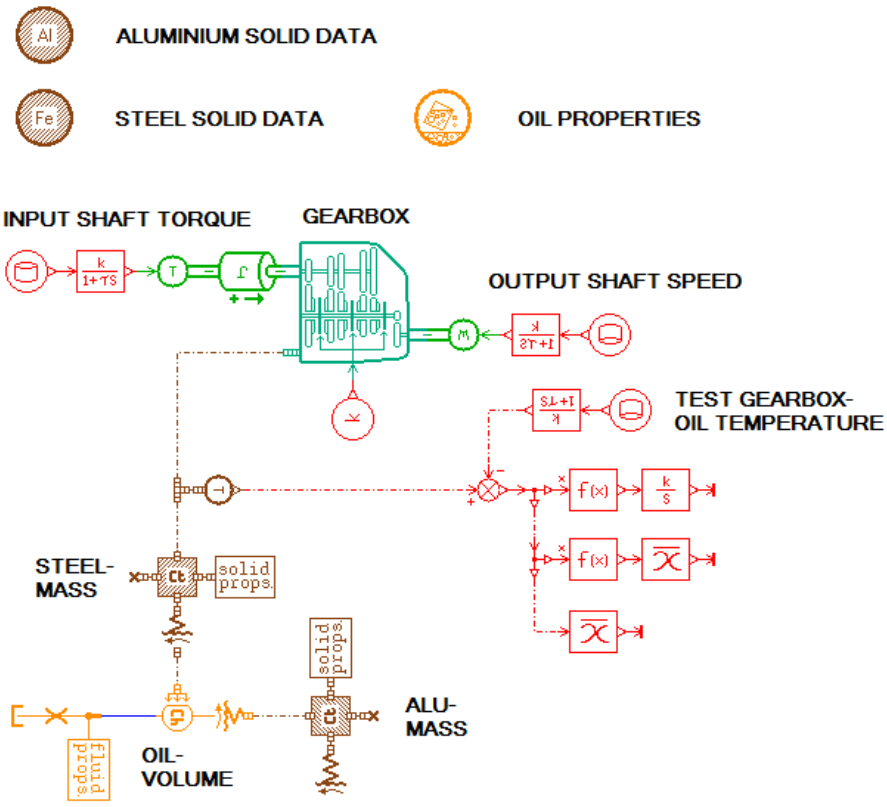

Figure 4-11: Gearbox simulation with thermal model

Gearbox model

The gearbox model shown in Figure 4-12 is used to compute the power loss of the gearbox at any load point. At port two and three the input and output quantities of the model are displayed. The gearbox model is usually used as n-ratio manual gearbox, with more than one forward gear and a reverse gear. For the simulation of an electric vehicles gearbox only one forward gear is required and this is done by setting the gear lever position at port one constantly with one. Therefore, during the whole simulation period the gearbox run in the first gear. At port four the power loss of the gearbox is the output and the input is the actual gearbox temperature. This port is used to connect the gearbox model with the thermal model of the gearbox. In the parameters of the model the gear ratio of 8.895 is defined. To calculate the power loss with that submodel, it is possible to choose between the calculation method with a constant efficiency or with a torque loss file which is temperature, output shaft speed and output shaft torque dependent. The torque loss file is generated out of the results gained in chapter 3.4 the power loss calculation of the gearbox. In gearbox model the change of the bearing preload dependent on the oil temperature is included due to the import of the temperature dependent KISSsoft/KISSsys bearing forces and therefore also considered in the power loss computation. For the generation of the coasting mode power loss map the gearbox simulation is repeated with the corresponding input parameters.

To reduce the deviation of the torque loss between the simulation and the test bench run, the torque loss maps are adjusted. These adjusted maps are used for the thermal simulation of the gearbox. The adjustment of the simulation results is described in detail in chapter 3.5.2.

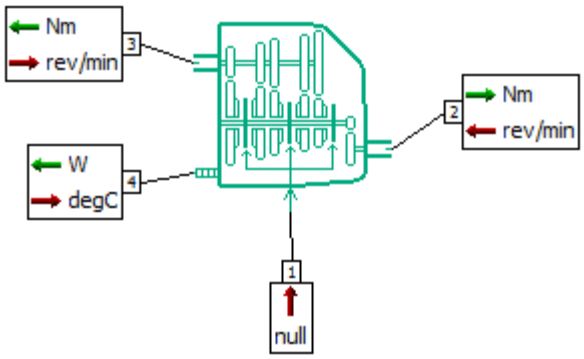

Figure 4-12: Transmission model

The torque loss of the gearbox reduces the secondary shaft torque T_s, which is equal to the output shaft torque, depending on the load point. In equation (4.4) the relation between the different torques is displayed. By means of the torque loss maps for different gearbox temperatures and linear interpolation, the values of the torque losses are calculated for every load point and for each gearbox temperature.

$$T_p \cdot u = -T_s + T_{loss} \tag{4.4}$$

T_p … Primary shaft torque

T_s … Secondary shaft torque

T_{loss} … Torque loss of gearbox

u … Gear ratio

Optimization of the convective heat exchange coefficient

The thermal model requires component specific input parameters. In case of the heat exchange coefficient it is necessary to compare the results of the simulation run with the measurement results to determine the appropriate value. In LMS Amesim it is possible to insert the gearbox temperature curve of the test run. The signal of the measured transmission temperature ϑ_a is subtracted from the computed transmission temperature ϑ_b and then squared. In equation (4.5) the calculation of the quadratic deviation over the whole simulation time is mentioned. With the deviation it is possible to form an optimization condition in the software tool.

$$\Delta\vartheta = \int \left(\vartheta_a - \vartheta_b\right)^2 \tag{4.5}$$

LMS Amesim offers a design exploration process which includes the optimization tool. The optimization process tries to optimize target values and especially in this application the temperature deviation is minimized. Target values for that optimization procedure are the heat exchange coefficients of the three different materials. As an input a default value and the upper and lower limit of the coefficients is set. Other target values which are set in the simulation model are the convective heat exchange areas and the masses of the three different materials. During the optimization process the solver changes the inputs to minimize the output, which is in that case the temperature deviation. The operation is stopped when the temperature deviation converged. To determine the suitable heat exchange coefficients for the gearbox, the optimization process is repeated with several different test run data. From the various simulation runs, the coefficients for the respective material are determined to obtain the optimum approximation of the simulated temperature curve to the measured temperature curve. The defined heat exchange coefficients of steel, aluminum, and the lubrication oil

are shown in Table 4-1. As mentioned before the masses and areas of the different gearbox components is measured by use of the 3D CAD model. In chapter 2.5 recommended values for the heat exchange coefficients are described. The heat exchange coefficients for the simulation are compared with the recommended values. The comparison shows that the coefficients defined in the table below are in the range of the recommended values.

Parameter	Unit	Value
Steel mass	kg	20
Area steel parts	m²	0.75
α steel	W/m²K	320
Aluminium mass	kg	11
Area aluminium parts	m²	0.6
α aluminium	W/m²K	30
Oil volume	dm³	1.2
Area oil volume	m²	0.6
α oil	W/m²K	300

Table 4-1: Thermal model input data

4.5 Comparison of simulation with measurement

The results of the simulation runs are compared with the measurement results. By using the optimized heat exchange coefficients, the deviation from the measured results is in a small range. It is important that the gearbox in the simulation has nearly the same heating and cooling behaviour to compute the losses referring to the actual transmission temperature. Another factor which influences the heating of the gearbox are the implemented torque loss maps. The torque losses of the gearbox are computed and deviate from the measured results. This deviation also causes a different heating and cooling of the gearbox at certain loads.

The measured and simulated temperature curve of the test run cycle M23 is shown in Figure 4-13. In that plot it is visible that different load points over a defined period are applied on the gearbox. The comparison of the simulated temperature curve with the measured temperature curve is described by means of the result plots for one test run. In the appendix the result plots of two other test cycles are displayed (test cycle M05 and M06). This different test runs are used to optimize the values of the heat exchange coefficients.

The orange curve shows the trend of the oil temperature during the test bench run and the blue curve displays the trend of the simulated gearbox oil temperature. Both trends lasts for 3400 seconds and two full load cycles are applied on the transmission. As displayed in the lower plot the input torque and the output rotational speed are varied over the time. During the driving mode the temperature curves show that the heating of the gearbox at the test bench and in the simulation has nearly the same inclination. In the upper plot is shown that the trend of the simulated and the measured temperature between 800 and 1700 rpm is not equal, but very similar characteristic.

The temperature deviation is computed by subtracting the measured gearbox temperature from the simulated gearbox temperature. To calculate the mean deviation equation (4.6) is used.

The standard deviation describes the deviation of values around the mean deviation. In equation (4.7) the computation of the standard deviation is shown. The standard deviation is computed by the square root of the variance and the variance is the expression below the square root. [21]

$$\bar{\vartheta}_{deviation} = \frac{1}{n}\sum_{i=0}^{n}\left(\vartheta_{i,simulation} - \vartheta_{i,measurement}\right) \tag{4.6}$$

$$s = \sqrt{\frac{\sum_{i=0}^{n}(x_i - \bar{x})^2}{n}} \tag{4.7}$$

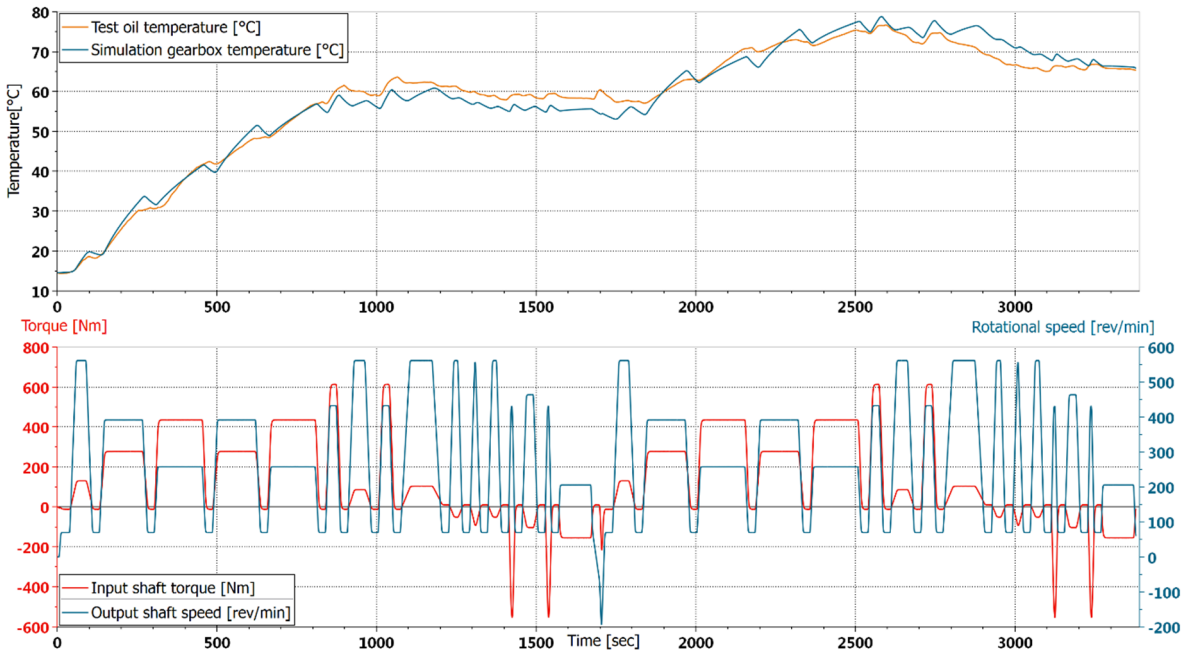

Figure 4-13: Temperature curves dependent of input shaft torque and output shaft speed

In Figure 4-14 the deviation curve of the test cycle M23 over the whole simulation period is displayed. By subtracting the measured temperature from the simulated temperature, the deviation is computed. The deviation of the temperature varies over the time, dependent on the recent load cycle. At low input torques and high rotational shaft speeds the simulated gearbox temperature is lower than the measured one and hence the deviation is negative in that range.

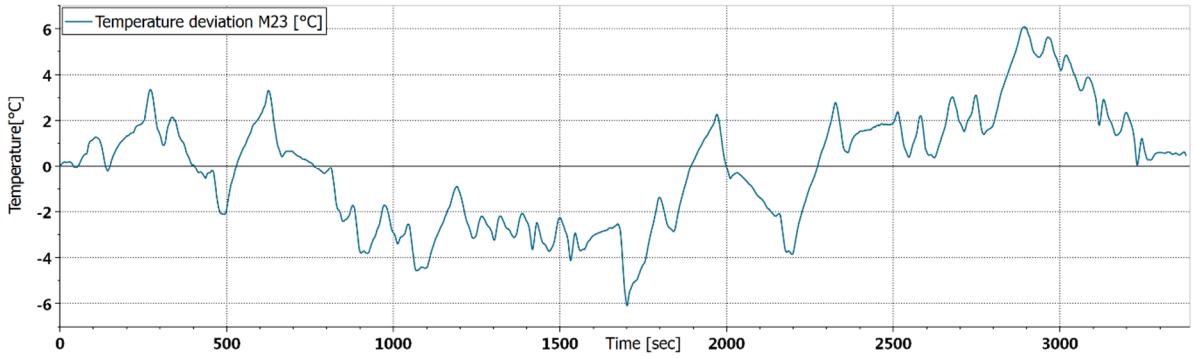

Figure 4-14: Temperature deviation plot

To evaluate the deviation of the three different test cycles the mean deviation and the standard deviation over the simulation time are computed. The results of these computations are displayed in Table 4-2. At all three simulations the mean deviation is in a range of -1 °C to 0 °C. At the M23 test run cycle a maximum standard deviation of 2.5 °C is reached, which is low compared to the temperatures reached at the simulation. The results are in the same range and therefore the heat exchange coefficients are defined as mentioned in Table 4-1. For further simulations of that gearbox in the entire vehicle model the parameters of the thermal model are used.

Parameter	**Unit**	**M23**	**M05**	**M06**
Mean deviation	°C	-0.02	-0.61	-0.87
Standard deviation	°C	2.5	0.95	1.47

Table 4-2: Simulation results of different test cycles

5 Vehicle simulation

In this chapter the determination of the gearbox power losses during different driving cycles with LMS Amesim is described. For this simulation an electric vehicle model is used. The analysed driving cycles are the WLTP, the city circuit in Graz, a driving section on the motorway A2 and a country road cycle. As an input quantity the slope and the velocity signal of the different cycles is needed. The WLTP is a standardized driving cycle and the data of the cycle is available in LMS Amesim. For the simulation of the other mentioned driving cycles measurement runs were made with different electric vehicles. During the measurements a lot of data was recorded, but for the mentioned simulations only the vehicle velocity and the slope is relevant. The measurement data was generated for another diploma thesis at the ECS by Feilmair [22]. In that former thesis the focus was the generation of load data for the development of electric drive units for electric vehicles. The data of the exploited driving cycles is used for the vehicle simulation in this thesis.

With the software tool LMS Amesim it is possible to set up whole vehicle models and simulate test driving cycles. In the other diploma thesis, the different types of vehicle models were analysed and the model which represents the test driving cycles in the best way was used for the simulation. The setup of such a simulation model is described in the next chapter in detail.

5.1 Setup of vehicle simulation model

In LMS Amesim a vehicle simulation model is set up to evaluate the gearbox losses. The general vehicle model setup is used from the other diploma thesis but with different input parameters and different single models. In Figure 5-1 the whole vehicle simulation model layout is displayed and the notation of the different models can be seen.

Generally, the eRAD245o gearbox was developed for the usage in a SUV and therefore for vehicles with a higher total mass. The measurement runs were done with electric vehicles with a lower weight than a SUV. Due to that the vehicle model is defined with the data of a BMW X3.

The important models in use of such a simulation are described in the next sections. All equations and conditions which are explained at each submodel are from the LMS Amehelp [9].

The most important parts of the model are:

- Vehicle model
- Tyre model
- Electric machine
- Battery
- Controller (Driver)
- Vehicle Control Unit (VCU)
- Gearbox with thermal model

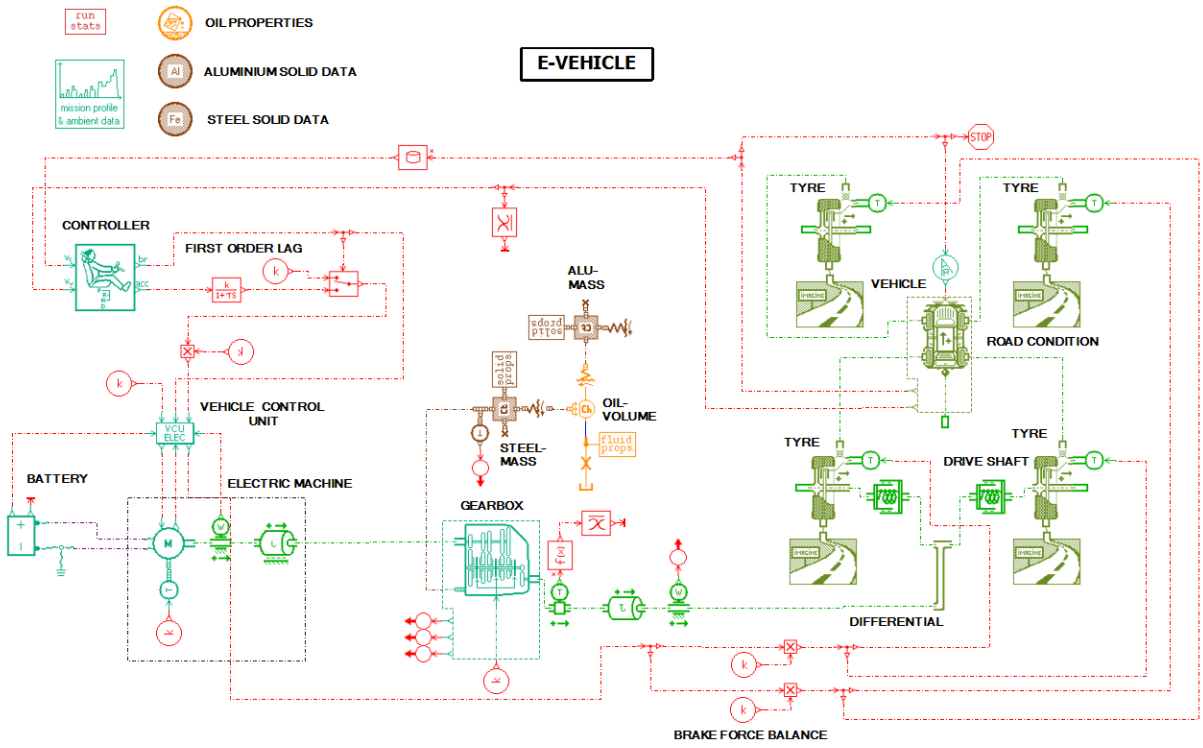

Figure 5-1: Vehicle simulation model layout

Vehicle model

Generally, the vehicle model is used to compute the vehicles longitudinal acceleration, displacement and speed. In Figure 5-2 the vehicle model with the several input and output quantities at the ports is displayed. To connect the vehicle model with the tyre model the ports two, three, five and six are used. At port four the road slope signal in percent is defined.

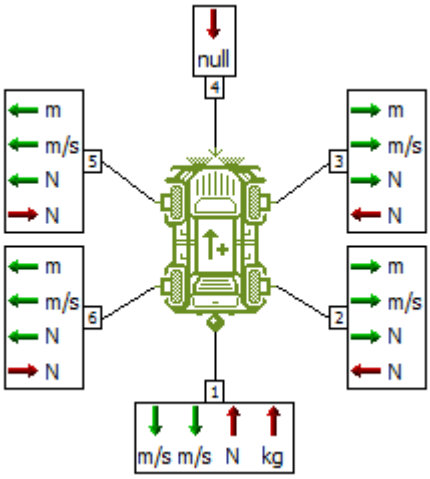

Figure 5-2: Mass transfer vehicle model

Basically, the equation of motion is used to define the several road resistances. At a vehicle the rolling, air, slope and acceleration resistance act. In equation (5.1) the different driving resistances of a vehicle are defined. [23]

$$Z = F_R + F_{Lx} + F_{St} + F_B \tag{5.1}$$

F_R … Rolling resistance

F_{Lx} … Air resistance

F_{St} … Slope resistance

F_B … Acceleration resistance

Z … Pulling force

The pulling force is defined in equation (5.2) by the sum of the drive torque and the static tyre radius. It is necessary that all resistances are transcended by the pulling force.

$$Z = \frac{M_{an}}{r_{stat}} \tag{5.2}$$

Rolling resistance [23]

The rolling resistance acts to an accelerated and braked tyre. At a tyre the pressure distribution is asymmetric because the tyre load is applied before the footprint centre. Equation (5.3) shows the computation of the rolling resistance force of one tyre. For the calculation of the rolling resistance for a whole vehicle the sum of the rolling forces is used.

$$F_R = f_R \cdot F_Z = \frac{e}{r} \cdot F_R \tag{5.3}$$

The rolling resistance coefficients f_{R0} and f_{R1}, shown in Table 5-1, are used for the computation of the rolling friction coefficient. These two coefficients were determined by coast down tests in the former thesis and were then used for the vehicle simulation. Equation (5.4) displays the computation of the rolling friction coefficient f_R. The formula consists of three different coefficients and it shows that the coefficient f_R is dependent on the vehicle velocity. During the coast down tests the vehicle velocity was below 130 km/h and at such velocities the coefficient f_{R4} has no influence on the rolling friction coefficient. At lower speeds the part of the equation including the coefficient f_{R4} is very small and thus is set to zero at the simulation. [22]

$$f_R = f_{R0} + f_{R1} \cdot \left(\frac{v}{100km/h} \right) + f_{R4} \cdot \left(\frac{v}{100km/h} \right)^4 \tag{5.4}$$

Slope resistance [23]

The resistance due to the slope of the roadway is defined with equation (5.5). This expression is described by the slope and the weight force. The slope is computed with the slope angle of the roadway. If the vehicle drives uphill the slope resistance is positive and when the vehicle drives downwards the slope resistance is negative.

$$F_{St} = G \cdot \sin\alpha \tag{5.5}$$

Air resistance [23]

The air resistance of a vehicle arises due to the airflow of the vehicle. In the case of flow against the vehicle, it is generally possible to distinguish between the flow around the vehicle and the flow through the components which are relevant for the engine cooling and air conditioning of the passenger

compartment. For the simulation only the flow around is considered by the usage of the vehicle specific drag coefficient.

$$F_{Lx} = c_x \cdot A \cdot \frac{\rho}{2} \cdot v_r^2 \tag{5.6}$$

In equation (5.6) the air resistance is calculated with the drag coefficient c_x, the air density ρ, the frontal area *A* and the vehicle longitudinal velocity v_r. The drag coefficient is a vehicle dependent dimensionless value and is defined for the simulated vehicle in Table 5-1. If the velocity of the vehicle increases the air resistance rises with the square of the vehicle speed. The density of the air at 25 °C and the drag relevant area *A* is also defined as mentioned in Table 5-1.

Acceleration resistance [23]

The vehicle acceleration is defined with equation (5.7) and consists of the total vehicle mass and the rotary inertia of the masses. To accelerate a vehicle the mass and the inertias are accelerated. The difficulty is to define the rotating masses. The mass of the vehicle can easily be measured.

$$F_B = \left(m + \sum_{j=1}^{n} \frac{J_{Rj}}{r_j \cdot R_j} \right) \cdot \ddot{x} \tag{5.7}$$

In Table 5-1 the most important input parameters of the vehicle simulation are shown. It includes parameters which are defined in the vehicle and the tyre model.

Parameters	**Unit**	**BMW X3**
Vehicle mass	kg	2500
Drag coefficient cw	-	0.35
Frontal area A	m²	2.65
Air density at 25 °C	kg/m³	1.18
Free tyre radius	m	0.336
Wheel inertia	kgm²	1.8
Rolling resistance coefficient f_{R0}	-	0.007
Rolling resistance coefficient f_{R1}	-	0.002

Table 5-1: Important input parameters of vehicle simulation model

The mass distribution of a vehicle has influence on the vertical tyre force. In case of the mass transfer vehicle model the vertical force is split up on each tyre equally. The computation of the vertical tyre force F_Z is described with equation (5.8). It shows that the total vehicle mass force is split up on each wheel. This vertical tyre force is used for further calculations in the tyre model.

$$F_Z = \frac{m \cdot g}{4} \tag{5.8}$$

Tyre model

The tyre model has several ports and at that ports different kind of input and output quantities are exchanged as displayed in Figure 5-3. This model is used for each tyre of the vehicle model and the forces acting on the tyres are the same per axle, because as mentioned before the vertical force is spit up equally. In case of the BMW X3 model the rear wheels are driven and the torque is applied on the rear axle. The front wheels are not driven but a brake force is applied to the tyres.

As described in the section above the vertical tyre force is equally at each wheel and this is used for the calculation of the longitudinal force. This force characterizes the maximum longitudinal force at each wheel per axle. In equation (5.9) and (5.10) the longitudinal force for the rear and front wheel is computed by multiplying the vertical tyre force with the friction coefficient. [23]

In the parameters of the tyre model some tyre relevant data are defined. One important parameter for the computation is the dynamic tyre radius which is dependent on the wheel size. For the calculation of the equation of motion the dynamic tyre radius is used. For some other calculations in theory the static tyre radius is used, but in LMS Amesim for all calculations the dynamic tyre radius is utilized. Other parameters which are defined are the rolling resistance coefficient f_{R0}, f_{R1} and the wheel inertia. The values for the rolling resistance and wheel inertia are used from the existing vehicle model defined in the mentioned former master thesis. [22]

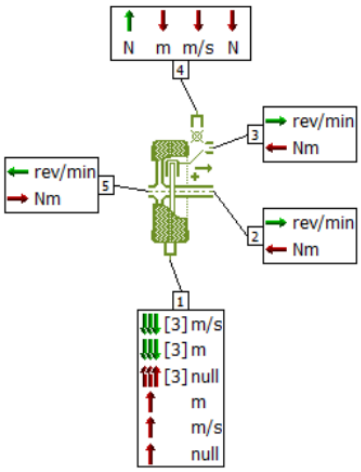

Figure 5-3: Tyre model

$$F_{x\_v} = F_Z \cdot \mu_v \tag{5.9}$$

$$F_{x\_h} = F_Z \cdot \mu_h \tag{5.10}$$

μ_v … Front wheel friction coefficient [-]
μ_h … Rear wheel friction coefficient [-]
F_{x_v} … Front wheel longitudinal force [N]
F_{x_h} … Rear wheel longitudinal force [N]
F_Z … Vertical tyre force [N]

Referring to Newton's second law the wheel acceleration is calculated with the equation (5.11). The torque at port two is always zero and the torque at port five is only zero at not driven wheels, this means at the front axle.

$$J_{wheel} \cdot \dot{\omega}_{wheel} = T_{in,p2} - T_{in,p5} - T_{brk} - T_{res} - F_x \cdot R_{roll} \tag{5.11}$$

Electric machine system

The electric machine which was chosen for the eRAD245o model is a six phase PSM with a distributed winding. For a better cooling efficiency, the rotor and the stator are water cooled. The electric machine has a maximum peak power of 245 kW, a maximum rotor shaft torque of 626 Nm and a maximum rotational shaft speed of 16500 rpm. In Figure 5-4 the torque characteristic curves for driving and coasting are displayed. The maximum recuperating torque of the electric machine is defined as 30% of the total braking torque of the vehicle (see page 64). This is the same percentage which is defined for the maximum braking torque of the rear axle. Due to vehicle handling reasons the recuperating torque is limited to the maximum braking torque at the rear axle of the vehicle, but the maximum recuperation power is defined with 245 kW.

The torque maps for driving and recuperation are defined in the parameters of the electric machine model. It is possible to define an efficiency map for the electric machine, but for the determination of the gearbox losses this efficiency is set constantly with one.

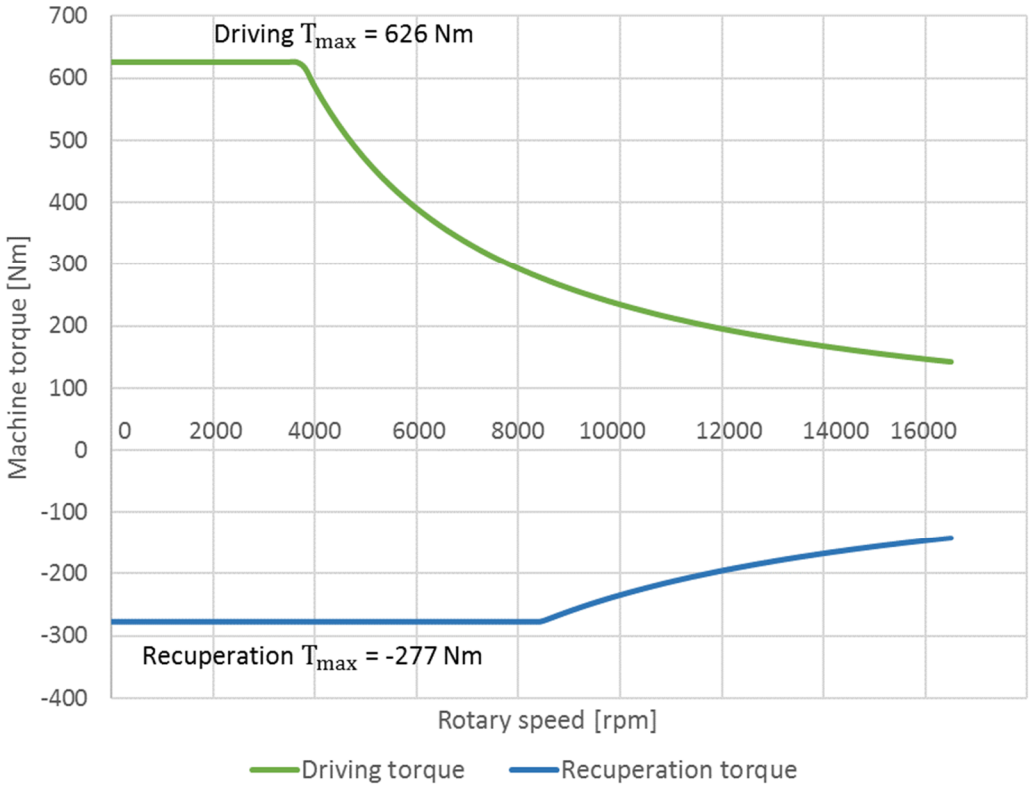

Figure 5-4: Torque characteristic curve of electric machine

An electric vehicle needs a battery and an electric machine to operate it. Figure 5-5 shows the models of the battery, the electric machine and the rotor shaft inertia. In the image the input and output ports of the three different models are displayed as well.

Concerning the battery, the voltage is set constantly with 340 V in the parameters of the battery model. It is possible to define a battery model that behaves like a battery in an electric vehicle. That means during a simulation run the charging status of the battery changes, but for the gearbox power loss computation the charging status of the battery is not of importance and not considered.

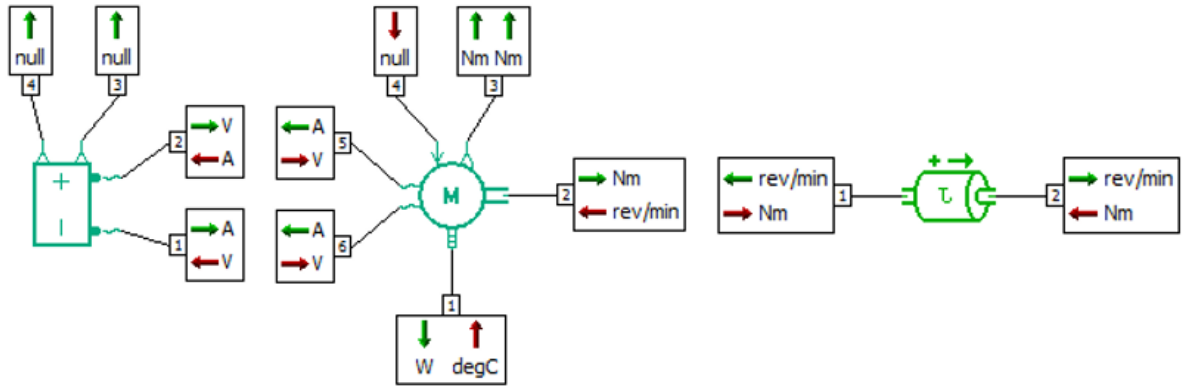

Figure 5-5: Electric machine, battery and rotary inertia model

The second model displayed in the image is the electric machine, which is operated as motor and generator. This model receives the torque command of the VCU at port four and computes the torque output at port two. At port one the temperature of the machine is set constantly with 25 °C. The output signal at port five is the current of the electric machine which is calculated by using equation (5.12) and it shows that the current is dependent on the mechanical power because the voltage is constant and the power loss is defined as constantly zero.

$$I_5 = \frac{P_{mech} - P_{loss}}{U} \tag{5.12}$$

With equation (5.13) the required torque of the electric machine, which is transmitted via port two to the gearbox, is computed. The computation of the output torque T_{motor} is done with the limited torque $T_{\lim}$ by using a first order lag with a user defined time constant t_r.

$$T_{motor} = \frac{1}{1 + t_r \cdot s} \cdot T_{\lim} \tag{5.13}$$

The third model in the image is the rotary motion inertia. This model computes the rotor acceleration and deceleration by using equation (5.14). The formula consists of the electric machine torque, the gearbox input torque and the inertia of the rotor. The rotor shaft inertia of approximately 0.072 kgm², is measured in the 3D CAD model.

$$\dot{\omega} = \frac{T_{motor} - T_{Gb}}{J_{Rotor}} \tag{5.14}$$

Controller

The so called controller or driver is used to accelerate and decelerate the vehicle in the simulation. For the power loss simulation, a specific controller, shown in Figure 5-6, with two input- and two output ports is applied. At port three a mission profile or a predefined vehicle speed profile is defined as input. The actual vehicle velocity is the input signal at port four.

Figure 5-6: Controller model

The driver model operates like a PID controller which compares the desired velocity with the actual vehicle speed. With equation (5.15) the deviation of the two velocities is calculated.

$$err = v_{cont} - v_{veh} \tag{5.15}$$

err … Deviation of vehicle velocity [m/s]
v_{cont} … Desired velocity[m/s]
v_{veh} … Actual velocity [m/s]

If the actual velocity is higher than the desired velocity the braking control output *brak* is applied because the velocity deviation is negative. The acceleration control *acc* is used when the vehicle deviation is positive. With a value range from zero to one the acceleration and braking signal is determined. The equation (5.16) and (5.17) describes the acceleration and braking control output computation.

$$acc = GP_{acc} \cdot err + GI_{acc} \cdot \int err \cdot dt + GA_{acc} \; dvcont \tag{5.16}$$

$$brak = -GP_{br} \cdot err - GI_{br} \cdot \int err \cdot dt - GA_{br} \; dvcont \tag{5.17}$$

acc … Acceleration control signal [-]
GP_{acc} … Proportional gain for acceleration control loop [s/m]
GI_{acc} … Integral gain for acceleration control loop [1/m]
GA_{acc} … Anticipative gain for acceleration control loop [s²/m]
$brak$ … Braking control signal [-]
GP_{br} … Proportional gain for braking control loop [s/m]
GI_{br} … Integral gain for braking control loop [1/m]
GA_{br} … Anticipative gain for braking control loop [s²/m]

In the parameters of the driver the proportional, integral and differential set value are defined. This set values influences the deviation of the vehicle speed and therefore have an impact on the input torque of the gearbox.

The values for the proportional gain of the acceleration and braking control loop are defined based on the simulations in the former master thesis of Feilmair. By use of the comparison with measurements the proportional gain of the acceleration GP_{acc} and the proportional gain for braking GP_{br} are set as follows. [22]

$$GP_{acc} = 2 \qquad \mathrm{GP}_{br} = 0.3 \tag{5.18}$$

One finding of his work was that the driver model has a kind of death time were no braking takes places during the switch of the acceleration to braking control. The simulations showed that the braking command is active over a speed difference of 0.02 m/s. This death time is useful for modelling a vehicle powered by a combustion engine, but in case of an electric vehicle this is not useful because a braking torque is applied instantaneously due to the recuperation if the acceleration command is equal to zero. The death time is set to zero to ensure a realistic behaviour. This skip of the delay had a negative impact on the convergence behaviour of the controller but this is solved by using the proportional gain for the acceleration and braking controller. [22]

Another problem appeared during his comparison of the measured and simulated data of the vehicle simulation. If there is a small deviation between the dedicated and actual vehicle velocity the torque signal of the drivetrain started to oscillate. This oscillation happened due to the acceleration signal of the controller model. Therefore, a first order lag (see Figure 5-7) has been used to prevent the drivetrain from being induced at its resonance frequency. Additionally a switch is used, because a problem occurred at the switching from the driving mode to the coasting mode. If the value of the braking signal is higher than 0.0001, the switch set the acceleration signal equal to zero. [22]

Figure 5-7: First order lag model

Vehicle Control Unit (VCU)

The used vehicle control unit is especially for the control of electric vehicles and receives as an input signal information from the driver, electric machine and the battery. With the control unit the torque which should be transmitted from the electric motor to the wheels is defined. An electric machine has the characteristic that it is used as a motor and as a generator to charge the battery. The vehicle control unit transmits at port one the requested motor torque to the electric machine and at port three the braking command is sent to the tyre models. All the other ports receive information from the driver and the electric motor. In Figure 5-8 the model of the vehicle control unit with the different ports is shown.

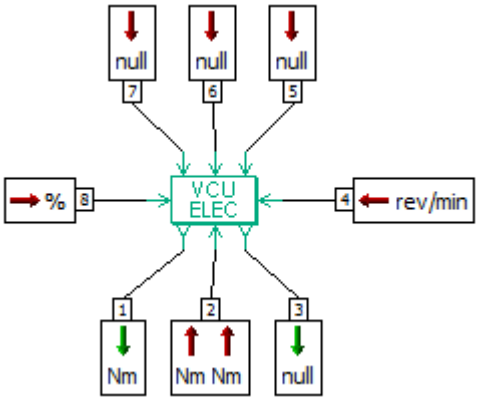

Figure 5-8: Vehicle control unit model

The acceleration command at port five can be defined in three different ways, but for this application the wheel torque is chosen in the parameters of the model. Thus, at port five the desired torque is the input signal. This desired torque is computed by the maximum torque of the electric motor and the acceleration command of the controller. The formula (5.19) displays the computation of the desired torque. With that computation procedure the controller deviation with increasing vehicle speed is avoided. [22]

$$T_{mot\_acc} = acc \cdot T_{mot\_max} \tag{5.19}$$

acc … Acceleration control signal [-]

T_{mot_acc} … Desired torque signal [Nm]

T_{mot_max} … Maximum torque of electric motor [Nm]

The control unit provides four different regenerative braking strategies. For the simulation runs the series strategy is chosen and in Figure 5-9 the diagram of this procedure is shown. In the parameters of the control unit model thresholds for the recuperation strategy are set. These thresholds are defined that the vehicle starts recuperating when the controller sent a deceleration signal. The recuperation strategy decelerates the vehicle with the recuperation torque of the electric motor. If the motor torque is not enough to brake the vehicle, the driver transfers a braking signal to the wheels.

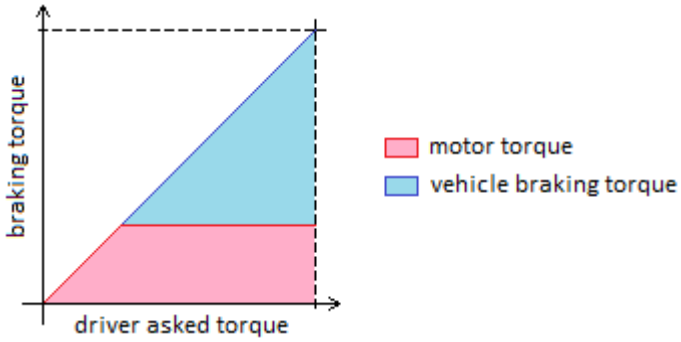

Figure 5-9: Diagram of regenerative braking strategy

For the braking command the type of the signal [0..1] is chosen which calculates the braking torque by multiplying the maximum braking torque with the braking command signal of the controller. Equation (5.20) shows the computation of the braking torque signal which is transmitted to the wheels.

$$T_{brake\_veh} = brak \cdot T_{brake\_max} \tag{5.20}$$

T_{brake_veh} … Braking torque of the vehicle [Nm]

T_{brake_max} … Maximum braking torque of the vehicle [Nm]

The maximum braking torque is defined in the parameters of the vehicle control unit. This maximum torque is computed with the vehicle mass, the friction coefficient and the dynamic tyre radius. In equation (5.21) the calculation of the maximum transferable force is displayed. With the maximum transferable force, the maximum braking torque for the vehicle is calculated. The equation (5.22) shows the computation with the dynamic tyre radius and the maximum transferable force. [22]

$$F_{brake\_max} = m_{veh} \cdot g \cdot \mu_{max} = 2500 \cdot 9.81 \cdot 1 = 24525\ N \tag{5.21}$$

$$T_{brake\_max} = F_{brake\_max} \cdot R_0 = 8240\ Nm \tag{5.22}$$

In the simulation model the brake torque distribution is defined with 70% of the brake torque is acting at the front axle and 30% of the braking torque is acting at the rear axle. That leads to a multiplication of the brake command with the maximum braking torque and the distribution factor of the axle. The result of that calculation is the braking torque for each wheel and this signal is transferred to the input port of the different wheels.

Gearbox with thermal model

For the vehicle simulation the gearbox with the thermal model which is explained in chapter 4 is used. The thermal model computes the change of the gearbox temperature and the power losses of the gearbox for the different driving cycles. Concerning the parameters of the gearbox these are the same as in the chapter thermal simulation of the gearbox. One parameter which is adapted for the driving cycle simulations is the starting and surrounding temperature which is set for each cycle to 25 °C.

Differential gearbox

The task of the differential gearbox is the splitting of the gearbox output torque to the two driven wheels of the vehicle. At each driven wheel half of the gearbox output torque is applied. The computation of the wheel torque is shown in equation (5.23) and the rotational speed of the tyre is the same as the gearbox output shaft speed.

$$T_{wheel} = \frac{T_{Gb}}{2} \tag{5.23}$$

Side shafts

For the connection of the gearbox model with the tyre model the rotary spring and damper model is used. This model is used as a substitute system for the side shafts. In a vehicle the output interfaces of the gearbox are connected via the side shafts with the wheel hubs. The simulated vehicle model was not built in hardware and therefore the characteristic parameters of the side shafts are taken from the simulation model of Feilmair [22]. The damper rating r_{tor} with 0.03 Nm/(rad/s) and the spring stiffness k_{tor} with 200 Nm/degree are defined in the parameters of the model. These two parameters are computed by knowing the dimensions of the side shafts. The drive torque transferred to the wheels (see equation (5.25)) and the angular displacement of the shaft (see equation (5.24)) are computed with that model.

$$\dot{\varphi} = \omega_1 + \omega_2 \tag{5.24}$$

$$T_{drive} = c_{tor} \cdot \varphi + r_{tor} \cdot \dot{\varphi} \tag{5.25}$$

3D table

The 3D table model with three inputs (see Figure 5-10) is used for post processing tasks, e.g. to find out the shares of the different power losses of the gearbox. At the three input ports the output shaft torque, the output shaft rotational speed and the actual gearbox temperature are defined as input parameters. With these parameters at the input the model computed by linear interpolation the specific value with the predefined torque loss table. To determine the different losses like gear and bearing losses of the gearbox during a driving cycle, the torque loss table of the gear and bearing loss is implemented in the 3D table model. The different torque loss tables are established by use of the adjusted results of the LMS Amesim power loss computation. For each load point the percentage of the total loss is calculated and saved in a table format. The output of that model is a percentage value which is multiplied by the total torque loss signal and the angular velocity. The result of this procedure is the share of the single power loss. With the use of the 3D table model the single power losses of the different vehicle simulations are computed.

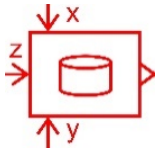

Figure 5-10: 3D table model

5.2 Analysed driving cycles

With the total vehicle simulation model, it is possible to simulate any kind of driving cycle. The model enables the use of standardized driving cycles like the WLTP or the NEDC. Standard driving cycles are available in the mission profile of the LMS Amesim simulation model and can be selected for simulations. But it is also possible to implement measurement data from vehicle test drives in LMS Amesim.

One task of this thesis is to analyse the gearbox power losses of a standardized driving cycle. For the evaluation of the gearbox losses the WLTP is simulated with the LMS Amesim model. The WLTP is the actual driving cycle which is valid for new developed vehicles on the market and hence chosen for the simulation. To get a better comparison of the standardized cycle with test driving conditions the measurement results from three different test cycles are used for simulation runs. These three different cycles are a driving around the city of Graz, a motorway part on the motorway A2 and a country road cycle in Styria. The test runs were done with three different electric vehicles but the most reliable results were gained from the BMW i3. [22] Therefore the simulation the velocity and the slope signal of the BMW i3 were used. Both signals are important because they are used as input for the simulation and thus these signals should be accurate to receive representative results. Another parameter which is defined is the stop duration of the vehicle, but this value is zero for the three test driving cycles.

In the following subchapters the different simulated driving cycles are described in detail with the help of the vehicle velocity curves.

5.2.1 WLTP

The worldwide harmonized light duty test procedure which is called shortly WLTP, is used for the evaluation of the power loss shares of the gearbox. In Table 5-2 the WLTP is compared with the NEDC to display the differences of these two cycles. One difference is the maximum velocity which increased from 120 km/h at the NEDC to 131 km/h at the WLTP. The average drive power increased from 4 kW at the NEDC to 7 kW at the WLTP.

The NEDC was the predecessor of the WLTP and was getting more and more outdated in the last years. Hence, the UNECE made the decision to define a new driving cycle which represents the real driving situations in a better way. The WLTP includes more acceleration and deceleration periods compared to the NEDC. Overall the WLTP covers driving in an urban area as well as driving on the motorway with higher velocity. For the new vehicle development, it is important to have a driving cycle which represents the reality as close as possible to reduce the effort of test runs. To determine the fuel consumption and the emissions of a vehicle in Europe the standardized driving cycle NEDC was used before the WLTP was introduced. New developed vehicles must fulfil the legal limit values. The tests are performed on a test bench with clearly defined boundary conditions which are not modified. The results of the standardized test run are used by the manufacturers as a legal basis for the certification of new developed vehicles. [24]

Parameters	Units	Driving cycle data	
Designation	-	WLTP	NEDC
Starting temperature	°C	25	25
Cycle time	min	30	20
Downtime share	-	13%	25%
Cycle length	km	23.25	11
Maximum velocity	km/h	131	120
Average velocity	km/h	46.6	34
Maximum drive power	kW	47	34
Average drive power	kW	7	4

Table 5-2: WLTP and NEDC data [24]

In Figure 5-11 the velocity curve of the WLTP is displayed in red. Until approximately 1500 seconds of the cycle the driving in an urban area and on a country road is simulated. In the last part of the cycle a motorway driving is simulated, which therefore includes a part with a higher velocity of 130 km/h.

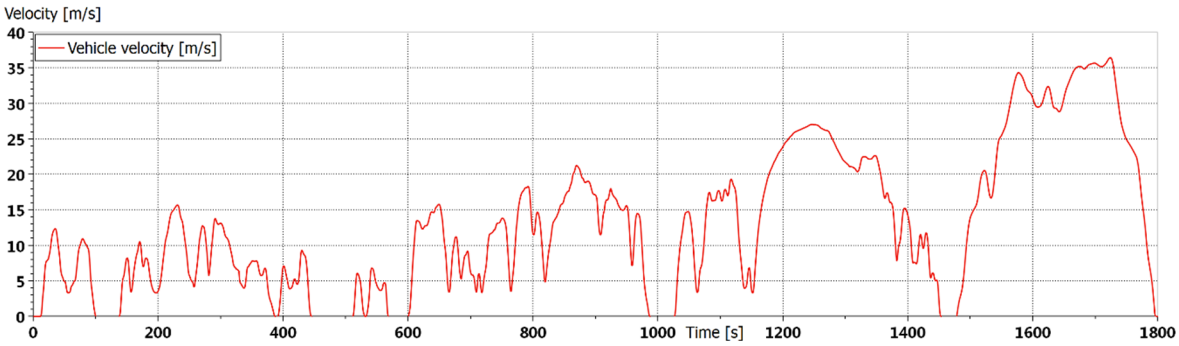

Figure 5-11: WLTP velocity curve

5.2.2 City test cycle in Graz with BMW i3

One measured driving cycle is the test cycle which was driven with the electric vehicle BMW i3 in Graz. The test vehicle was equipped with several measurement devices to collect data about the behaviour during the driving situation. This generated data, especially the velocity information, is used for the simulation of the gearbox losses. The slope measurement of the city cycle is incorrect and thus as an assumption the slope of the city cycle road is set to constantly zero. In Figure 5-12 the velocity profile of the city cycle over nearly 1.97 hours (7100 seconds) is shown. The curve provides information about the maximum and minimum velocities during the cycle. The graph shows that the vehicle is accelerating and decelerating very often during the driving cycle, as it is usual in city driving.

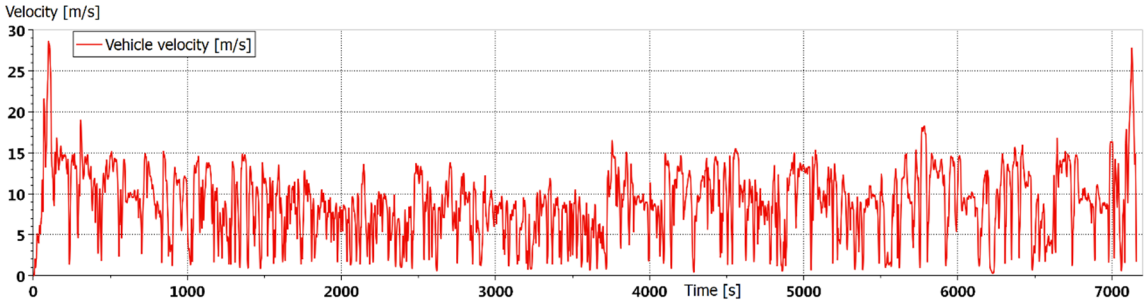

Figure 5-12: Velocity curve of city test cycle Graz with BMW i3

5.2.3 Motorway A2 with BMW i3

Contrary to the city cycle, the cycle on the motorway has only sections with high speeds and low shares of acceleration and deceleration. In Figure 5-13 the speed curve describes the trend of the velocity for the measurement cycle. During that cycle the electric vehicle BMW i3 is driving on the motorway for approximately 24.2 minutes (1450 seconds). The vehicle reaches a maximum speed of 130 km/h and this speed is held over most of the time. In case of the motorway simulation the slope measurement signal of the test runs is plausible and therefore used as input parameter.

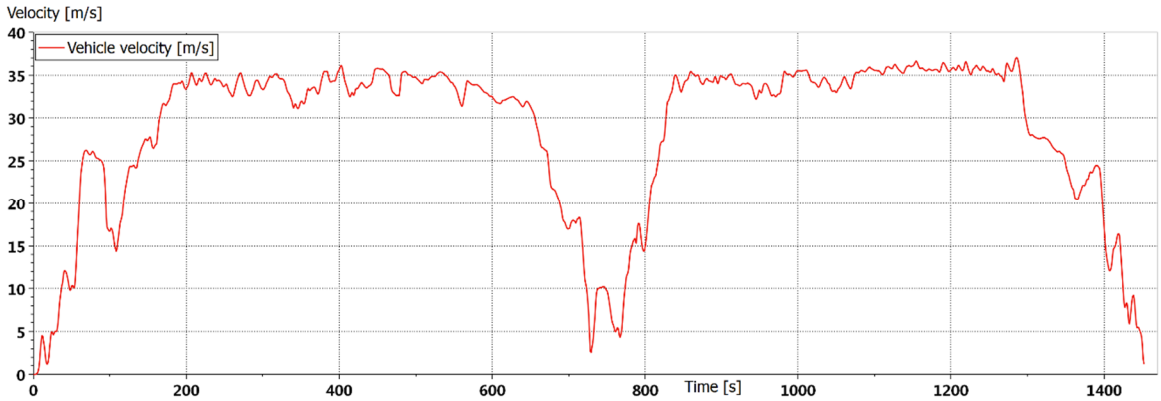

Figure 5-13: Motorway cycle velocity curve with BMW i3

5.2.4 Country road cycle with BMW i3

The country road cycle through Styria (see Figure 5-14) is kind of mixture of lower and higher velocities, but there are also short maximum velocity peaks. This driving cycle has a lot of long acceleration and braking periods where the electric vehicle BMW i3 is in motor and generator mode. Due to the driving on a country road the slope of the road has an influence on the driving torque applied to the vehicle. During this driving cycle, the vehicle travels uphill and downhill, reaching maximum inclinations of 15%.

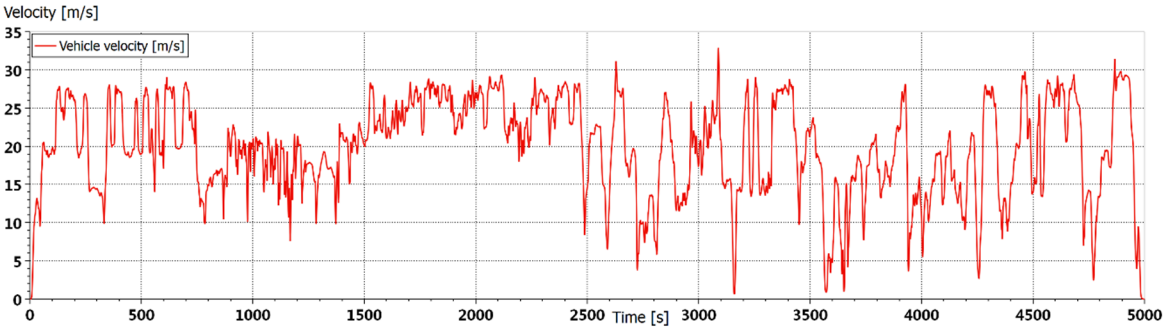

Figure 5-14: Vehicle velocity profile of the country lane cycle with BMW i3

5.3 Results of driving cycle simulation

In this subchapter the results of the various driving cycles are specified and the different losses are analysed. To display the results in a comparable way, pie charts of the different single losses are generated. With these charts the allocation of the power loss generating elements of the gearbox are identified. Additional to the single power loss charts, charts of the separate bearing power losses in the gearbox are established. With the information of the loss distribution at the different driving cycles loss generating components could be optimized to increase the efficiency of the gearbox.

The percentage values of each power loss term are mean values which are computed out of the simulation results. By calculating the mean value of each power loss term over the total simulation time, the percentage of every single loss term is determined.

Another evaluation method is used to interpret the results of the simulation runs. Therefore, the gear, bearing, sealing ring and paddling power loss are classified over the axle torque and axle rotational speed. This classification is done over the whole simulation time and so the power loss is multiplied with the time and leads to the total energy loss of the corresponding loss component. The classification of the power loss signals is done with the software tool FEMFAT Lab, which is a special software developed at ECS. As input the power loss file including the respective axle torque and speed is used. The signals are scanned with a sampling rate of 1 Hz. To classify the different loss signals the classification boundaries and the number of classes are defined identical for each classification. The number of classes is defined with 10. With the defined boundaries and number of classes the so called dwell classification is done. The result is an Excel file where 10 maps are plotted, that means for each axle rotational speed class width one map. On the x-axis of the maps are the axle torque and on the y-axis the power loss classes inscribed. In the maps the dwell for each rotational speed and power loss class are inserted. To display the energy loss for each axle torque and axle speed class only in one table, a further calculation is performed. The final output energy loss values in each cell of the table are computed by multiplying the power loss class mean with the dwell time of every torque and rotational speed class. This classification procedure is separately done for every single power loss component and for every driving cycle.

To display the results of the classification procedure in a graphical way, the data is plotted by use of MATLAB. The plots of the WLTP cycle are displayed in the following section and the energy loss plots of all other driving cycles are shown in the appendix.

WLTP with BMW X3

The results of the simulation are generated with the use of the loss share tables. With that tables the power loss for every print interval step of the simulation are determined. In Figure 5-15 the result plot of the WLTP simulation including the different losses, the vehicle velocity and the gearbox output power are displayed. The different power loss curves are shown in the upper plot and in the lower plot the vehicle speed curve in purple and the gearbox output power in orange are represented. The red curve in the upper plot is the gear power loss and this curve shows the trend that the gear losses increase with the rise of the output power. At sections of higher vehicle speeds the gear losses decrease due to the lower torque applied on the gearbox. The bearing loss curve is displayed in blue in the upper plot and it shows that the bearing losses increase and decrease with the change of the velocity. In the upper plot the remaining two curves are the sealing ring loss curve in black and the paddling loss curve in green. These two part losses have a lower share compared to the bearing and gear losses. The paddling and sealing ring losses are rotational speed dependent and not load dependent and hence increase with the rise of the vehicle speed.

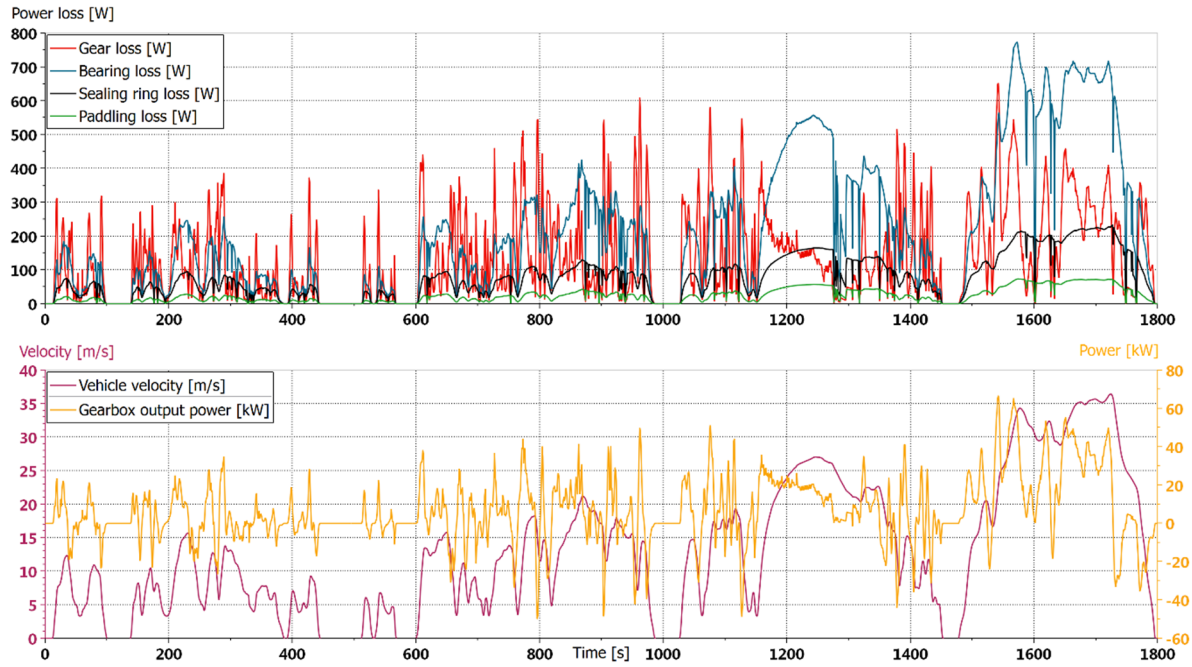

Figure 5-15: Plot of different power loss, vehicle velocity and gearbox output power

To show the shares of the losses in a compact way, the mean values of the different loss shares are represented in a pie chart. In Figure 5-16 the gear, bearing, sealing ring and paddling loss shares of the WLTP driving cycle are displayed. The bearing losses generate the highest share of the losses at the WLTP and the gear losses the second highest share. During the WLTP the absolute mean gearbox output torque is 339 Nm and the mean rotational output speed is 367 rpm. Another impact on the distribution of the gear and bearing losses has the gearbox temperature. During the WLTP the gearbox reaches a maximum temperature of 54 °C and therefore the distribution of the power losses is approximately in the same range as the power loss distribution at 40 °C.

The gear losses have loss peaks at high torques as displayed in Figure 5-15. In a wide range of the cycle the applied rotational speed is in a range of the mean rotational speed and in this load range the gear losses are lower than the bearing losses. To determine the distribution of the gear losses of each gear stage, the mean loss value per stage is computed. At the WLTP 39.4% of the gear losses are generated by gear stage one and 60.6% of the total gear losses are generated by gear stage two. For the computation of the gear losses at gear stage two the load dependent and non-load dependent losses are summed up. At the second gear stage the gear wheel is immersed in the oil bath and thus the paddling losses are generated at the second gear stage.

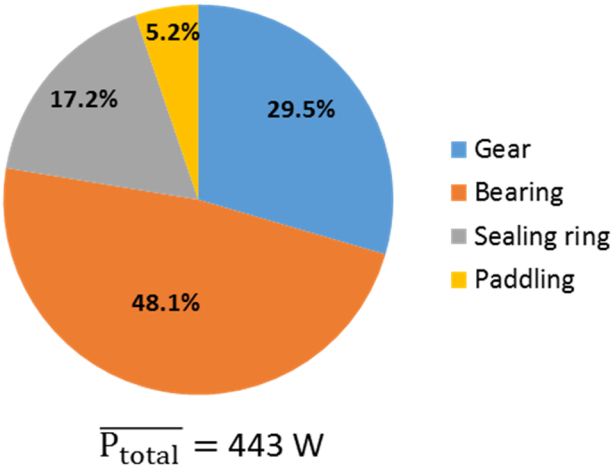

Figure 5-16: WLTP share of single power losses

In Figure 5-17 the share of the single bearing losses of the gearbox at the WLTP cycle are represented. The pie chart shows that the ball bearing at the input shaft, bearing B12, has with 18.5% the highest loss share of the total bearing losses. A comparison of the losses of the intermediate shaft bearings, B21 and B22 with the losses of the rotor shaft bearings, B01 and B02 show that the bearings of the two shafts have a similar share of the total bearing power loss. The two output shaft bearings, B31 and B32 at the differential cause a smaller share compared with the intermediate and input shaft bearings.

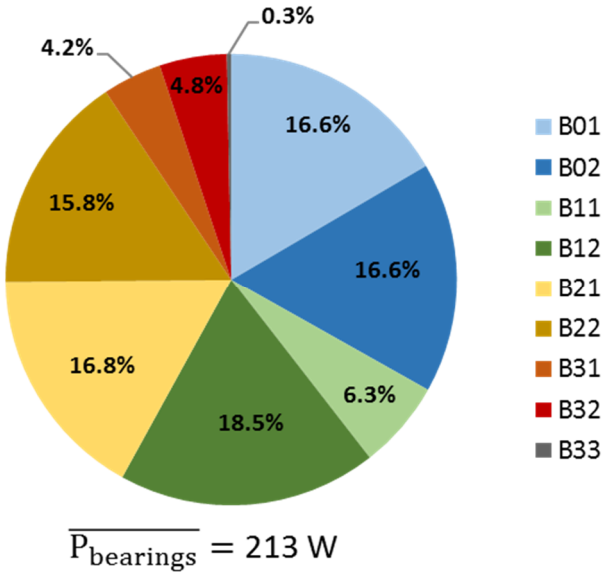

Figure 5-17: Single bearing losses of WLTP cycle

The power loss of each components cause an energy loss over a driving cycle. To represent for example the energy loss of the gears, the classification mehtod is used and the results are plotted as a image with the help of MATLAB. By use of the energy loss plots the load ranges of the WLTP are displayed and the plots describe the impact of the power losses regarding the WLTP.

In Figure 5-18 the gear energy loss of the gearbox at the WLTP is shown over the axle torque and axle speed. By use of such a plot the axle speed and axle torque ranges where the highest energy loss occur can be identified. The plot of the gear energy loss points out that most of the energy loss occur around the absolute mean axle torque of 339 Nm. At higher axle speeds the maximum gear energy loss are reached, but also at lower axle speeds the energy loss is in the range of 3 Wh. In the plot the seperation

between driving and coasting is shown. If the axle torque sign is negative the vehicle is in generator mode. At the WLTP the deceleration of the vehicle is done by regenerative braking, this means by operating the electric machine in generator mode. The energy loss plot shows that the energy loss generated during coasting are lower compared to the losses generated at driving.

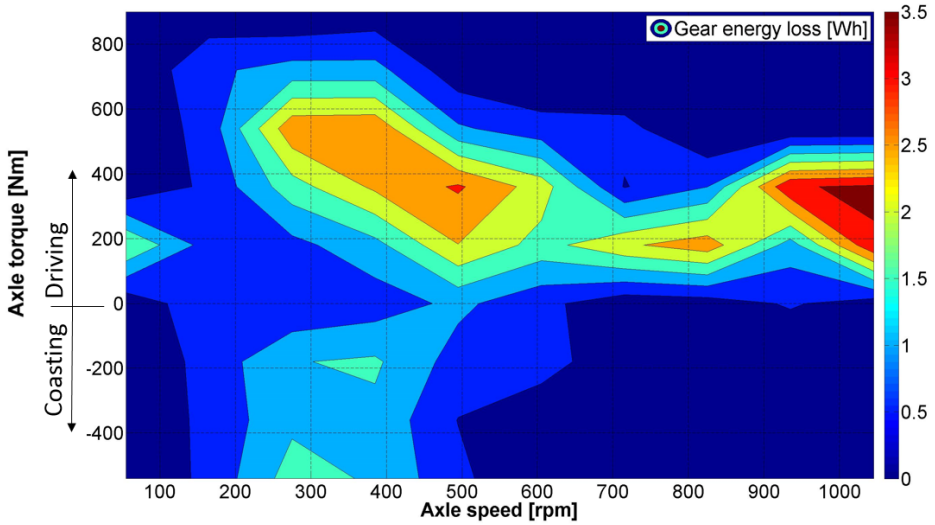

Figure 5-18: Gear energy loss at the WLTP

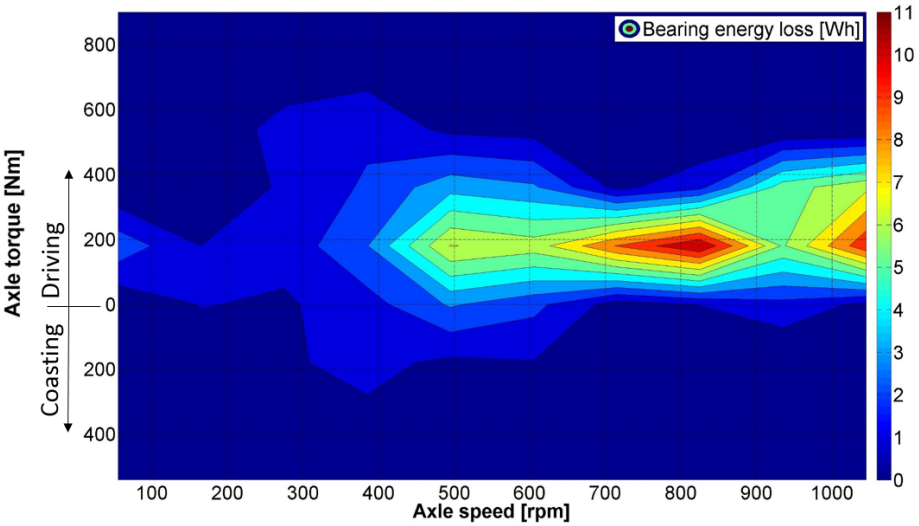

Figure 5-19: Bearing energy loss at the WLTP

The energy loss of the bearings at the WLTP are represented with the plot in Figure 5-19. A comparison of the gears energy loss with the energy loss of the bearings shows that the energy loss of the bearings is higher and distributed in a different way over the axle torque and speed range. The bearing losses reach an energy loss of up to 11 Wh at determined axle speeds and axle torques. Referring to the energy loss at driving and coasting, only a small part of the bearing energy loss is generated during coasting.

In Figure 5-20 the plot of the sealing rings energy loss is displayed. The distribution of the sealing rings energy loss is nearly the same as the distribution of the bearing loss, but the range of the energy loss differs. With a maximum of 3 Wh the energy loss of the sealing rings have nearly the same maximum energy loss as the gear energy loss but overall the energy loss of the gears is higher than the sealing ring losses.

The paddling energy loss at the WLTP are displayed in Figure 5-21 with a maximum energy loss of up to 1 Wh. Regarding the energy loss distribution, the paddling losses have the maximum energy loss in the same load range in relation to the sealing ring losses. At the WLTP between 600 and 1100 revolution per minute, most of the energy loss occur.

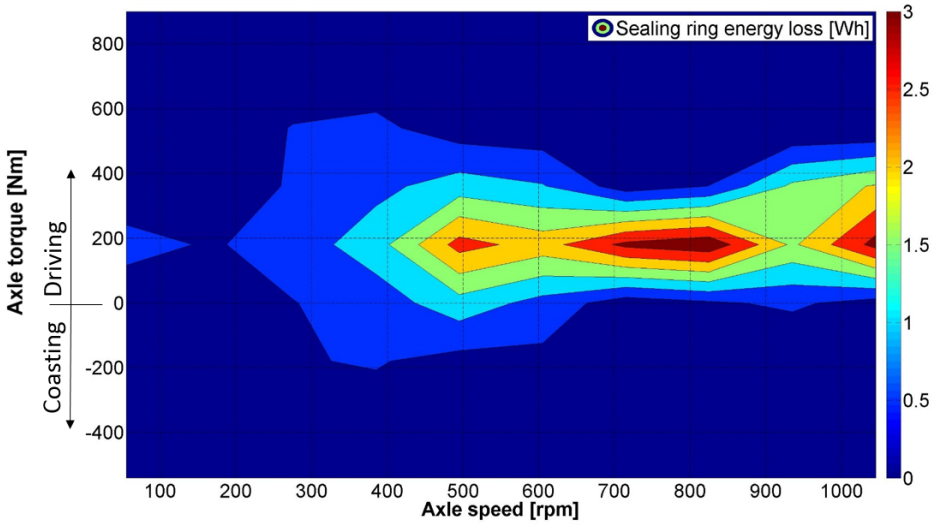

Figure 5-20: Sealing ring energy loss at the WLTP

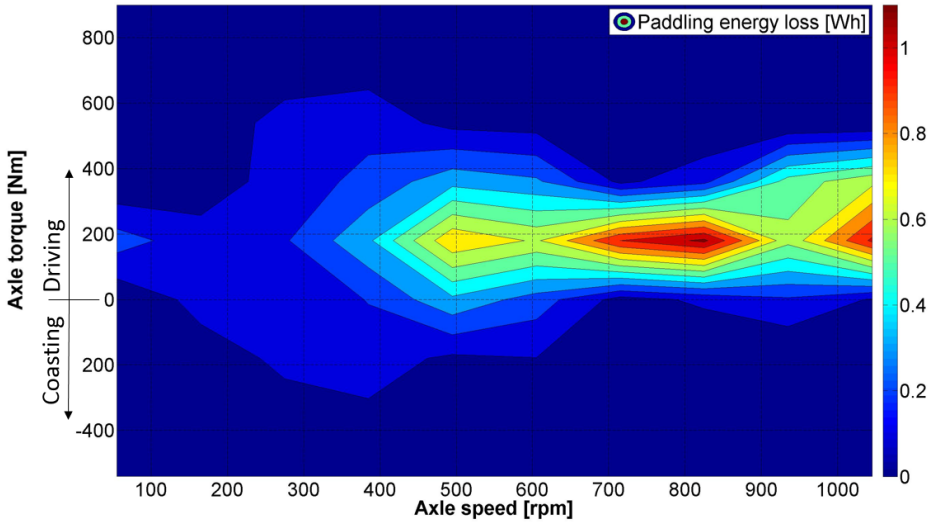

Figure 5-21: Paddling energy loss at the WLTP

City circuit in Graz with BMW X3

During driving in a city, a lot of acceleration and deceleration phases occur and therefore a lot of torque peaks act on the gearbox. In the appendix a segment of the total plot with the different losses, the vehicle velocity and the gearbox output power is shown. The peaks of the gear losses are displayed in that image and it can be detected that the gear losses are higher over the simulation time section. Over the whole city driving cycle an average velocity of 31.9 km/h (8.86 m/s), an absolute mean axle torque of 428.8 Nm and a mean axle speed of 252 rpm is reached.

In Figure 5-22 the pie chart of the individual loss shares and the loss shares of the single bearings are displayed. Contrary to the WLTP the loss share of the gears is larger than the share of the bearings. One reason for the higher gear loss share at the city driving is the high number of torque peaks in the gearbox. That means at higher axle torques the loss of the gears is increasing and getting larger than the bearing losses. At the city driving a maximum gearbox temperature of 46 °C is reached, which has

an influence on the distribution of the losses. The second pie chart in Figure 5-22 shows the share of the single bearing losses and in that chart the loss share of the bearings on the intermediate shaft is the largest fraction. Generally, only small changes in the distribution of the single bearing losses compared to the shares of the WLTP are detected. Concerning the single gear losses, 41.2% of the total gear losses occur at the first gear stage and 58.8% of the total gear losses are generated by gear stage two.

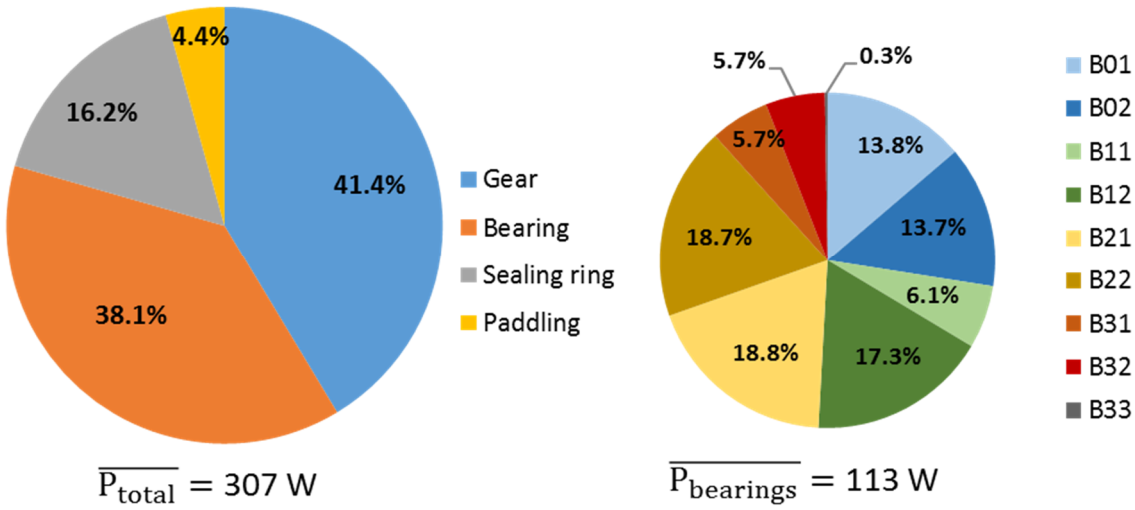

Figure 5-22: Share of power losses at city driving cycle

Motorway A2 with BMW X3

The driving cycle on the motorway has a very monotonic trend and the load changes during that cycle are low. With an average velocity of 103.3 km/h (28.7 m/s) and an average axle speed of 816 rpm, the average velocity and the average axle speed are the highest of all four cycles. The mean axle torque is 358.3 Nm and is in the same range as the WLTP. Concerning the gearbox temperature, during the highway driving a maximum oil temperature of 69 °C is achieved. To get a better understanding of the distribution of the power losses, the evaluated diagram of the transmission losses is shown in the appendix. The image consists of two plots, the first one shows the different power losses and the second one shows the vehicle velocity and the transmission output power.

In Figure 5-23 the power loss shares are displayed and in the left pie chart the distribution of the individual losses is presented. The share of the bearing losses is half of the total losses and the gear losses have a share of 26.1%. Due to the higher vehicle speed during the driving on a motorway, the bearing losses are higher than the gear losses and therefore for the whole cycle the main component of the total losses are the bearing losses. The sealing ring losses have a higher share at the motorway driving cycle than at the other analysed cycles. Referring the single losses of the bearings, the ball bearing at the input shaft B12 has the highest loss share. The rotor shaft bearings and B21 of the intermediate shaft are in the same range. Concerning the distribution of the gear losses the power loss of gear stage one has a share of 37.9% and the losses of gear stage two has a share of 62.1%.

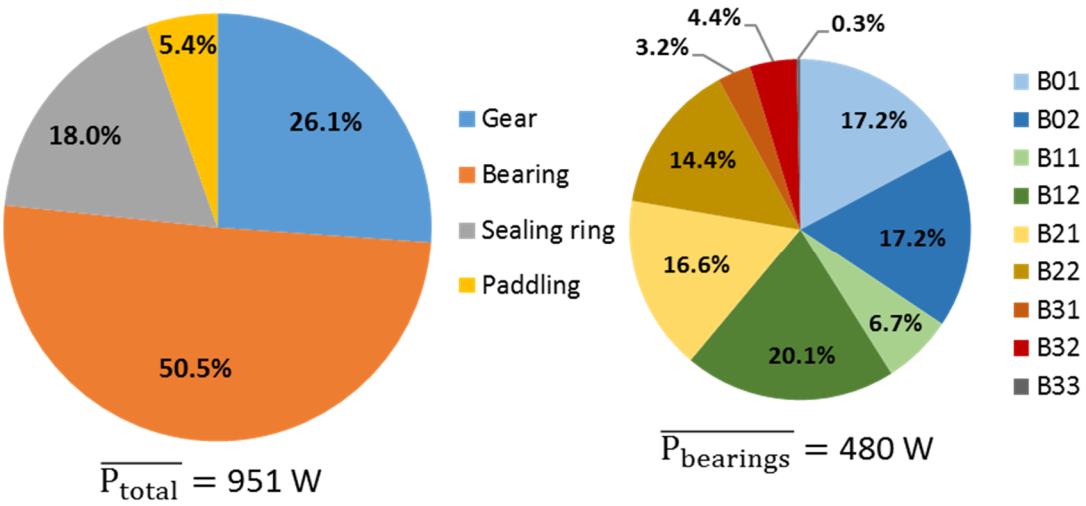

Figure 5-23: Share of power losses at the motorway cycle

Country road cycle with BMW X3

At the country road cycle a few sections with higher axle torque occurred due to the slope of the road. The slope signals of the country road test cycles are plausible and thus considered in the simulation. Over the entire driving cycle a mean velocity of 69.5 km/h (19.3 m/s), an average axle speed of 549 rpm and an absolute mean axle torque of 503 Nm is reached. With that mean axle torque the highest value compared to the other driving cycles is achieved. The gearbox temperature which is reached at the country road cycle is also higher compared to the other cycles. Over the entire simulation of that cycle the gearbox temperature is in a range of 70 °C and reaches a maximum of 74 °C at certain load levels.

In Figure 5-24 the pie chart of the individual losses show that the gear losses have the highest share and the bearing losses have the second highest one. The reasons for the higher gear losses are the range of the axle torque which is achieved during the driving cycle and the gearbox temperature. With increasing loads, the share of the gear losses increases and gets larger compared to the share of the bearing losses. Sealing ring and paddling losses stay nearly the same in the country road cycle in comparison with the other cycles. The gear losses are split up in the losses of gear stage one and gear stage two. Gear stage two generates the higher share of the gear losses with 59.7%. The remaining percentage of 40.3% is the share of the power loss which is generated by gear stage one. In the right pie chart shown in Figure 5-24 the intermediate shaft bearings, B21 and B22, and the roller bearing at the input shaft B12 have the highest share of the bearing losses. The sum of these three bearings represent nearly 60% of the total bearing losses of that driving cycle. All other bearings have a lower power loss share, e.g. the rotor shaft bearings, B01 and B02, have a share of 25% of the total bearing power loss.

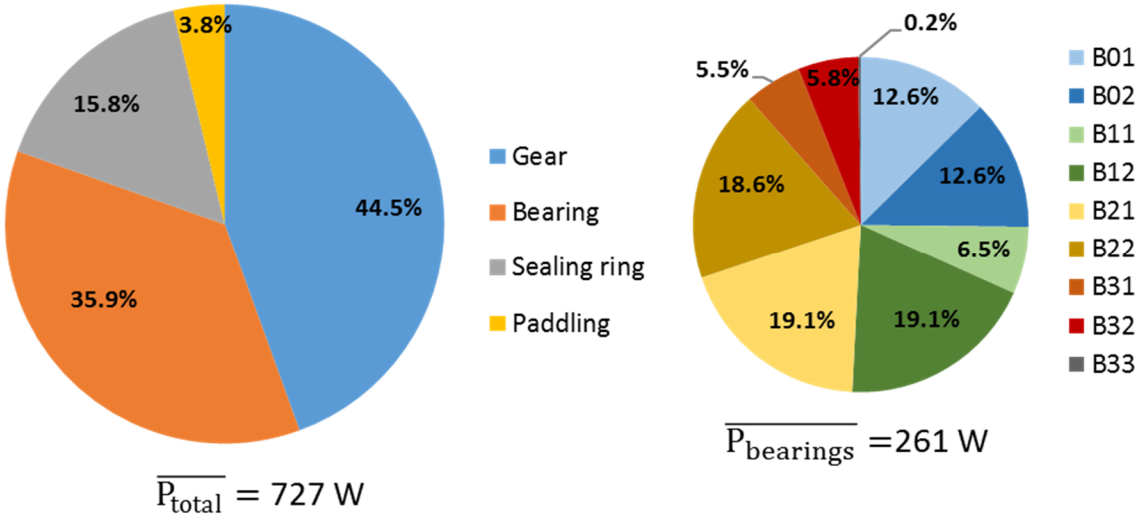

Figure 5-24: Share of power losses at the country road cycle

6 Summary and conclusion

The aim of this thesis was to generate a gearbox simulation model in LMS Amesim and compare it with the KISSsoft/KISSsys model. With the LMS Amesim model it is possible to determine the single loss shares of a high speed, electric vehicle transmission. It is the first time at the ECS that the gearbox losses are computed with the software tool LMS Amesim. In general, these efficiency computations are performed with the KISSsoft/KISSsys computation software. To investigate and understand the differences of these two software tools, the power loss computation methods were analysed in detail. The gear losses were calculated in a different way in both software tools and therefore the results of the gear losses are not equal. In KISSsoft/KISSsys the load and non-load dependent gear loss is computed with diverse equations. For the determination of the bearing and sealing ring losses the same methods are in use.

The electric transmission model was setup by the different mechanical models of the LMS Amesim library. With LMS Amesim it is possible to compute the torque losses for every load point, but for each load point a new simulation must be started, hence the simulation was automatized by use of Microsoft Excel. One thing which must be considered is that the bearing forces are computed in KISSsoft/KISSsys and used for the loss simulation in LMS Amesim. The simulation process is started in Excel and the specified boundary conditions are automatically imported in LMS Amesim. Thereafter the simulation is performed and the results are automatically exported to Excel were the final evaluation was conducted.

The KISSsoft/KISSsys model was adapted with the drive shaft bearing to get representative results. In KISSsoft/KISSsys the load spectrum is defined and the power loss is computed for each load point. To achieve comparable bearing loss values, the simulation must be repeated with the appropriate oil heights. The simulation time needed for the load spectrum runs is longer in relation to the LMS Amesim simulation. Comparing the simulation results with the measurement results indicates that deviations occur. The deviation of the LMS Amesim results is higher for the two different gearbox temperatures in relation to the KISSsoft/KISSsys simulation results. For further simulations the single torque losses of the LMS Amesim simulation are multiplied with calibration factors to reduce the deviation. The adjusted torque loss maps are used for the thermal simulation model and for the vehicle simulation model.

To consider the heating and cooling of a gearbox a thermal model is needed. The losses generated in the gearbox leads to an increase of the transmission temperature. For the setup of a thermal model, gearbox relevant data like the oil volume, steel and aluminium mass are defined. In a gearbox different heat exchange processes occur such as convection, conduction and radiation. To present the components of the E-Drive transmission in the simulation, point masses are used. These point masses have the properties of the different materials and they are connected by the convective heat exchange models. One important parameter for a convective heat exchange is the convective heat exchange coefficient, which is not known for the different heat exchanges in the gearbox. Before the determination of the heat exchange coefficients the constraints are defined. The constraints are the surfaces of the different heat exchanges and the masses of the different point masses.

The temperature trend of the gearbox was measured at the test bench with several test runs. To determine the heat exchange coefficients the results of the measurement are used and hence the LMS Amesim gearbox simulation model is configured identical to the measurement setup. By comparing the temperature curve of the test run with the temperature curve of the simulation the heat exchange coefficients are determined by an optimization process. The optimized heat exchange coefficients are used for all three heat exchange processes and therefore the deviation between the simulated and the

measured temperature curve is in a small range. With the identified parameters the thermal model is used for further simulations in a vehicle simulation model.

To identify the power losses in a gearbox during different driving cycles a whole vehicle model was setup in LMS Amesim. The temperature dependent gearbox model computes the torque losses of the gearbox for the different load points. For the setup of the vehicle model different LMS Amesim submodels are employed. Important elements of the simulation model are the controller, the vehicle control unit, the electric machine, the mass transfer vehicle model and the gearbox including the thermal model. The vehicle model requires a velocity and slope signal to simulate the selected driving conditions in LMS Amesim.

For the evaluation of the power losses, four driving cycles were analysed. The WLTP is a standardized driving cycle which is used to simulate different driving conditions. All other simulated cycles are test driving cycles, which were measured with a test vehicle. In the gearbox model the torque loss maps at three different temperatures are implemented. These maps are used to calculate the total torque loss for each simulated load point. With the total power loss the heating of the gearbox is computed during a driving cycle. To determine the individual torque losses of the gearbox at the different driving cycles, torque loss share tables for each individual torque loss are employed. The share tables are based on the LMS Amesim loss computations.

With the identification of the individual losses, the shares of power loss sources were evaluated for each driving cycle. Depending on the driving cycle the bearing or the gear losses have the highest power loss share. The sealing ring and paddling losses are non-load dependent losses and have nearly the same power loss share at every driving cycles. The power loss computation in LMS Amesim enables the determination of the loss share for every single bearing and the loss share of each spur gear stage. Therefore, the share of the power losses for each bearing and gear stage are identified for the driving cycles. Comparing the different cycles with each other shows that the bearings on the intermediate shaft, the rotor shaft and the ball bearing on the input shaft generate the largest share of the total bearing loss. The second gear stage generates a higher share of the total gear losses in relation to the first gear stage.

The results of the individual power losses were then used for the determination of the energy loss during the driving cycles. Hence, a classification process was performed and as a result the individual energy loss at the different axle torque and rotational speed classes was computed. The classification tables show at which load ranges of the cycles which amount of energy loss occur. With these results it is possible to identify the load ranges with the highest impact on the energy loss.

The energy loss of the gearbox has an impact on the cruising range of an electric vehicle. To increase the range of such a vehicle, a high efficiency of the whole drivetrain unit needs to be considered. Each component of the gearbox has the potential for a loss reduction. By simulating the power loss possible improvements and their effectiveness regarding the increase of the efficiency can be analysed. The combination of the power loss computation with the vehicle simulation enables the evaluation of the impact due to the improvements at different driving cycles.

With the thermal gearbox model the oil temperature of the gearbox was computed during a driving cycle. The trend of the oil temperature is displayed dependent on the load and the actual gearbox power loss. If the trend shows critical temperatures modifications can be simulated and compared to the initial situation.

The results of the WLTP simulation showed that the bearing losses have the highest share of the total power loss. That leads to the conclusion that as primary priority the bearing efficiency should be increased in order to reduce the power losses at the WLTP. Factors which influence the bearing power loss are the bearing forces which are dependent on the gear forces and the oil viscosity which is temperature dependent. During the gearbox development the lifetime, the static and dynamic safety of the bearings are main factors which have an influence on the choice of the bearing type. These factors are of higher importance in the project concept phase than the losses generated by the bearing. Nevertheless, the power loss of the bearings should be considered in the early prototype development stage to design an efficient gearbox.

In the chapter of the gearbox power loss computation the distribution of the single losses at different load points are displayed. The results of the load spectrum simulations show that the gear losses have a large share at higher load ranges and hence are beside of the bearing losses the main loss generating component. At the driving cycle simulation especially at the WLTP the bearing losses have the highest share and the gear losses the second highest share. The load ranges are lower compared to the other simulated cycles and thus the gear losses have a smaller share. At the country road cycle and the city cycle the gear losses have the highest share and generate most of the gearbox losses due to the higher loads applied on the gearbox. The paddling losses are the non-load dependent part of the gear losses and at the eRAD245o the gear at the output shaft generates the paddling loss because the gear is immersed in the oil bath. Summing up the load and non-load dependent gear losses, they are one of the main loss generating element of a gearbox. That leads to the conclusion that the gear efficiency should be increased as much as possible.

At the eRAD245o gearbox sealing ring losses have power loss shares which can't be neglected because at the WLTP the sealing ring losses generate 17% of the total power loss. The sealing ring losses are generally friction losses which are dependent on the axle speed and the contact area. For the computation of the sealing ring losses only the shaft diameter and the shaft speed is used. Other methods exist which considers the contact area of the sealing ring for the sealing ring loss computation. Generally, for future developments it would be interesting to reduce the proportion of the sealing ring losses by use of contactless sealing technologies.

Regarding the thermal simulation, the determination of the heat exchange coefficients is one important part. The setup of the thermal model itself is not difficult but the determination of the coefficients without measurement data is challenging. Due to the fact that the different power losses are temperature dependent, the thermal behaviour of the gearbox has a main impact on the simulation results. If no measurement results are available, general heat exchange coefficients of a gearbox can be used for first computations. The result of the thermal simulation represents the temperature trend of the gearbox. If the increase or decrease of the gearbox temperature is not plausible, the coefficients must be adapted and the simulation repeated. To obtain representative results it is better to carry out measurement runs and determine the heat exchange coefficients with the help of the measurement results.

The comparison of the simulation results of both computation software tools showed that the KISSsoft/KISSsys computation is more accurate, especially the computation of the gear loss. At the load spectrum simulation the main difference is the computation of the gear loss, because the bearing and sealing ring losses are calculated with the same equations. The LMS Amesim simulation results show that the gear loss computation method of Amesim is less accurate compared to the calculation method implemented in the KISSsoft/KISSsys software tool. One advantage of the LMS Amesim simulation is the reduced computation time of the gearbox losses compared to the KISSsoft/KISSsys simulation. For the computation of 33 load points the LMS Amesim simulation lasts for a few minutes and the KISSsoft/KISSsys simulations lasts for approximately one hour, depending on the computer power.

During the development phase of a transmission the different components e.g. gears, bearings are defined and computed with the software tool KISSsoft/KISSsys. Due to the fact that the power loss computation is more accurate in KISSsoft/KISSsys, my recommendation is that the power loss simulation should be performed with this software tool. If the power loss simulation would be conducted in LMS Amesim a new gearbox simulation model is required which leads to an additional time effort. The LMS Amesim model must be updated parallel to the KISSsoft/KISSsys model if the gearbox design changes. This additional required time effort is currently not considered in the early development phase. Due to mentioned reasons in the sections above it does not make sense to compute the gearbox power losses with LMS Amesim as well.

In the concept phase of the transmission development the results of the KISSsoft/KISSsys simulation are used for the optimization of the gearbox efficiency. If the transmission design is in an advanced development stage a LMS Amesim vehicle simulation model can be build up, to evaluate the gearbox losses at different driving cycles. With the results of the KISSsoft/KISSsys simulation torque loss maps for different operating temperatures can be established. The torque loss maps are required for the vehicle simulation model, because the maps are implemented in the gearbox model. The LMS Amesim gearbox model can be implemented in different vehicle models and used for all kind of driving cycles to evaluate the power loss distribution of the gearbox. This is a big advantage of LMS Amesim compared to KISSsoft/KISSsys. In summary it makes sense to use KISSsoft/KISSsys for the gearbox power loss simulations and LMS Amesim for the whole vehicle simulations.

7 Outlook

The LMS Amesim gearbox power loss simulation model can be used as a template for new developed transmissions. The gearbox specific parameters must be defined in the different loss generating elements. Furthermore, the Excel file is a template for the new developed gearboxes and the corresponding bearing loads must be implemented in this file. After updating the parameters, the power loss simulation of the transmission can be performed.

The determined calibration factors for the adjusting of the gearbox results are only valid for the eRAD245o gearbox. In the early development phase of a new gearbox design no hardware parts are available and no measurement runs are carried out. Therefore, the simulated results can't be compared with measured results. For further simulations it would be interesting to define a calibration equation which is load and rotational speed dependent. Then the adjustment is more general and applicable for other gearboxes as well.

In the LMS Amesim simulation the load dependent gear losses are split up in slipping and rolling losses, although the slipping losses cause the main part of the load dependent gear losses. To reduce the deviation of the simulation results compared to the measured results, the formula of the slipping coefficient should be analysed in detail. By testing another gearbox and comparing the results of the measurement with the simulation, the formula of the slipping coefficient can be revised. With an improved computation method, the simulation results should differ from the test results in a smaller range. Thus, the first simulation results of a new developed gearbox are more precise and predictable, without adjusting it with test results.

With the vehicle simulation model including the transmission model it is possible to determine the different power losses generated in a gearbox. In the vehicle simulation different vehicles can be defined by implementing the respective vehicle data. Therefore, the gearbox power losses can be evaluated for every vehicle where the gearbox will or might be installed in the future. It is interesting for new developed transmissions to identify the losses generated at different driving cycles, especially at the WLTP. To consider the temperature dependency of the gearbox the thermal model of the gearbox must be redefined, because the identified parameters are only valid for the eRAD245o gearbox. In order to define the heat exchange coefficients, the simulations temperature trend must be compared with the trend of the test runs.

List of Figures

List of Tables

Bibliography

[1] M. Hucko, “2026 kommt das Aus für den Verbrennungsmotor,” *Der Spiegel,* http://www.spiegel.de/auto/aktuell/elektromobilitaet-der-durchbruch-kommt-2022-a-1166688.html.

[2] C. Lund, W. Maister, C. Lange and B. Beyer, “Innovation durch Co-Simulation!,” in *Wärmemanagement des Kraftfahrzeuges VI*, Berlin, 2008.

[3] P. Hofmann, Hybridfahrzeuge, Vienna: Springer-Verlag, 2010.

[4] JVAUTO, 2016. [Online]. Available: https://jvauto.wordpress.com/2016/06/17/basics-of-electromobility-the-main-components-of-an-electric-vehicle/.

[5] G. Niemann and H. Winter:, Maschinenelemente Band II Getriebe allgemein Zahnradgetriebe – Grundlagen, Stirnradgetriebe, vol. 2. Auflage, Springer Verlag, 1983.

[6] H. Ohlendorf, “Verlustleistung und Erwärmung,” in *Stirnradgetriebe-Zahnreibung*, Braunschweig, Vieweg Verlag, 1964.

[7] W, Benedict G. H. & Kelley B., “Instantaneous coefficients of gear tooth friction,” in *Tribology Transactions*, vol. 4, 1961, pp. 59-70.

[8] B. Roulet, Modélisation de l'évolution de la dissipation de puissance et du comportement thermique d'une boîte de vitesse manuelle, Paris, 1995.

[9] Siemens AG, LMS Imagine.Lab Amesim 15.1 Help, 2016.

[10] ISO/TR 14179-2, “Thermal load-carrying capacity,” in *Gears-Thermal capacity*, Part 2 ed., 2001.

[11] W. Mauz, “Hydraulische Verluste bei Tauch- und Einspritzschmierung von Zahnradgetrieben,” FVA Forschungsvorhaben Nr.44/III, FVA Forschungsheft Nr. 185, 1985.

[12] H. Rahnejat, in *Tribology and Dynamics of Engine and Powertrain: Fundamentals, Applications and Future Trends*, 2010, pp. 807-811.

[13] A. S. Terekhov, “Hydraulic losses in gearboxes with oil immersion,” in *Russian Engineering Journal*, vol. 55, 1975, pp. 7-11.

[14] Schaeffler Technologies, Wälzlager, 2014, pp. 37-51.

[15] J. R. Welty, C. E. Wicks, R. E.Wilson and G. L. Rorrer, Fundamentals of Momentum, Heat and Mass Transfer, 5 ed., John Wiley & Sons, Inc., 2002.

[16] P. v. Böckh and T. Wetzel, Wärmeübertragung, 6 ed., Springer Verlag, 2015.

[17] H. Linke, Stirnradverzahnung, Carl Hanser Veralg München Wien, 1996.

[18] KISSsoft AG, [Online]. Available: http://www.kisssoft.ch/english/products/.

[19] Siemens Product Lifecycle Management Software Inc., "LMS Imagine.Lab Amesim," 2014. [Online]. Available: https://www.plm.automation.siemens.com/en/products/lms/imagine-lab/amesim/index.shtml#lightview-close.

[20] H. Watter, Hydraulik und Pneumatik, Springer Fachmedien Wiesbaden, 2013.

[21] T. Steinfeld, "Mathepedia," [Online]. Available: http://www.mathepedia.de/Standardabweichung.html.

[22] T. Feilmair, Lastdatengenerierung für die Auslegung von elektrischen PKW-Antrieben, St.Valentin, 2017.

[23] M. Mitschke and H. Wallentowitz, Dynamik der Kraftfahrzeuge, vol. 5, Wiesbaden: Springer Fachmedien Wiesbaden, 2014.

[24] D. J. Seiler, "Verband der Automobilindustrie (VDA)," [Online]. Available: https://www.vda.de/de/themen/umwelt-und-klima/abgasemissionen/wltp-weltweit-harmonisierter-zyklus-fuer-leichte-fahrzeuge.html.

A. Appendix

A.1 Thermal simulation results

In that section the simulation results of the thermal simulation are displayed. Here the plots of measurement run M05 and measurement run M06 are shown. For each simulation the two temperature curves, the input shaft torque, the output shaft speed and the temperature deviation are represented by the images.

M05 measurement run

In the image below the two temperature curves, the input shaft torque and the output shaft speed are displayed.

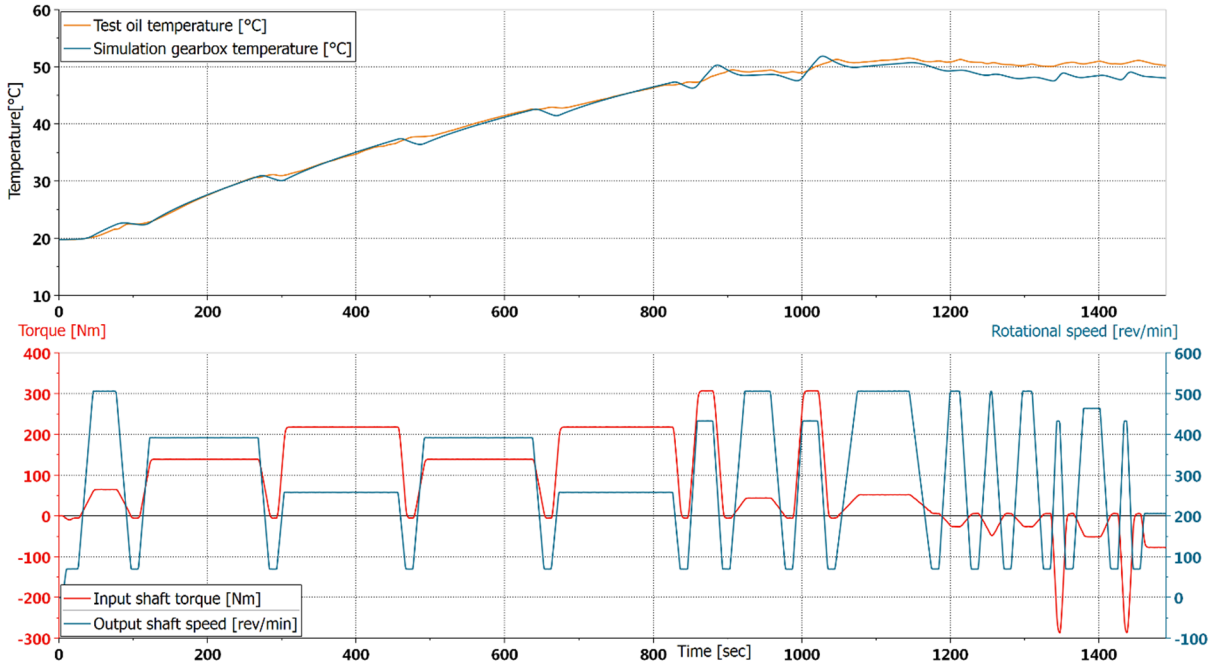

M05 measurement run simulation results

The blue curve in the plot below shows the temperature deviation over the test cycle time.

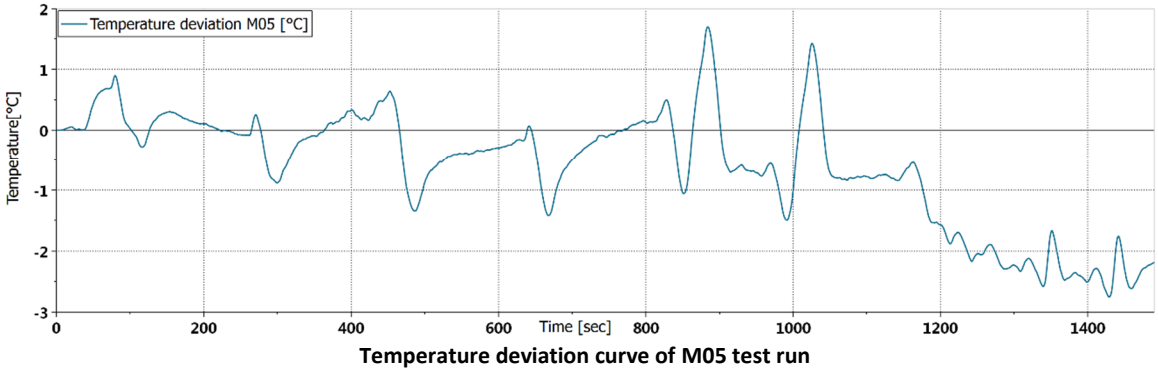

Temperature deviation curve of M05 test run

M06 measurement run

The upper plot shows the simulated and tested gearbox temperature curve. In the lower plot the load spectrum applied to the gearbox is displayed.

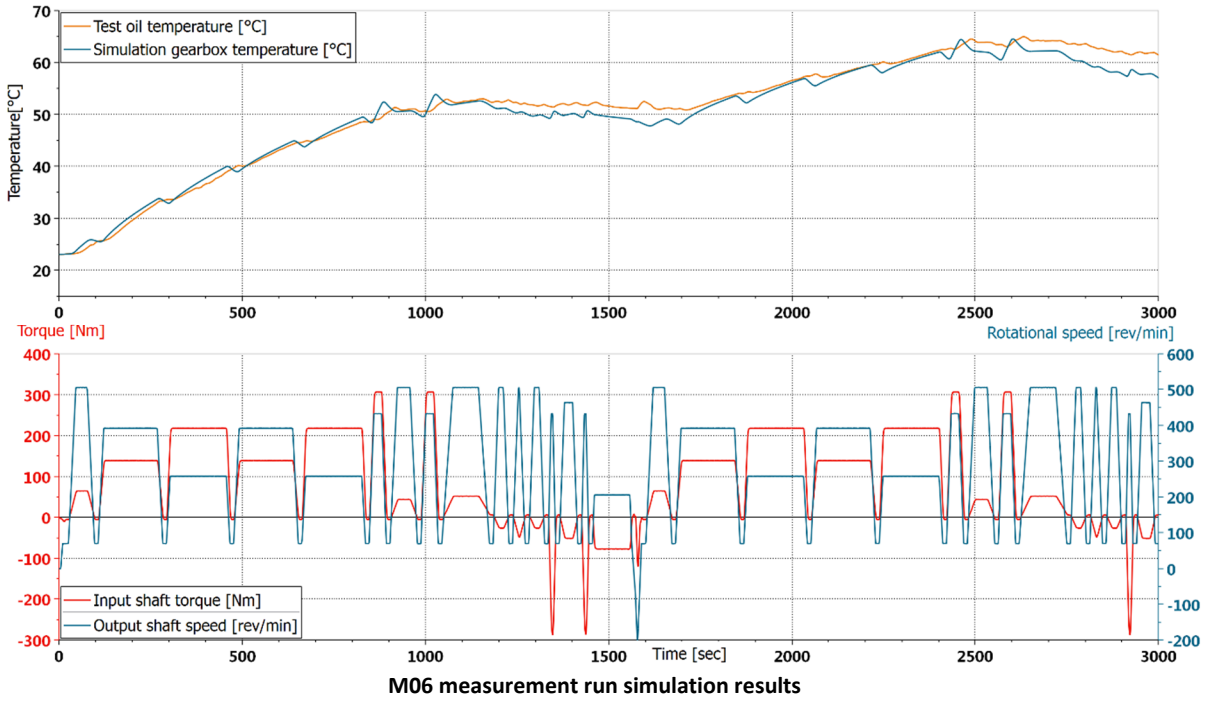

M06 measurement run simulation results

The temperature deviation during the M06 test cycle is shown in the figure below. At certain load levels the temperature deviation reaches a maximum of -4 °C but generally over the whole cycle the mean deviation is in a range of -1 °C.

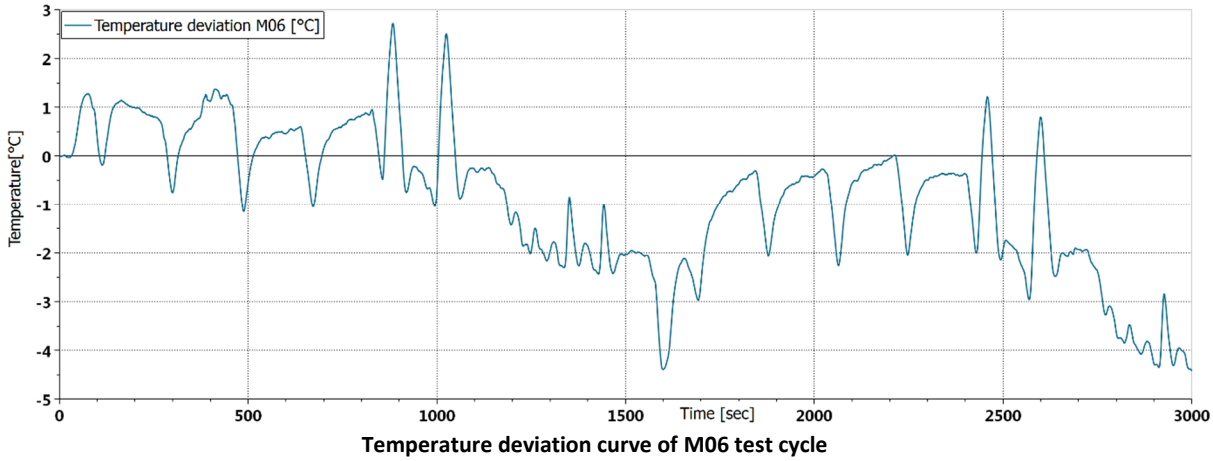

Temperature deviation curve of M06 test cycle

A.2 Vehicle simulation result plots

Here the simulation result plots and the plots of the energy loss of the three test driving cycle simulations are displayed.

City test cycle in Graz with BMW X3

In the image in the upper plot a section of the power losses is displayed. The whole city test cycle lasts for 1.97 hours (7100 seconds), to illustrate the trend of the different losses only section of 1000 seconds is shown in the graph. In the lower plot the vehicle velocity and the output power are represented.

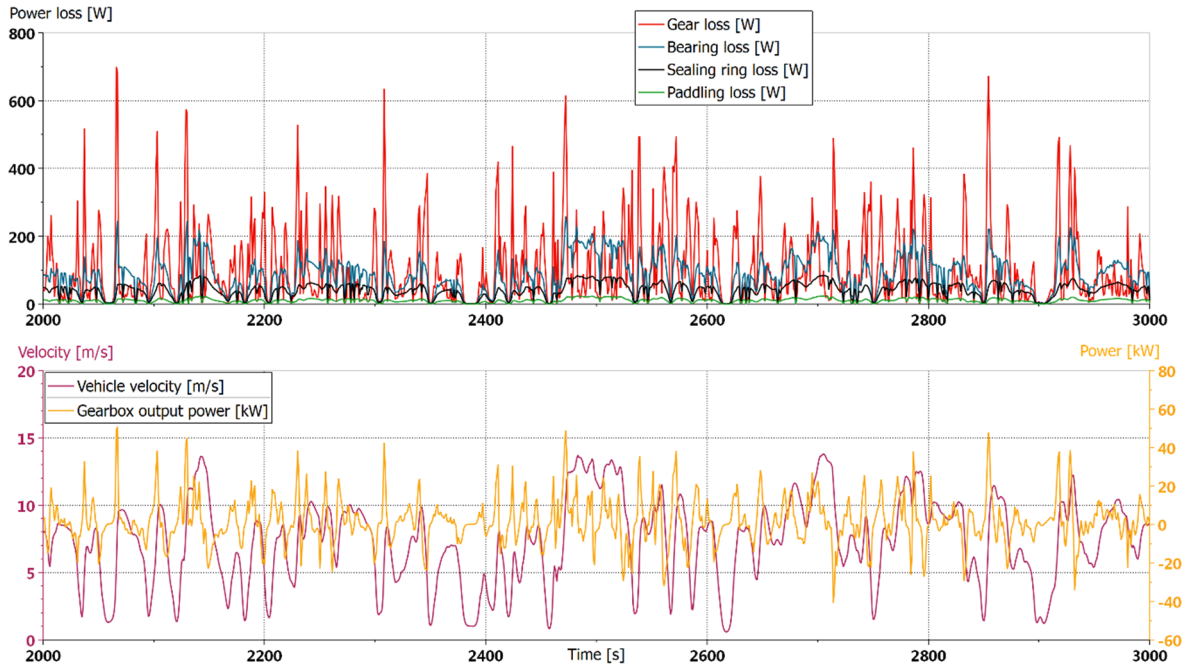

Different power losses, vehicle speed and output power of city test cycle section

The image below shows the gear energy loss over the city driving cycle. Due to the lower velocities during driving in a city, the energy loss occur in a range of lower axle speeds and lower axle torques. The gear energy loss reach losses up to 70 Wh at lower axle loads and speeds.

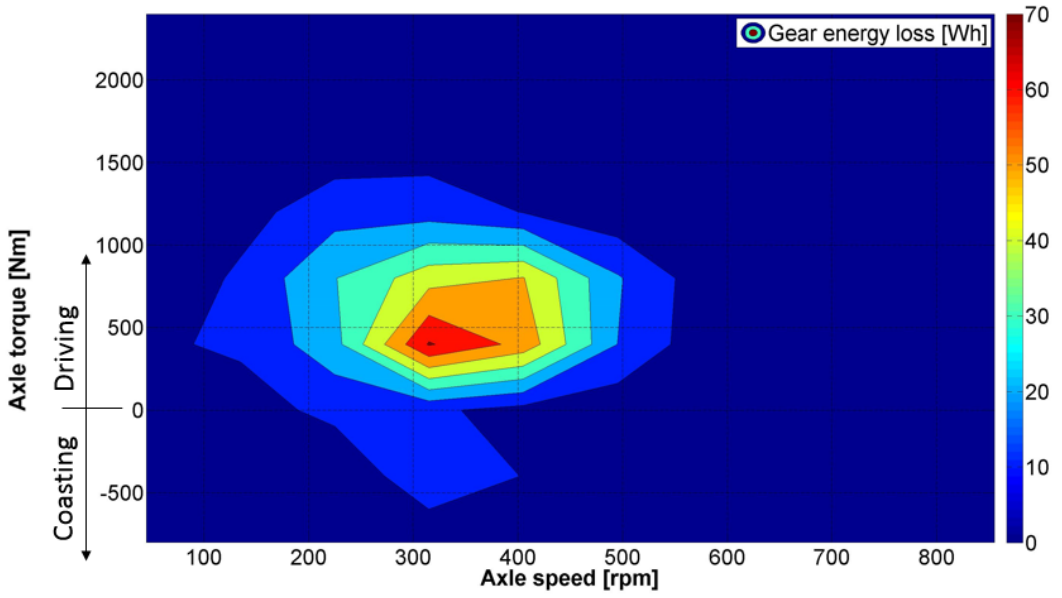

Gear energy loss of city test cycle

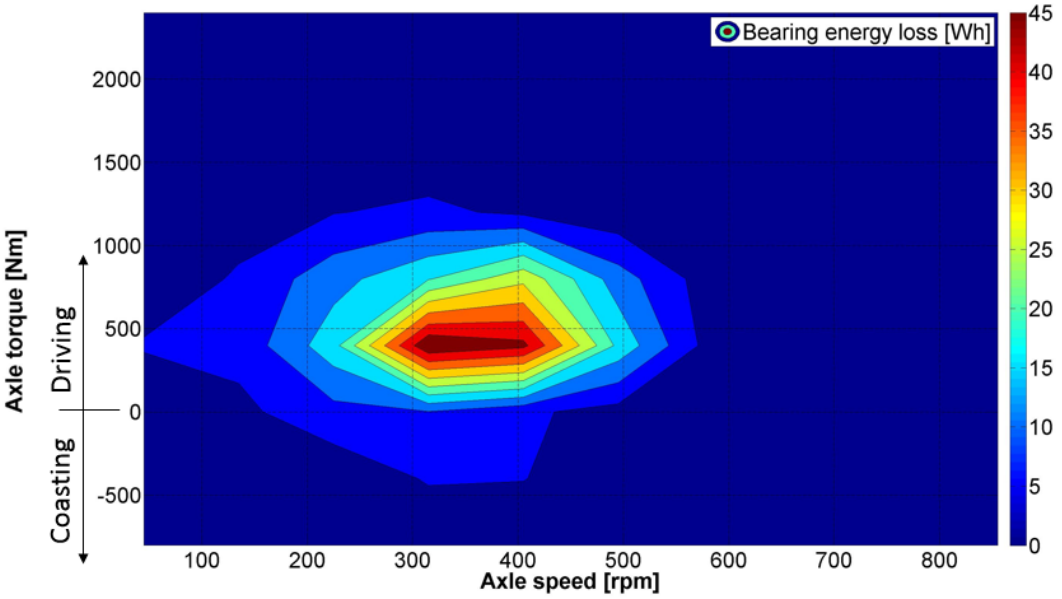

Bearing energy loss of city test cycle

The bearing energy loss reach a maximum of 45 Wh and the higher amount of the energy loss occur in the same load spectrum. During driving in a city a vehicle is accelerating and decelerating very often and therefore the gearbox is operated in the same load ranges over the whole cycle time. The sealing ring energy loss are in a scope of 20 Wh at the city specific load points.

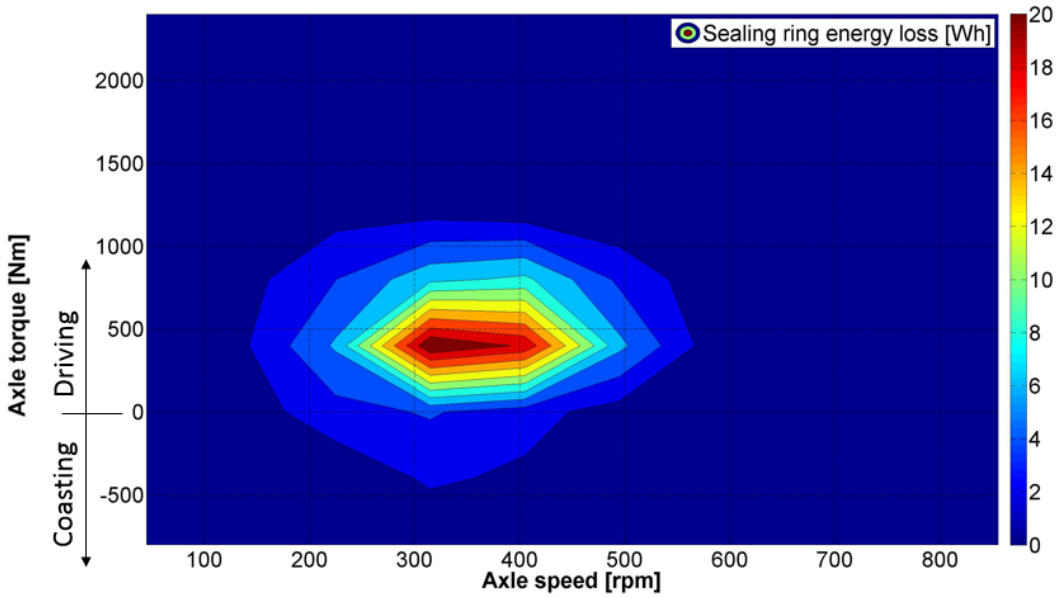

Sealing ring energy loss of city test cycle

The amount of energy loss due to paddling are in a lower range. A maximum energy loss of 5 Wh is generated during the cycle in the same range as the sealing ring losses.

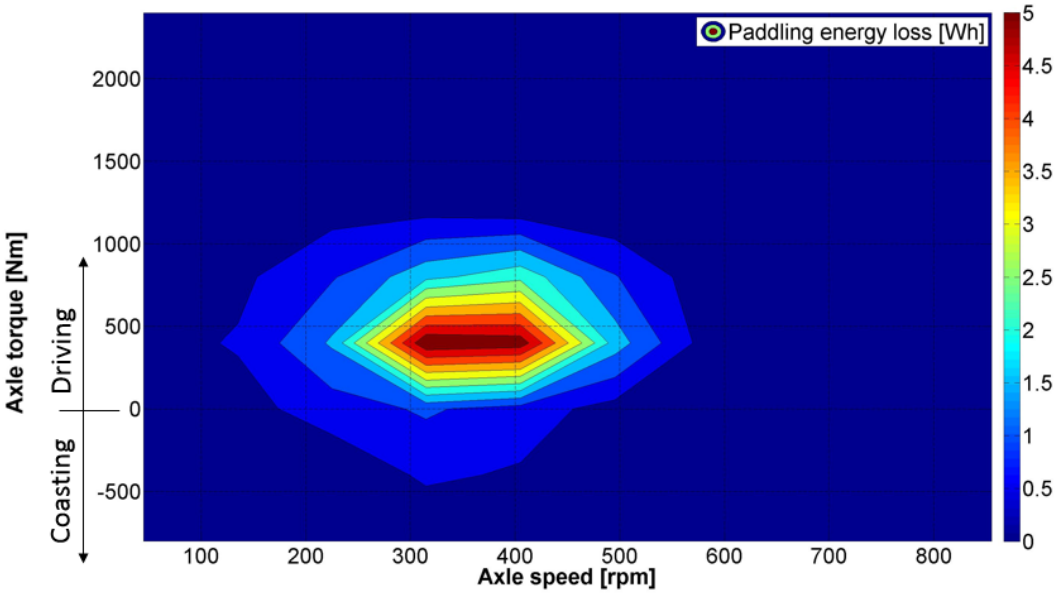

Paddling energy loss of city test cycle

Motorway A2 with BMW X3

In the figure below the power losses of the whole motorway cycle are shown. The power losses are displayed in the upper plot and the vehicle speed and the gearbox output power are displayed in the lower plot. During driving on a motorway the vehicle velocity is in a range above 130 km/h and at such speeds the bearing losses have the highest share of the power losses. At the short acceleration periods the gear losses have a peak but overall the bearing losses are dominating during the whole cycle.

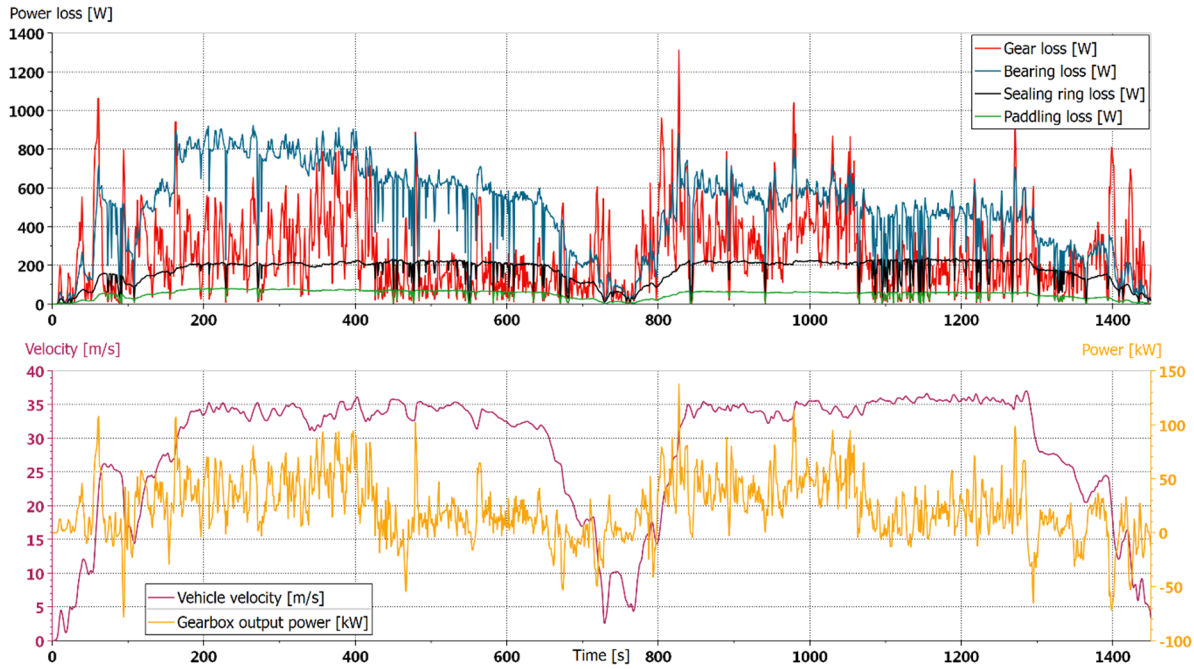

Different power losses, vehicle speed and output power of motorway cycle

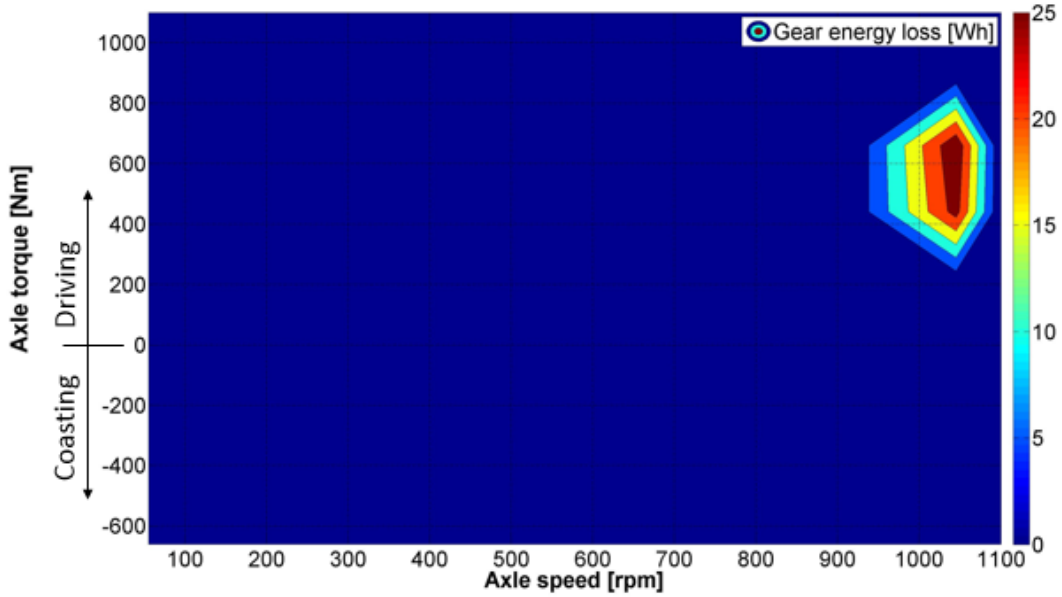

Gear energy loss of motorway cycle

Due to the characteristic of that driving cycle the energy loss is focused at the high axle speed and at axle torques between 200 and 900 Nm. The gear energy loss reaches a maximum of 25 Wh which is lower compared to the bearing energy loss which reach a maximum of up to 80 Wh. During the motorway cycle the power losses at coasting are low and hence the energy loss is in a low range and not displayed in the plot.

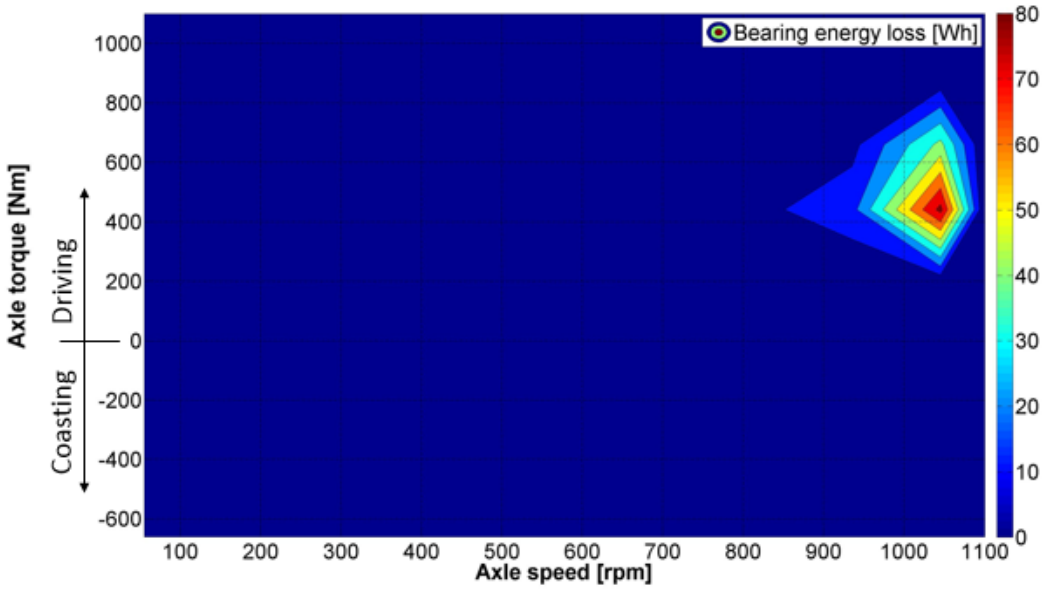

Bearing energy loss of motorway cycle

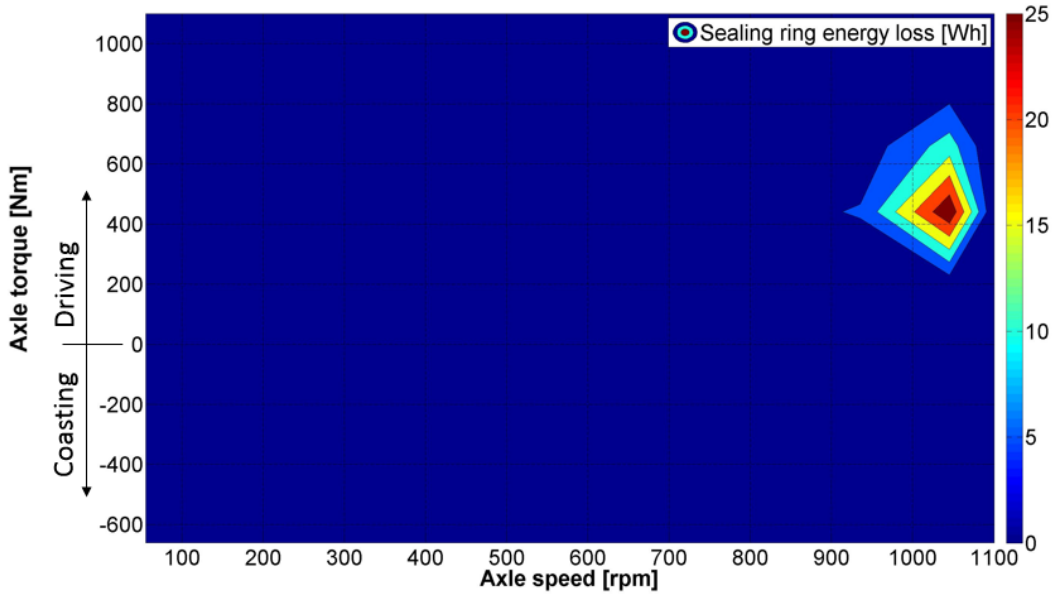

Sealing ring energy loss of motorway cycle

For the sealing ring and paddling losses it is the same, the energy loss are focused in the same load range. The sealing ring losses reach an energy loss of up to 25 Wh which is higher compared to the paddling energy loss.

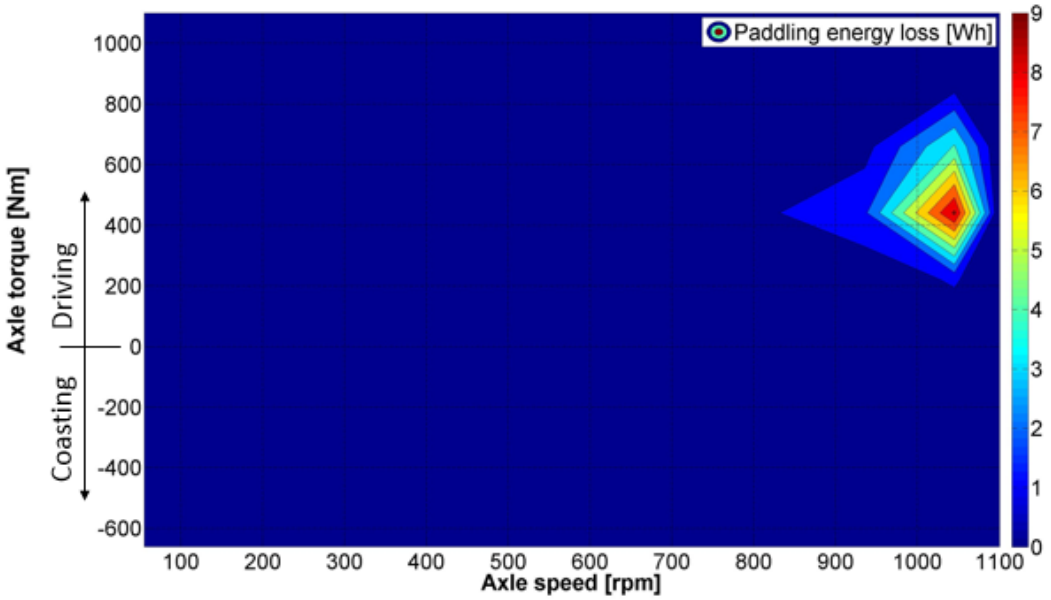

Paddling energy loss of motorway cycle

Country road cycle with BMW X3

In the upper plot a section of the country road cycle including the different power losses are displayed. The gear losses are represented in red and over the time section the proportion of the gear losses is larger than all the other losses. In the lower plot a section of the vehicle velocity profile is displayed in purple and it shows that velocities up to 130 km/h are reached at the country road cycle.

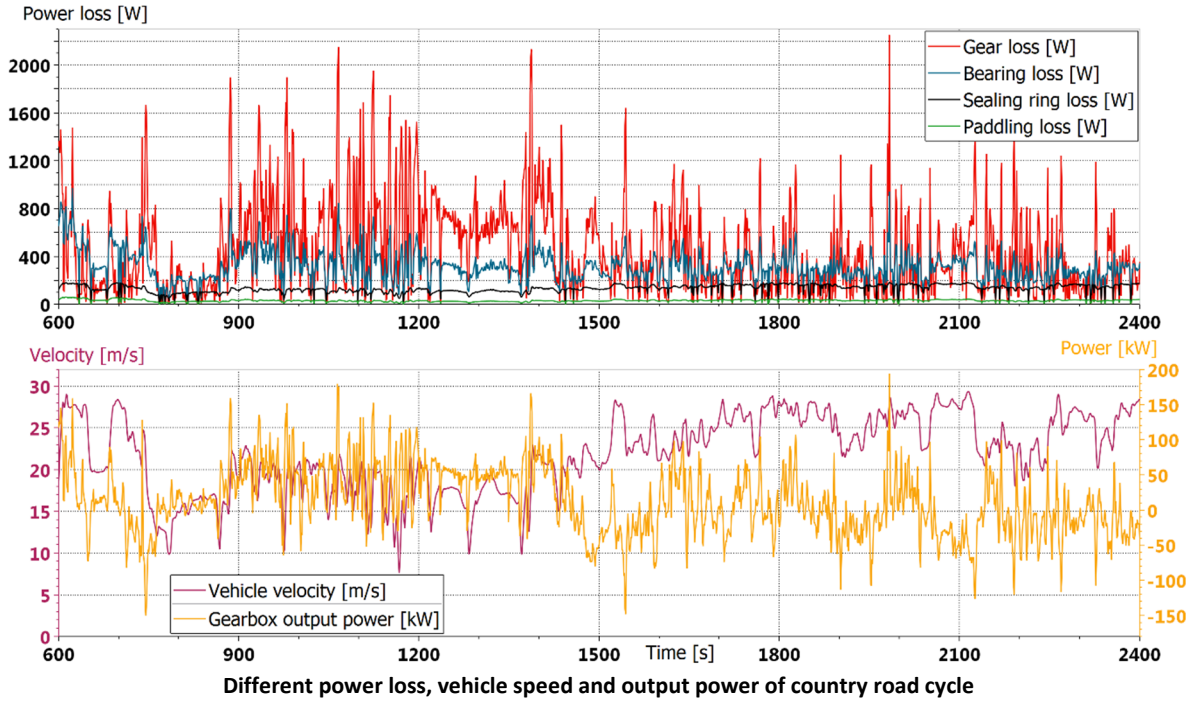

Different power loss, vehicle speed and output power of country road cycle

At the country road cycle the gear energy loss are distributed over the axle speed range from 400 to 900 rpm. The gear energy loss reach a maximum of 35 Wh at different axle rotational speeds and axle torques. During that cycle the energy loss not only occur at driving, also at coasting gear energy loss up to 25 Wh occur. Due to the slope of the country road the gear energy loss at coasting are not negligible low.

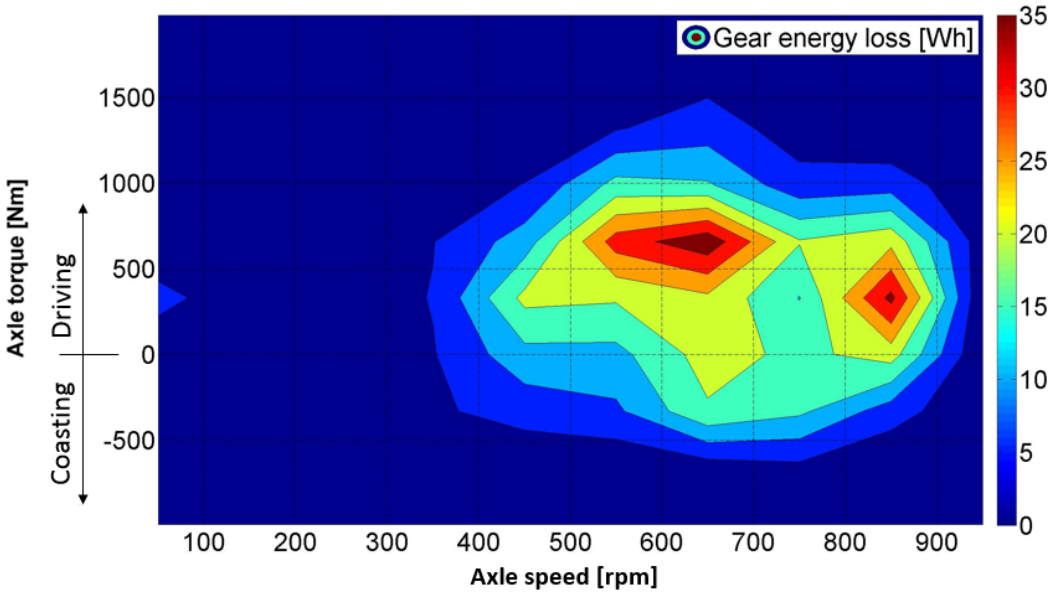

Gear energy loss of country road cycle

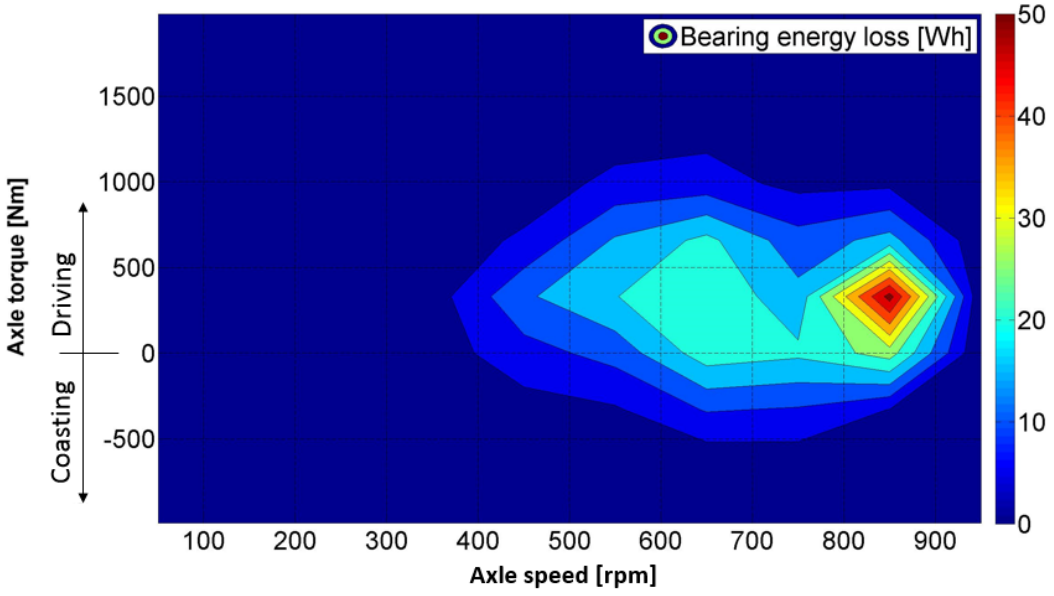

Bearing energy loss of country road cycle

The bearing energy loss at the country road cycle reach a maximum of 50 Wh at 850 rpm. At coasting bearing energy loss up to 25 Wh occur, but only at lower axle torques. The sealing ring energy loss have nearly the same distribution as the bearing energy loss, but the range of the losses is a different one because 20 Wh are the maximum sealing energy loss at that cycle.

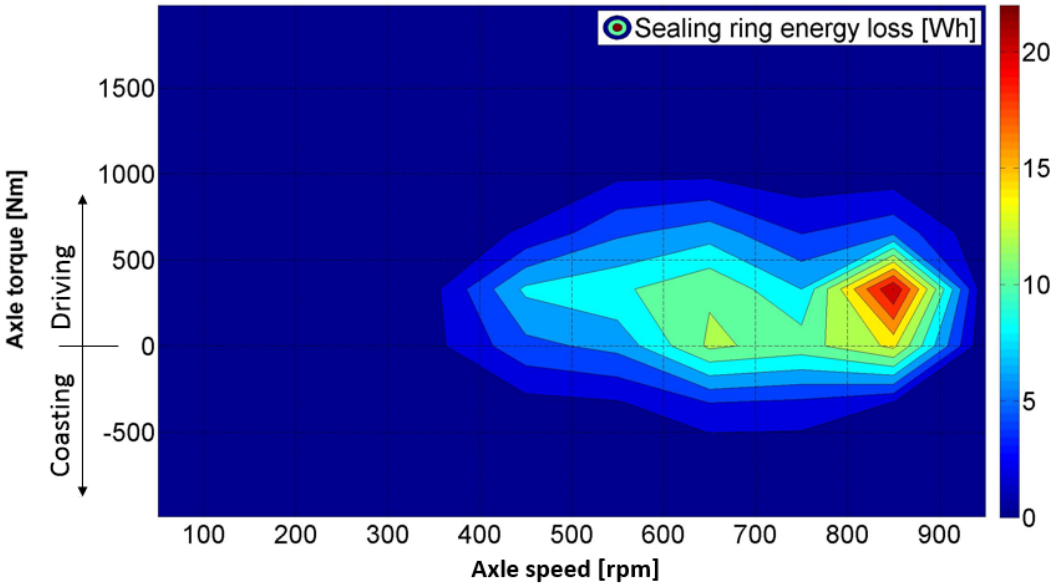

Sealing ring energy loss of country road cycle

The paddling energy loss generate a smaller amount of the entire energy loss during the country road cycle. A maximum of 6 Wh energy loss is reached at 850 rpm. At coasting also the paddling of the gears generate a low amount of energy loss.

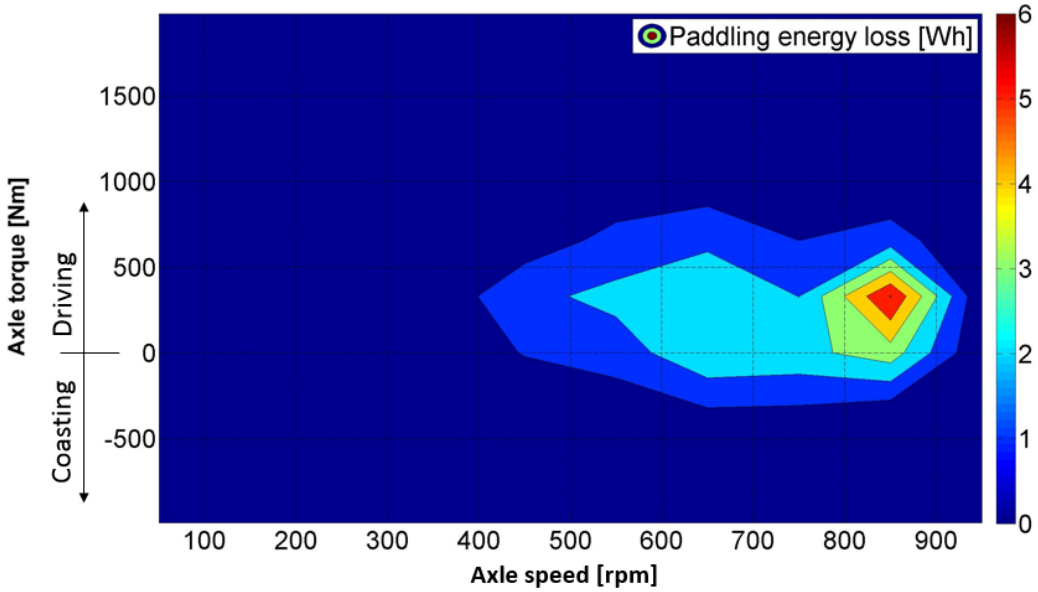

Paddling energy loss of country road cycle